PREPARATION AND SURFACE MODIFICATION OF MAGNETIC PLGA NANOPARTICLES FOR SUSTAINING NATURAL INTERFERON RELEASE

Ph.D. THESIS

By:

QUAZI TANMINUL HAQUE SHUBHRA

DOI: 10.18136/PE.2014.553

SUPERVISORS:

PROF. JÁNOS GYENIS

DR. TIVADAR FECZKÓ

UNIVERSITY OF PANNONIA

DOCTORAL SCHOOL OF MOLECULAR- AND NANOTECHNOLOGIES

RESEARCH INSTITUTE OF CHEMICAL AND PROCESS ENGINEERING

HUNGARY

2014

PREPARATION AND SURFACE MODIFICATION OF MAGNETIC PLGA NANOPARTICLES FOR SUSTAINING NATURAL INTERFERON RELEASE

Értekezés doktori (PhD) fokozat elnyerése érdekében

Írta: Quazi Tanminul Haque Shubhra

Készült a Pannon Egyetem Molekuláris- és Nanotechnológiák
Doktori Iskolája keretében

Témavezetők: Dr. Gyenis János, professor emeritus
Dr. Feczkó Tivadar, tudományos főmunkatárs

Elfogadásra javaslom (igen / nem)

…….

(aláírás)

A jelölt a doktori szigorlaton .....%-ot ért el,

Az értekezést bírálóként elfogadásra javaslom:

Bíráló neve: …..... ….....) igen /nem

…….

(aláírás)

Bíráló neve: …..... ….....) igen /nem

…….

(aláírás)

A jelölt az értekezés nyilvános vitáján ….....%-ot ért el.

Veszprém, …….
a Bíráló Bizottság elnöke

A doktori (PhD) oklevél minősítése….....

……
Az EDHT elnöke

TABLE OF CONTENT

List of abbreviations

BBB	Blood brain barrier
BCA	Bicinchoninic acid
BSA	Bovine serum albumin
D_{mean}	Mean hydrodynamic particle size
DCM	Dichloromethane
DOE	Experimental design
Dox	Doxorubicin
EE	Encapsulation efficiency
ELISA	Enzyme-linked immunosorbent assay
GA	Glycolic acid
HSA	Human serum albumin
IFN-α	Interferon alfa
LA	Lactic acid
MNPs	Magnetic nanoparticles
MPs	Microparticles
MPS	Mononuclear phagocyte system
MRI	Magnetic resonance imaging
Ms	Saturation magnetization
NPs	Nanoparticles
PBS	Phosphate-buffered saline
PEG	Poly(ethylene glycol)
PLA	Poly(lactic acid)
PLGA	Poly(lactic-co-glycolic acid)
PVA	Poly(vinyl alcohol)
RES	Reticuloendothelial system
SEM	Scanning electron microscope
SPIO	Superparamagnetic iron oxide
TEM	Transmission electron microscopy

V_{HSA}	Volume of the introduced HSA solution (internal phase)
V_{PLGA}	Volume of the introduced PLGA/magnetite solution (intermediate organic phase)
V_{PVA}	Volume of the outer aqueous phase (PVA solution)
W/O/W	Water-oil-water
O/W/O	Oil-water-oil
X_{Fe3O4}	Relative mass of the introduced magnetite compared to the mass of PLGA
X_{PLGA}	Concentration of PLGA in the intermediate oily phase
X_{HSA}	Concentration of HSA in the inner aqueous phase
X_{VOLR}	Volume ratio of the outer aqueous phase to the intermediate oily phase
X_{time}	Time of the second sonication

ABSTRACT

The aim of this Ph.D. work was to create sustained and targeted drug delivery device for natural interferon alfa (IFN-α) which is an effective medicine mainly applied against hepatitis viruses and viral hepatocellular carcinoma. Thus, IFN-α and superparamagnetic iron oxide (Fe_3O_4) nanoparticles (NPs) were co-encapsulated inside poly(lactic-co-glycolic acids) (PLGA) matrix. PLGA NPs were prepared using double emulsion solvent evaporation method, and the relation between the process variables, in order to obtain small sized NPs sterilizable by ultrafiltration with high encapsulation efficiency; the surface modification to evade macrophages in the bloodstream; and the *in vitro* IFN-α release were investigated. Process optimization and functionalization were carried out using human serum albumin model drug. By experimental design and statistical analysis with STATISTICA® software, the number of experiments was reduced to 90 instead of 243 for five important process variables and the results were analyzed. The mean hydrodynamic size and encapsulation efficiency of NPs ranged from 115-329 nm and 18 to 97%, respectively depending on the process conditions. The optimization process, carried out by exact mathematical tools using GAMS™/MINOS software, enabled to find out optimum process conditions to achieve high encapsulation efficiency (92.3%) for relatively small sized PLGA NPs (155 nm). NPs prepared with selected optimum condition were subjected to surface modification to prolong their lifetime in the bloodstream by using triblock copolymer poloxamer. Surface functionalization was verified by size, zeta potential and isothermal titration calorimetry investigations. In blood serum protein adsorption measurements, bovine serum albumin tended to be adsorbed 50% less on the surface modified NPs in comparison to the unmodified ones. In vitro IFN-α release study carried out using enzyme linked immunosorbent assay test showed that prepared PLGA NPs are capable to sustain the release of interferon, and protect it from the quick degradation. Interferon release from poloxamer modified PLGA NPs was much slower than that for unmodified ones.

KIVONAT

A PhD munka célja késleltetett és célzott hatóanyag leadási rendszer létrehozása természetes interferon alfa (IFN-α) számára, mely a hepatitisz vírusok és a virális hepatocelluláris karcinóma egyik hatékony gyógyszere. E célból poli(tejsav-glikolsav) (PLGA) mátrixban IFN-α és szuperparamágneses vas-oxid nanorészecskéket együttesen mikrokapszuláztak. A PLGA nanorészecskéket összetett emulziós oldószer elpárologtatásos módszerrel állították elő, és vizsgálták az eljárás változói közötti összefüggést annak érdekében, hogy ultraszűréssel sterilizálható kisméretű, nagy kapszulázási hatékonyságú részecskéket nyerjenek; a felületi módosítást, hogy a véráramban elkerüljék a makrofágokat; és a nanorészecskék in vitro IFN-α kibocsátását. Az eljárás optimalizálását és a részecskék funkcionalizálását humán szérum albumin modell gyógyszerrel végezték. A STATISTICA® kísérlettervező és statisztikai analízis szoftverével a kísérletek számát 243-ról 90-re csökkentették az öt legfontosabb folyamatváltozó figyelembevételével, és az eredményeket elemezték. A nanorészecskék átlagos hidrodinamikai mérete és a kapszulázási hatékonysága az eljárási körülmények függvényében 115-329 nm és 18-97 % tartományban változott. Az optimalizálás egzakt matematikai eszköze a GAMS™/MINOS szoftver lehetővé tette a legjobb eljárási körülmények megtalálását magas kapszulázási hatékonyság (92,3 %) és viszonylag kisméretű (155 nm) PLGA nanorészecskék eléréséhez. Az optimális körülmények között előállított nanorészecskék felszínét poloxamer triblokk kopolimerrel módosították, hogy megnöveljék a véráramban az élettartamukat. A felszíni funkcionalizálást méret, zeta potenciál és izotermális titrációs kalorimetriás analízissel támasztották alá. Vér szérum fehérje adszorpciós vizsgálata során a felületmódosított nanorészecskék 50 %-kal kevesebb bovine szérum albumint adszorbeáltak, mint a nem módosított nanorészecskék. In vitro IFN-α leadási vizsgálat enzimhez kapcsolt immunszorbens meghatározással kimutatta, hogy a PLGA nanorészecskék képesek az interferont késleltetetten kibocsátani, és megvédeni a gyors lebomlástól. A poloxamerrel módosított PLGA nanorészecskék lényegesen lassabban adták le az interferont, mint a nem módosított részecskék.

AUSZUG

Das Ziel der Ph.D These war Herstellung eine Vorrichtung für nachhaltige und gezielte Arzneimittelabgabe welche naturgemäß Interferon Alpha (IFN-α) enthält. Interferon Alpha ist eine effektive Medizin vorzugsweise verwendet gegen Hepatitis-Viren und virales Leberzellkarzinom. So IFN-α und superparamagnetischen Eisenoxid (Fe_3O_4) Nanopartikeln (NPs) waren innerhalb einer Matrix von Poly(Milchsäure-co-Glykolsäure) (PLGA) co-gekapselt. PLGA NPs waren mit der Hilfe einer Doppelemulsion Methode präpariert. Die Relation zwischen Die Prozessvariablen und die in vitro IFN-α Freigabe war untersucht um feinen NPs zu beschaffen, die für Sterilisation durch Zentrifugation geeignet sind, und eine hohe Verkapselung Leistungsfähigkeit haben, und mit Oberflächenmodifizierung Makrofagen in den Blutstrom zu vermeiden können. Die Optimierung des Verfahrens und die Funktionalisierung waren Aufwendung von Humanes Serumalbumin als Modell Arzneimittel durchgeführt. Die Anzahl von Experimenten war von 243 bis 90 Prozessvariablen Aufwendung das Versuchsdesign und statistische Analyse von Statistica Software reduziert. Der hydrodynamischen Durchschnittskerngröße und Verkapselung Leistungsfähigkeit von NPs waren 115-239 nm und 18-97 %, beziehungsweise abhängig von den Prozessbedingungen. Die Optimierung des Verfahrens, die mit exaktem mathematischem Instrument, der GAMS™/MINOS Software durchgeführt war, hat ermöglicht zu finden optimal Verfahren Bedingungen zu erreichen eine hohe Verkapselung Leistungsfähigkeit (92,3 %) von relativen kleinen PLGA NPs (155 nm). NPs, die mit ausgewählten optimalen Verfahren Bedingungen hergestellt waren zu prolongieren ihre Lebensdauer in den Blutstrom, waren mit Hilfe dreiblock copolymer Poloxamer Oberflächenmodifizierung untergezogen. Oberflächenfunktionalisierung war mit Korngröβe- und Zetapotenzialanalyse, und isometrische Kalorimetrie Titrieren geprüft. In der Blutserum Absorption Messungen Bovines Serum Albumin was tendieren zu absorbieren 50 % weniger auf die oberflächenmodifizierte NPs als auf die Unmodifizierten. Die in vitro IFN-α Freigabenuntersuchung zeigte, was mit der Enzyme verbundenen immunosorbens Probe durchgeführt war, daβ die präparierten PLGA NPs fähig sind zu retardieren die Freigabe von Interferon, und die Oberflächenmodifizierung bewährt die NPs von einer schnellen Degradierung. Freigabe von Interferon mit Poloxamer modifizierten PLGA NPs war viel langsamer als von Unmodifizierten.

1 INTRODUCTION

Last two decades have witnessed tremendous efforts by researchers for developing potent drugs to treat cancer and viral diseases. Cancer has overtaken heart disease as the number one killer and as a single entity, cancer takes highest number of human lives worldwide with an estimated 8.2 million deaths in 2012. World cancer report 2014 forecasted 75% increase in cancer cases worldwide over next two decades which is going to result in 25 million cancer cases. The estimated total annual economic cost of cancer was approximately US$ 1.16 trillion in 2010. This amount is equivalent to 2% of total global GDP (gross domestic product). According to recent report released by Centers for Disease Control and Prevention on World Hepatitis Day (July 28, 2013), viral hepatitis is a leading cause of infectious disease mortality globally, each year causing approximately 1.4 million deaths. Most of these deaths occur among the approximately 400 million persons living with chronic hepatitis B virus or hepatitis C virus infection.

Nanoparticles (NPs) are solid colloidal particles with diameters ranging from 1-150 nm, nevertheless, regarding microencapsulation, 1-1000 nm is generally termed as nano size range. Numerous NP-based drug delivery and drug targeting systems are currently under development and many of them are already developed [1]. Especially since 1980s, scientists have been trying to develop potent drug carriers and deliver medicines to targeted sites. The primary cause behind tremendous development of medical industry is recognizing essentiality for developing current therapies for drugs already marketed and yet to be marketed. Drug loaded magnetic nanoparticles/nanocapsules (NPs) are very promising tools to realize targeted and sustained drug delivery, especially in fighting against cancer. Several disease related bioactive molecules/drugs are successfully encapsulated by appropriate matrices to improve bioactivity, bioavailability and applied for controlled delivery. Nanomedicines of the diseases such as AIDS, cancer, tuberculosis, diabetes, malaria, prion disease, etc. are in different trial phase for the testing and some of them are commercialized [2]. Probably that’s why recent years have witnessed not only unprecedented growth of research, but also vast applications in the area of nanoscience and nanotechnology. Therapeutic NP technologies are able to revolutionize the drug development process and capable of changing the landscape of the pharmaceutical industry. Encapsulation of

medicinal drugs by nanocarriers increases specificity, drug efficacy, therapeutic index of corresponding drugs and tolerability.

1.1 Objectives

The aim of this Ph.D. work was to create sustained and targeted drug delivery device for natural interferon alfa (IFN-α). IFN-α and superparamagnetic iron oxide (Fe_3O_4) NPs were co-encapsulated inside poly(lactic-co-glycolic acids) (PLGA) matrix. PLGA NPs were prepared using suitable method of production and the relation between the process variables to obtain smaller sized NPs with higher encapsulation efficiencies, surface modification to evade macrophages in the bloodstream and in vitro IFN-α release were investigated. Due to high cost of IFN-α, process optimization and functionalization were carried out using human serum albumin (HSA) model drug instead of IFN-α. IFNs exhibit antiviral and antitumor activities. Magnetic NPs can target IFN-α loaded PLGA NPs to liver and spleen and can be used to cure cancers of respective body parts. On the other hand, due to the presence of magnetic NPs, targeting any body part with the help of magnetic field (by external or internal magnet) may be possible and drug uptake process might also be visualized by MRI (Magnetic resonance imaging).

2 REVIEW OF THE LITERATURE

2.1 Interferon (IFN)

Interferon (IFN) was first discovered in 1957 by Alick Isaacs and Jean Lindenmann [3]. Interferon (IFN) is a class of cytokines (cell signaling proteins) with immune stimulating activity carrying out important physiological functions in higher vertebrates. IFNs are a family of small proteins and glycoproteins. They are produced and secreted in vivo by cells mainly in response to infections caused by viruses and also in response to synthetic or biological inducers. IFNs are being used widely for the biologic therapy of infectious viral diseases such as hepatitis C and B and for the treatment of several cancers.

IFNs are divided into type 1 and type 2 based on common biochemical features and/or amino acid sequence similarities. IFN-γ is the only type 2 member having dissimilar structure than type 1 IFNs. Type 1 IFNs share a common cell surface receptor. Type 1 IFN is subdivided into several types depending on the basis of nucleotide and amino acid sequence identities, species-restricted distributions or unique biological functions. Among different subtypes, two most ancient and best-characterized type 1 IFNs are 'IFN-α' and 'IFN-β' which are the most broadly distributed type 1 IFNs among mammals.

2.1.1 Natural interferon alfa (IFN-α)

Natural IFN-α proteins are partially glycosylated, whereas recombinant IFNs are not. Natural IFN-α has certain advantages over recombinant products. Natural IFNs show comparatively lower side effects than recombinant or synthetic IFNs, which is their main advantage and the reason behind the use of natural IFN-α in this study. Cell culture-derived "natural" IFN products contain a multiplicity of IFN types or species, thus, are expected to provide potentially better therapeutic efficacy, than single-species recombinant IFN products. Since each subtype has its own specific biological activity, it is expected that natural IFN-α has more balanced effect against a variety of diseases. Therefore, it can be considered more advantageous for patients to be treated with natural product that potentially elicits an effective immune response, and is tolerated to a higher extent by the treated patients.

IFN-α is produced by leukocytes (T cells, B cells, macrophages and null cells) upon exposure to viruses, B cell mitogens, tumor cells or foreign cells [4]. IFN-α is the

most extensively studied interferon species. Each subtypes of IFN-α showed different growth inhibitory, antiviral and other biologic activities. Regarding antiviral activity, IFN-α1 was the least, while IFN-α8 was the most potent.

IFN-α is used in more than 40 countries for treating more than 14 types of cancers, including some hematological malignancies (chronic myeloid leukemia, hairy cell leukemia, some B and T cell lymphomas) and certain solid tumors, such as melanoma, renal carcinoma and Kaposi's sarcoma [5].

2.1.2 The mechanisms of action

IFNs show numerous and diverse actions, functioning at the physiological and molecular level. They bind to specific membrane receptors on the cell surface to show their cellular activities. After being bound to the cell membrane, IFNs initiate a complex sequence of intracellular events, including the up-regulation of certain other cytokines, suppression of cell proliferation, induction of certain enzymes, inhibition of virus replication in virus-infected cells, immunomodulating activities such as enhancement of the phagocytic activity of macrophages and augmentation of the specific cytotoxicity of lymphocytes for target cells.

In spite of years of intense works in animal tumor models and considerable experiences in the clinical use of IFNs, the exact mechanisms underlying the antitumor response are not fully understood. Likewise, not too much is known about why some tumors are highly responsive to IFN treatments, while others show little or no response. IFN-α plays very important role in the antiviral defense by regulating the immune system or by direct inhibition of the intracellular viral lifecycle [6]. IFN-α has the ability to stimulate the host cell to resist viral infection and can inhibit many steps of viral replication. The major antiviral action is the affecting of translation of the viral genome. IFN-α inhibit viral transcription, enzymatically degrade viral RNA, reduce the translation of viral proteins by interfering with the normal host cell translation mechanism, modify glycosylation patterns of viral proteins (which could influence virus packaging, release, or virulence) and can alter the cell membrane (e.g. increasing cell membrane fluidity) which may influence virion maturation and release. IFNs inhibit cell growth and division by increasing the length of the multiplication cycle, enhancing cell lysis through cytotoxic mechanisms, depleting essential metabolites, inhibiting the

expression of oncogenes, inducing the expression of tumor suppressor genes and inducing apoptosis.

IFN-α is eliminated from the body mainly by the kidney, where they are totally filtered through the glomeruli. In the kidney, during tubular reabsorption, they undergo rapid proteolytic degradation resulting in negligible reappearance of intact IFN-α in the systemic circulation. Minor pathways of elimination for IFN-α involve liver metabolism and subsequent biliary excretion [7]. For healthy people, IFN-α exhibited an elimination half-life of 3.7 to 8.5 hours (mean 5.1 hours).

Primary adverse effect is "flu-like" symptoms (headache, fever, myalgias, etc.) which are in most cases mild or moderate, and transient, and does not affect the treatment. Alfa IFNs have suppressive effect on the bone marrow, which may lead to a fall in the white blood cell count, the platelet count and less commonly the hemoglobin concentration. Moreover, abnormalities in the blood clotting mechanism have been observed. These effects can enhance the risk of infection, thrombosis and hemorrhage.

2.2 Model drug

To make the research more economical, researchers frequently use model drug during the development of drug loaded NPs/microparticles (MPs) since in many cases drugs are quite expensive. In this study, HSA was selected as a model drug, since natural interferon accompanied with a number of other cytokines and proteins is secreted as a protein mixture from the human blood, and HSA is the most abundant protein in this mixture. HSA is not removed from the mixture, since it was found that it assures appropriate medium to cytokines, and preserves their activities and prevents them from environmental damages. HSA concentration is higher than 95% in the natural interferon mixture (Trigon Biotechnological Zrt.), therefore in the encapsulation process it affects strongly the properties of the obtained NPs. HSA is a monomeric multi-domain macromolecule, which is the most abundant plasma protein in the human body with a plasma concentration of 0.6 mM [8]. HSA consists of 585 amino acids that form three structurally similar α-helical domains.

2.3 Nanoparticles in drug delivery

The use of nanotechnology in medicine, specifically for drug delivery has been increasing day by day. From a positive viewpoint, NPs have the ability to access into the cell and various cellular compartments including the nucleus, and they have the potential to cross the blood brain barrier also. Currently a multitude of substances are being investigated for the preparation of NPs for drug delivery. Not too much is known regarding all aspects of nanoparticle toxicology in the field of drug delivery, however, vast number of research is being carried out to explore that.

Many studies have demonstrated that NPs possess several advantages over MPs [9]. For example, NPs are capable of travelling through the bloodstream without blockage or sedimentation of the microvasculature. Small NPs can circulate throughout the body and penetrate tissues e.g. tumors. NPs having unique small size can strongly influence drug loading, drug release, stability of the therapeutic agents, etc. Because of their small size, unique qualities are shown by NPs that are not found in the same material at larger size [10]. Drug release is strongly affected by the size of particles. Smaller particles possess larger surface-area-to-volume ratio, and most of the drugs associated with small particles normally remain at or near the particle surface, which leads to a faster drug release [11]. NPs have relatively high cell uptake in comparison to MPs. They are useful for a wider range of cellular and intracellular targets because of their mobility and small size. NPs can be taken up by cells through natural routes e.g. endocytosis. These vehicles can be designed in a way so that they will represent biophysical characteristics that are unique to the target cells, and are capable of minimizing drug loss and toxicity that can occur due to the delivery to the non-desired tissues. Similar study showed that NPs penetrated throughout the submucosal layers of a rat intestinal loop model, whereas MPs were predominantly localized in the epithelial lining [12]. This indicates that particle distribution can be tuned by controlling size of particles. In recent years, significant researches have been done on NPs as oral drug delivery vehicles, and the major interest for this purpose was lymphatic uptake of the NPs by the Peyer's patches in the gut associated lymphoid tissue. There are lots of reports on the optimum size for Peyer's patch uptake ranging from < 1 μm to < 5 μm [13]. Results show that MPs remain in the Peyer's patches, while NPs are systemically disseminated. Another advantageous feature of NPs smaller than 220 nm is that they

could be easily sterilized by ultrafiltration, since the sizes of bacteria and viruses are larger [14].

One big challenge for nanomedicinal formulations is scaling up. Nanodrug formulation to a large-scale is not always easy. It is much easier to maintain the size or composition of NPs at the laboratory scale than at a large scale. A number of technologies for the production of nanodrug may not be compatible with large-scale production due to the type of preparation method need to be used and high cost of materials employed. Although there are a good number of patents published on nanodrug delivery technologies, commercialization is still in its early stage [15].

2.3.1 Characteristics of NPs for drug delivery

Particle size is one of the most important characteristics of NPs intended for drug delivery applications. Size plays vital roles in particle functions, in vivo distribution, targeting, drug loading, drug release, toxicity, degradation, clearance and uptake mechanisms, etc. [16]. Depending on size, particles show different diffusion characteristics, velocities and adhesion properties which result in different uptake efficiencies. The size of NPs must be large enough to prevent rapid leakage in blood capillaries and at the same time small enough to escape the capture of macrophages in the reticuloendothelial system (RES).

The surface properties of NPs also control the fate of nanoparticles in the circulation. Opsonization and mononuclear phagocyte system (MPS) clearance are the two most important factors that are strongly affected by NP surface properties. Generally, positively charged NPs are internalized by cells due to electrostatic interaction with the negatively charged cell membrane by non-specific endocytosis [17]. On the other hand, negatively charged NPs show more selective internalization due to slight charge repulsion effect. Higher surface charge (either positive or negative) lead to an increase in macrophage surveillance, followed by MPS clearance. The in vivo biodistribution studies showed that highly negatively or highly positively charged NPs accumulated in the liver due to MPS cells uptake, whereas slightly negatively charged NPs accumulated in the tumor tissue and were excluded by the MPS system [17].

NPs used for drug delivery purpose should have desirable release profile. Both drug release and biodegradation of nanocarriers need to be considered significantly during the development of nanoparticulate delivery systems. Drug release is a complex process and depends on many factors like drug diffusion through the NP matrix, drug

solubility, desorption of the adsorbed or surface-bound drug, NP matrix degradation or erosion, the combination of diffusion and erosion processes, etc. [13]. Polymeric coating of nanocarriers can also affect the release of drug.

2.3.2 Toxicological hazards of nanoparticles

Safety and toxicological issues need to be strongly considered for the use of nanotechnology in nanomedicines. NPs have significant negative impact on human body due to the interactions between NPs and biological systems, which is termed as "nanotoxicology". Preliminary nanotoxicological studies have revealed that NPs can contribute to free radicals formation, undesirable penetration through the epidermis or other physiological barriers to enter different areas of the body that are more susceptible to toxic effects and damage of brain cells [15]. The cationic NPs (e.g. gold, polystyrene, etc.) may cause blood clotting and hemolysis, whereas anionic NPs are nontoxic in comparison to cationic ones. However, scientists have been working on the surface coatings and modifications of NPs to make them comparatively safer and more effective [18].

2.3.3 Forces acting on nanoparticle systems

The primary attractive force among NPs dispersed in a liquid is van der Waals force. For two nanospheres of radius 'R_1'and 'R_2' separated by a distance 'D' that is much smaller than 'R', the van der Waals interaction energy can be written: $V = -\{AR_1R_2/6D(R_1+R_2)\}$ where A is the effective Hamaker constant of the system [19]. If this attraction is strong enough, the NPs will hit each other and coalesce to form large particle. If only van der Waals forces would operate in a particle system, we could expect all dissolved particles to coagulate immediately and precipitate out of solution as a mass of solid material. Fortunately this does not happen due to the existence of repulsive forces between particles suspended in water or any liquid of high dielectric constant. Particles suspended in liquid are usually charged and can be prevented from coalescing by repulsive electrostatic forces. Other repulsive forces capable of preventing coalescence are solvation and steric forces.

Electrostatic repulsion arises when electric charge exists at the surface of the NPs. These charges may originate from the adsorption of charged ions at the surface (e.g. the adsorption of $–OH^-$ groups to the water-air or water-polymer interfaces that charges them negatively), or they may be due to ionization of chemical groups (e.g.

ionization of carboxyl group to carboxylate ion). In immediate vicinity of the NP surface, solution composition is in fact relatively complex. It is often described by a double-layer model: the inner layer (also known as the Stern layer), where the water molecules are highly structured by solvation of surface charges, and the diffuse layer involving counterions.

In case of very small separations between the surfaces or particles (e.g. few nanometers), the non-DLVO (Derjaguin and Landau, Verwey and Overbeek) forces such as the solvation forces and hydrophobic interaction forces become important. Solvation forces may arise from the ordering of the solvent molecules into discrete layers between particle surfaces in a highly restricted space. When NPs are immersed in a liquid, particle surfaces may be solvated. If two solvated surfaces come close enough together so that the solvation layers overlap, repulsive force originates. The repulsion may be caused because of the hydrated groups at the surfaces when they approach each other. Sometimes, solvation forces are also called structural force. Hydrophobic interaction occurs due to the water-fearing property of hydrocarbons by releasing water from the surface or hydrophobic particles resulting in interaction between hydrophobic groups.

Steric repulsion helps to stabilize colloidal particles and provides a more general method, exploiting the fact that the strength of van der Waals forces falls off very quickly with the distance. Colloidal particle surfaces can be coated with neutral and hydrophilic molecules that are long enough to maintain a certain distance between the particles, thereby rendering the van der Waals attraction negligible. In a physiological medium, extremely hydrophilic macromolecules like dextran or poly(ethylene glycol) (PEG) are often used to stabilize colloidal particles, since they interact strongly with the particle surface, and that they cannot form ‘bridges’ between different particles.

2.4 Microencapsulation methods

Microencapsulation is a process of enclosing submicron/micron sized particles of solids/droplets of liquids/gasses in an inert shell, which in turn protects and isolates the particles from the external environment. Microcapsules consist of two parts: the core and shell. The core is the intrinsic part (contains the active ingredient) and is protected by the shell (the extrinsic part). The obtained products of microencapsulation process are termed as microparticles/microcapsules/microspheres depending on the internal

structure and the morphology. If the particle size goes below 1 μm, they are termed as nanoparticles, nanocapsules, nanospheres, respectively.

The morphology of microcapsules mainly depends on the arrangement of core material inside the shell and deposition process for shell material. Microcapsules may be regular and irregular in shapes. Based on their morphology, microcapsules can be classified as matrix, mononuclear and polynuclear type (Fig. 1).

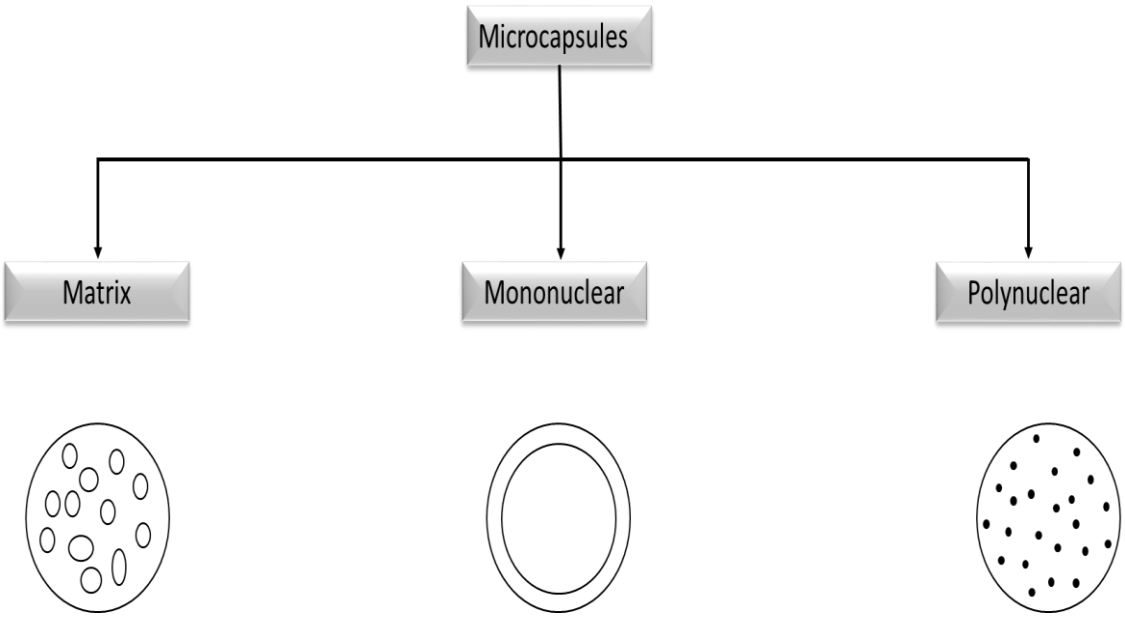

Fig. 1: Morphology of microcapsules.

Matrix type microcapsules exhibit homogeneous distribution of the core material inside the shell material. Mononuclear (also known as core-shell) type microcapsules contain a shell around the core. Many cores are encapsulated within the shell in polynuclear microcapsules. Beside these three primary morphologies, multiple shell mononuclear microcapsules are also observed.

The goals of the microencapsulation are diverse, however, most important directions are: (i) protection of the sensitive substances from the external environment, (ii) masking of organoleptic properties such as odor or taste, (iii) enzyme and microorganism immobilization, (iv) controlled, sustained or timed release of drug, (v) for safe handling of the toxic materials, (vi) better processability (improving flowability, solubility, dispersibility), etc.

Several techniques are used for the encapsulation of core materials. Broadly these methods can be divided into three types [20]:

(i) Chemical methods: In-situ processes like suspension, emulsion, precipitation or dispersion polymerization, interfacial polycondensations, etc. are the most widely used chemical techniques for microencapsulation.

(ii) Physico-chemical methods: Among physico-chemical methods, most common microencapsulation process is coacervation. Coacervation is based on aggregation of macromolecules by partially desolvating fully solvated macromolecules. Coacervation can be divided into two types: simple coacervation and complex coacervation. In simple coacervation processes, addition of salt or alcohol, change in temperature or pH issues in phase separation. On the other hand, oppositely charged polymer, when added to the polymer solution, forms a coacervate phase via anion–cation interactions in complex coacervation process. Sol-gel encapsulation, layer-by-layer (L-B-L) assembly, supercritical CO_2-assisted microencapsulation, etc. are also physico-chemical methods of microencapsulation used for specific applications.

(iii) Physico-mechanical methods: There are several physico-mechanical methods which are being used widely. Solvent evaporation technique finds widespread applications in different pharmaceutical industries. It facilitates the release of drug in a controlled way, which has a lot of clinical benefits. The core material to be encapsulated is dissolved or dispersed in the solution of coating polymer. The coating polymer is dissolved in a volatile solvent. The forming solution is added to a stirred solution containing a suitable stabilizer to form small polymer droplets containing encapsulated material. From the mixture, solvent is evaporated. As a result, coating material shrinks around the core material encapsulating the core.

2.4.1 Double emulsion method

A double emulsion is a complex liquid dispersion system in which the droplets of a dispersed liquid are further dispersed in another liquid. In a double emulsion, the inner dispersed droplets/globules are separated (compartmentalized) from the outer liquid phase by a layer of another phase. So far, different types of double emulsions have been documented. Some may have single internal compartment, while others may contain many internal droplets (known as “multiple-compartment emulsions”). Two common types are the water-oil-water (W/O/W) and oil-water-oil (W/O/W) double

emulsions. The most common and widely used double emulsion is W/O/W type, although O/W/O emulsions are needed for some specific applications.

Potential applications for double emulsions are well documented and a large number have been patented [21]. The important applications are in pharmaceuticals, agriculture, foods and cosmetics. In most cases, double emulsions are used to achieve slow and sustained release of active matter from an internal reservoir into the continuous phase (mostly water).

Usually a two-step emulsification process is used to form double emulsions using high pressure valve homogenizers or conventional rotor-stator. The primary emulsion of either type (W/O or O/W) is prepared under high-shear conditions to obtain inner droplets of small size, while less shear is applied during the secondary emulsification step to avoid rupture of the liquid membrane between the innermost and outermost phase. However, the second step can affect encapsulation efficiency and might reduce it, if homogenization is too intensive. It can also result in highly polydisperse outer drops, if homogenizing conditions are too mild.

Double emulsions can alternatively be produced by other methods e.g. by forcing a primary emulsion through a microporous membrane or microfabricated channel arrays into a continuous phase liquid. Much less shear is needed in this case, than in the conventional emulsification processes. As a result, the droplets are intact and both monodispersity and high entrapment efficiency can be achieved.

Double emulsions possess two different interfaces and require two sets of different types of emulsifiers. For O/W/O type emulsions, the first set of emulsifiers needed for the internal interface must be hydrophilic. For the same type of emulsion, the second set of emulsifiers needed for the external interface must be hydrophobic. In case of W/O/W type of double emulsions, the order of the emulsifiers is just opposite. The inner emulsifiers must be hydrophobic, while the outer ones need to be hydrophilic. In many cases a mixture of two or more emulsifiers in each set is used for better stabilization results. Too little emulsifier might fail to give a stable emulsion, whereas too much emulsifier may lead to toxic effects and can even cause destabilization.

By double emulsion, active materials are generally entrapped in the inner aqueous/organic phase. It is well documented in the literature that, due to the osmotic pressure difference, the active matter tends to diffuse and migrate from the internal phase to the external interface; in most cases through a mechanism known as “reverse micellar transport”. Stability of emulsion is very important for its industrial

applications. Flocculation, aggregation, coalescence are the major factors affecting the instability of the double emulsions, resulting in the separation of the phases and the rupture of the droplets. Double emulsions with low molecular weight emulsifiers (so called monomeric emulsifiers) are mostly thermodynamically unstable. This is because in the second stage of the emulsification severe homogenization or shear takes place forming large droplets. Proper and more suitable combinations of emulsifiers can improve the emulsion stability and reduce the droplet sizes. Among different surfactants, partially hydrolyzed poly(vinyl alcohol) (PVA) is mostly used since it is capable of producing smallest particles [22].

2.4.2 $W_1/O/W_2$ double emulsion solvent evaporation techniques

$W_1/O/W_2$ double emulsion solvent evaporation technique is normally used to prepare hydrophobic biodegradable micro/nanospheres containing hydrophilic proteins, pharmaceuticals and polypeptides for sustained release applications.

For the generation of transient $W_1/O/W_2$ emulsions, a two-stage emulsification process is used. The basic principle of the encapsulation in this process is based upon inducing phase separation of the polymer dissolved in a volatile organic solvent (O phase) due to partial extraction of the solvent in a large volume of the outer water phase (W_2 phase) and finally evaporation of the volatile solvent. The polymer then forms a coacervate which encloses the internal aqueous phase (W_1) that contains the active compound. MPs/NPs are hardened upon the removal of the residual solvent. Suitable solvents for this technique need to be volatile and immiscible with water. Dichloromethane is being employed frequently due to its low boiling point which facilitates the removal of residual solvent from the finished product. The other aspects include high dissolving power for a wide range of polymers, its partial solubility in water, and toxicity profile. The hydrophilic active substance (e.g. drug) is dissolved either in buffer or water and represents the internal water phase (W_1). Stabilizing excipients can be added for the protection of drug in the core of the microspheres. W_1/O emulsion is resulted upon the homogenization of W_1 phase with the O phase. The resulted primary emulsion is then rapidly added to a large volume of an external aqueous solution (W_2) that usually contains emulsifier(s) (e.g. PVA), and then emulsified to obtain a double $W_1/O/W_2$ emulsion.

Particles are formed based on coacervation. Because of its initial diffusion into the continuous W_2 phase, the solvent is extracted from the polymer containing O phase

inducing phase separation of the polymer. The organic solvent elimination occurs by two steps: firstly by extraction and secondly by evaporation. For further removal of the organic solvent and particle hardening, the system is continuously stirred at a constant rate for few hours. After complete solidification, the MPs/NPs are isolated either by filtration or centrifugation and washed several times with water to remove residual PVA and non-encapsulated drug. Depending on the glass transition temperature of the polymer, the MPs/NPs are lyophilized or dried in a vacuum at room temperature.

The main advantage of the $W_1/O/W_2$ double emulsion technique is that hydrophilic drug substances can be encapsulated under very gentle process conditions. Additionally, high yields and encapsulation efficiencies can be obtained.

2.5 Polymers used for drug delivery

Polymeric materials used for formulating NPs and MPs include both natural and synthetic polymers. Natural polymers in most cases are less expensive and have aqueous solubility. They have not been widely employed for biomedical purpose, since they vary in purity, show variability from batch-to-batch, and often require crosslinking that could denature the embedded drug. Synthetic polymers have a number of advantages including high control of polymer properties, such as molecular weight and functionality, and are feasible for commercial-scale production. Synthetic polymers show more reproducibility and can be prepared with the desired copolymer compositions, molecular weights and degradation rates. Synthetic polymers such as PLGA, poly(lactic acids) (PLA), poly(ε-caprolactone) (PCL), poly(methyl methacrylates) and poly(alkyl cyanoacrylates) or natural polymers such as gelatin, chitosan, albumin, collagen or alginate, etc. are commonly used as drug carriers. It is reported in the literature that polyesters alone and in combination with other polymers are most commonly used for the formulation of NPs and MPs. PLGA and PLA are highly biocompatible and biodegradable. They have been employed since the 1980's for numerous in vivo applications (biodegradable implants, controlled drug release, etc.).

2.5.1 Poly(lactic-co-glycolic acid)

PLGA is one of the most successfully used biodegradable polymers. PLGA is approved by the US Food and Drug Administration (FDA) and European Medicine Agency (EMA) in various drug delivery systems in humans.

This unique carrier system has the potential to change the current scenario of cancer research and diagnosis in real time. Encapsulation or conjugation of drugs in PLGA carriers can reduce several undesirable shortcomings. PLGA particles loaded with drugs can prolong the in vivo circulation time of the therapeutics from minutes to hours and are also able to reduce the cellular uptake along the endocytic route [23]. A very significant property of PLGA is the capability to manipulate its physico-chemical properties in order to tailor its degradation rate, which subsequently affects the release profile of the encapsulated molecules. Tailoring the release of encapsulated drugs from the polymeric particles reduces the use of frequent doses in the treatment regimen. The degradation rate of PLGA depends mainly on the hydrophilicity, molecular weight and crystallinity of the polymer. More hydrophilic and lower molecular weight PLGA exhibits an increased rate of polymer degradation. Ratio of PLA and PGA monomers present in the copolymer mainly determines the hydrophilicity of PLGA. Glycolic acid (GA) is more hydrophilic than LA (lactic acid). If the PLGA contains higher proportions of GA, increased degradation rate of the NP formulations is observed due to higher hydrophilicity of PLGA. The only exception to this rule found in the literature is the co-polymer having 50:50 GA:LA ratio which shows fastest degradation rate (half-life ($t_{1/2}$) about 2 weeks) among PLGA polymers of different GA:LA ratios even those with higher GA content. This is because of the amorphous nature of PLGA 50:50. At 50:50 GA:LA ratio the PLGA polymer possesses least crystallinity in its structure and more prone to hydrolysis and degradation than other PLGA polymers with higher or lower GA:LA ratios.

PLGA particles are biodegradable in the body since in the presence of water they undergo hydrolysis of their ester linkages leading to two metabolite monomers: LA and GA, which, under normal physiological conditions, are byproducts of several metabolic pathways in human body [24]. The degradation rate for PLGA polymer depends on the monomer ratio. The degradation products (LA and GA) are endogenous and easily metabolized by the body via the Krebs cycle, and are eliminated. It leads to very minimal systemic toxicity related with using PLGA for drug delivery or biomaterial applications. According to a review by Athanasiou et al., many in vitro and in vivo studies associated with the toxicity/biocompatibility demonstrated that PLGA biomaterials show absence of significant toxicity and satisfactory biocompatibility [25]. In vivo studies investigated applications in articular cartilage, bone and meniscus. A mentionable number of studies had been carried out in situ in some soft tissues and

muscle. The results of all those studies supported the in vivo application of PLA-PGA biomaterials, although some cases showed inflammatory responses [24,25]. Biodistribution studies demonstrate that delivery by PLGA NP enhances accumulation of therapeutic/diagnostic agents by the enhanced permeability and retention effect [24].

PLGA is soluble in a wide range of common solvents including acetone, chlorinated solvents, tetrahydofuran, ethyl acetate, etc. The glass transition temperature (Tg) of PLGA copolymers are higher than the physiological temperature, hence they are glassy in nature. Thus, their chain structure is fairly rigid, which gives them good mechanical strength to be used for the formulation of drug delivery devices. PLGA polymer goes through bulk erosion during its degradation. The degradation bulk erosion model of release is considered advantageous in vaccine delivery, since it hinders the early release of large adjuvants or antigens from the delivery system before the particle is taken up by dendritic cells and reduces the systemic distribution of encapsulated molecules.

2.6 Magnetic nanoparticles (MNPs)

NPs show physical and chemical properties that differ from the characteristic of their atom and the bulk counterparts. MNPs have large surface area that dramatically changes some of the magnetic properties. Each MNP can be considered as a single domain, which is the reason why MNPs can exhibit superparamagnetic property and quantum tunneling of magnetization. Superparamagnetism is a type of magnetism observed in small ferromagnetic or ferrimagnetic NPs. Superparamagnetism is especially important in applications like MRI or drug delivery, where NPs exhibit no magnetic properties upon removal of the external field and therefore possess no attraction for each other eliminating the major driving force for aggregation. More importantly, superparamagnetic NPs show better control over the application of their magnetic properties since they are capable to provide strong response to an external magnetic field.

To date, iron oxide particles such as magnetite (Fe_3O_4) or maghemite (γ -Fe_2O_3) are by far the most commonly employed for clinical use, although nickel, cobalt, neodymium–iron–boron, etc. are also magnetically responsive materials. This is because magnetite and maghemite may be nontoxic, show good chemical stability, biological compatibility, and relatively ease of manufacture. Nickel and cobalt are

highly magnetic materials, but they are both toxic and susceptible to oxidation and hence are of little interest [26].

Size can strongly influence properties of MNPs. As shown in Fig. 2 [27], size of NPs defines the NP regime and hence magnetic behavior of that NP. With the decrease in size of the MNP, the magnetic anisotropy energy per NP decreases. Magnetic anisotropy energy is the energy needs to keep the magnetic moment in a particular orientation. The anisotropy energy becomes equal to the thermal energy at a characteristic size for each type of MNP allowing random flipping of the magnetic moment. The flipping is observed at sizes below r_o (transition point from superparamagnetic to single domain), and the nanoparticle is then defined as being superparamagnetic [28].

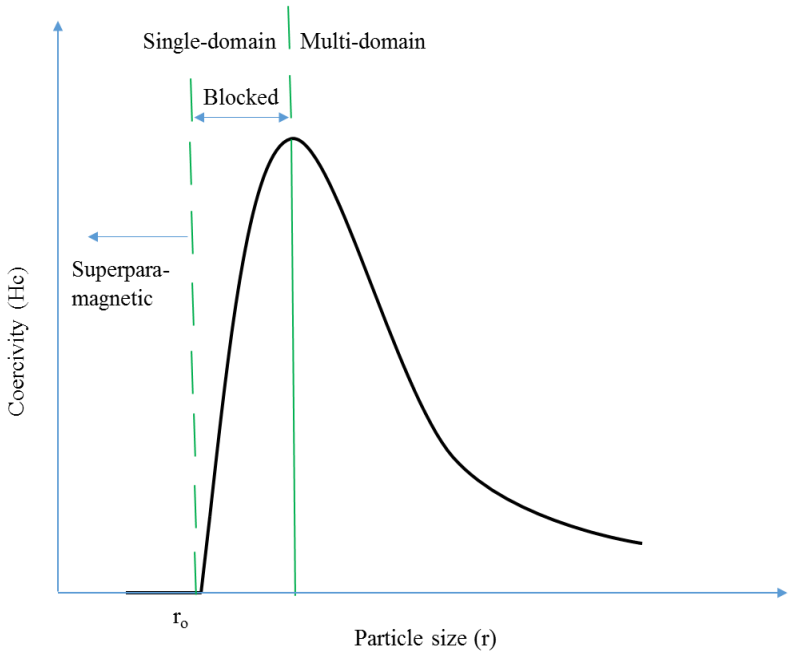

Fig. 2: Relationship between size and coercivity for MNPs.

Generally saturation magnetization (Ms) increases linearly with size until it reaches the bulk value. Above a certain size (typically 5-40 nm) known as critical particle diameter (Dc), nanoparticles become multi-domain instead of single domain. Multi-domain nanoparticles show bulk magnetism, become either ferro/ferri or antiferromagnetic. Iron nanoparticles in the size range below 20 nm are superparamagnetic (range of 10–20 nm).

Above a temperature called blocking temperature (T_B), both ferromagnetic and ferrimagnetic NPs exhibit superparamagnetic behavior. A blocking temperature T_B can be defined as the temperature between the blocked and the superparamagnetic state. Blocking temperatures rapidly increase with particle size as can be seen from the following equation [28]:

$$T_B = KV/25k_B = K(4\pi r_o^3/3)/25k_B$$

where k_B is the Boltzmann constant, K is an anisotropy constant, V is the volume of one MNP and r_o is the MNP radius.

During nanoparticle synthesis, if the MNP size is maintained below a critical volume/size, the MNPs tend to develop as single magnetic domain structures and at the smallest sizes, NPs exhibit superparamagnetic behavior under standard conditions.

Increasing size of MNPs would undoubtedly aid attraction to external magnets. Generally, larger particles possess shorter plasma half-life and cleared from the body quickly, whereas smaller nanoparticles (smaller than 10 nm) are subjected to rapid renal elimination. Though the smaller the magnetic carrier, the higher the efficiency of cell uptake. MNPs smaller than 4 μm are removed by the RES, mainly in the liver (60–90%) and spleen (3–10%) [29]. Spleen usually filters MNPs larger than 200 nm. MNPs up to 100 nm are mainly phagocytosed by liver cells [29].

Drug loaded magnetic nanoparticles target the liver cells, since iron oxide is accumulated in the liver. Jia et al. found higher antitumor activity for doxorubicin (DOX) drugs in comparison to free DOX when co-encapsulated with magnetite inside PLGA [30]. In the presence of magnetic field, the antitumor activity of the DOX-MNPs was higher also. Akbarzadeh et al., studied cytotoxicity of DOX loaded magnetic PLGA-poly (ethylene glycol) (PEG) using magnetite and found from the in vitro cytotoxicity test that the Fe_3O_4 had no cytotoxicity and were biocompatible [31].

2.6.1 Surface modification of magnetic nanoparticles

In the absence of any surface coating, magnetic iron oxide NPs have a large surface-to-volume ratio possessing high surface energies. As a result, they tend to aggregate so as to minimize the surface energies. Additionally, uncoated iron oxide NPs show high chemical activity, and oxidized easily in air (especially magnetite), generally causing loss of magnetism and dispersibility [32].

Magnetic iron oxide NPs have hydrophobic surfaces and agglomerate to form large clusters resulting in increased particle size due to hydrophobic interactions between the NPs. Clusters of MNPs possess strong magnetic dipole–dipole attractions between them and exhibit ferromagnetic behavior. Type and geometric arrangement of surface coatings on the NPs determine the overall size of the colloid and play a significant role in the biokinetics and the biodistribution of NPs in the body [32].

Generally, the types of specific coatings for these MNPs depend on the end application, and should be chosen by keeping the intended application in mind.

The coated surfaces are suitable for further functionalization by the attachment of various bioactive molecules. Although MNPs are considered biodegradable, the iron in MNPs can be reused/recycled by cells using normal biochemical pathways for iron metabolism. Such recycling of iron may evoke adverse effects on homeostasis, causing damage to critical cells in the heart, liver and other metabolically active organs [33]. Modification of surface can also decrease these side effects by avoiding exposure and preventing the leaching of magnetic cores and facilitating intact excretion of MNPs through the kidney [33].

Surface modification with polymers can significantly increase the half-life of MNPs by retarding RES clearance. Opsonization involving opsonin binding is a major step in the phagocytosis process of MNPs. To avoid opsonization of MNPs, both non-biodegradable and biodegradable inorganic and organic coatings are used to retard detection and uptake by macrophages. MNPs can be coated with organic stabilizers (e.g. oleic acid), polymeric stabilizers (e.g. PVA, PEG) and with inorganic molecules (e.g. silica, gold).

2.6.2 Applications of MNPs

Most promising use of colloidal MNPs is in drug delivery to carry drugs to specific site for site-specific delivery of drugs. Ideally, MNPs are capable to bear pharmaceutical drug on their surface or in their bulk that can be driven to organ of target and released there. They can also be co-encapsulated with drug molecules inside a matrix and can be administered for targeting specific sites. For drug delivery application, the charge, the surface chemistry of the MNPs and most importantly the size strongly affect both the bioavailability of the NPs within the body and the blood circulation time. Both larger and smaller particles are removed from the circulation system very quickly and not useful for drug delivery purpose. Particles in the range of ca. 10 to 100 nm are optimal for intravenous administration and exhibits most prolonged blood circulation time. NPs in this range of size are small enough not only to evade RES of the body, but also capable of penetrating very small capillaries within the body tissues. As a result, they can offer the most effective distribution in specific tissues. Ex vivo experiments on the toxicity of magnetite-loaded polymeric particles or magnetite have demonstrated that

the former one has rather low cytotoxicity, and magnetite itself has many adverse effects. Nevertheless, particle size must be considered very strongly, because any fraction greater than 5 μm can cause capillary blockade, and must be avoided [34].

Superparamagnetic iron oxide (SPIO) NPs are extensively used as MRI contrast agents, to better differentiate pathological and healthy tissues. These contrast agents find particular application for imaging organs associated with RES (e.g. spleen, liver), which is where SPIO NPs tend to be amassed quickly after intravenous administration. The ultra small SPIO NPs show the tendency to accumulate in the lymph nodes and are used as contrast agent for MR-based lymphography. Cell tracking by iron oxide NP based MRI is now getting popular, and is very useful tool in the field of biomedicine.

2.6.3 Toxicity of MNPs

There are several reports indicating the potential toxicity of MNPs. Iron is an innate metal and essential for life, mainly because of its ability to donate and accept electrons readily by switching between ferrous (Fe^{2+}) and ferric (Fe^{3+}) ions. This oxidation-reduction reaction plays crucial role in energy production and in many important metabolic pathways. The total amount of iron in the body is strictly regulated, because excess iron can be very toxic.

High levels of free iron ions resulted from MNPs will cause an imbalance in body homeostasis leading to aberrant cellular responses including oxidative stress, DNA damage, epigenetic events, and inflammatory processes [33]. Many researchers have reported probable toxicity because of overloaded iron and several conditions that affect toxicity of MNPs. One of them is mitochondrial activity, because the toxic mechanism of iron is evident from the generation of reactive oxygen species (ROS). As a result, organs having highly active mitochondria such as liver, heart, and pancreatic beta cells are vulnerable to iron toxicity. Gender and age can also affect the degree of iron toxicity due to different normal serum ferritin ranges (6–155 mg/ml for women and 15–320 mg/ml for men). Age-related macular degeneration (AMD), Alzheimer's disease and atherosclerosis are accelerated by excess iron. Hence, for practical application of MNPs, strategies to avoid possible toxic effects of therapeutics involving MNPs should be developed and focus can be given to the use of lower quantity of MNPs.

2.7 Drug Release

The release profile of drugs from NPs depends on both the physicochemical nature of the encapsulated drug molecules and the type of matrix material. Mode of the drug attachment and/or encapsulation (e.g. covalent conjugation, surface adsorption, dispersion homogeneity of drug molecules in the polymer matrix), matrix hydration and/or degradation controlling parameters, and the physical state of the drug within the matrix (such as crystal form) are the factors that affect the release profile.

Drug release from biodegradable polymers occurs in one of the two ways: erosion and diffusion. In vivo release from biodegradable polymers is generally governed by a combination of both erosion and diffusion mechanisms, which depend on the relative rates of them. Erosion is the physical dissolution of a polymeric material due to its degradation. Most of the biodegradable polymers used for drug delivery are degraded by hydrolysis (reaction between typically ester bonds in the polymer backbone and water molecules, which repeatedly cuts the polymer chain until it is returned to monomers). Other biodegradable polymers degrade enzymatically, which also takes place by chain scission. Upon the breakage of chemical bonds along the polymer chain by water molecules, the physical integrity of the polymer degrades allowing the release of the drug. There are two possible mechanisms of erosion. First one is the confinement of water to the matrix surface, as in the case of a hydrophobic polymer chain scission is limited only on the surface. Hence, the drug will be released due to the erosion of the polymer matrix. On the other hand, if the water penetrates the polymer matrix faster than it hydrolyzes the bonds on the surface, erosion will take place throughout the entire material (also known as bulk erosion). In many cases, in vivo erosion of a polymer matrix is some combination of these mechanisms. Degradation by surface erosion alone is preferred in many cases, since the rate of degradation can be controlled through the surface area of the matrix.

For diffusion-controlled release, concentration gradient of drug inside the polymer matrix is the driving force for drug molecules to diffuse out into the surrounding medium. The diffusion of any drug molecule through the polymer matrix depends on several factors like the molecular weight of the drug, the solubility of the drug in the polymer matrix and the surrounding medium, the diffusion coefficient of the drug molecule, the distance necessary for diffusion, its concentration throughout the polymer matrix, etc. Drugs can be either evenly distributed throughout the polymer

matrix or they can be encapsulated as a reservoir. For the reservoir system, the release rate also depends on the membrane area and thickness. Practically, a lag period is often observed for reservoir system after placement in vivo, and burst release is present in most other systems. When a drug is dissolved in the matrix and released by diffusion mechanism, the driving force for the release is the concentration gradient and the release can be predicted based on Fick's laws of diffusion. Cumulative release from diffusion-controlled matrix devices is inversely proportional to the square root of time [35]. This presents an engineering challenge since smaller surface area resulted from the degradation decreases the release rate.

2.8 Microencapsulation of interferon alpha by PLGA

Development of drug carriers for the delivery of drug in a bio-available and safe manner to targeted sites is now becoming an exceedingly important area of biopharmaceutical researches. As a result of vast number of researches carried out by researchers all over the world, various effective drug delivery technologies with significant outcomes have been reported. Among various available biodegradable polymers, PLGA is most popular due to its favorable degradation characteristics, long clinical experience and possibilities for sustained drug delivery [36]. PLGA has been extensively studied in the literature to illustrate the delivery of large number of various drugs, proteins, peptides, gene, etc. Among various drugs, different types of interferons (natural, synthetic, interferon-α, interferon-γ, etc.) have been investigated by many researchers. To the best of our knowledge, until now no study has been carried out to prepare nanoparticles co-encapsulating natural interferon-α and magnetite for targeted delivery using PLGA. Below, results of similar studies are shown by emphasizing that none of them investigated the entrapment of natural interferon-α along with magnetite inside NPs.

Zhou et al. encapsulated IFN-α loaded magnetic PLA and PLGA microspheres (MPs) with mean size of 2.5 μm [37]. The microparticles were prepared by modified solvent evaporation method.

Yang et al., studied IFN-α loaded PLGA MPs varying the concentrations (5%, 10%, 15%, 20% and 25%) and the viscosities (0.39, 0.6, 0.89 and 1.13 dL/g) of PLGA using double emulsion solvent evaporation method without magnetic particles [3]. Nine groups of rats were injected intramuscularly with three doses (0.5, 1 and 2 MIU) of

commercial lyophilized IFN-α-2b injection or IFN-α-2b MPs. The author found that their IFN-α-2b MPs containing 15% of 0.89 dL/g PLGA provided a sustained drug effect for up to 21 days in rats.

In another study, Yang et al., prepared IFN-α loaded PLGA MPs by a double emulsion solvent evaporation method. Characteristics, such as morphology, drug loading, encapsulation efficiency, in vitro release and degradation of IFN-α loaded PLGA NPs were investigated. The IFN-α MPs were prepared by using PLGA of different viscosities (0.17–1.13 dL g^{-1}) ([dl/g]: inherent viscosity, 0.1% in $CHCl_3$, 25ºC) and concentrations (between 5–25%), which not only affected the drug loading and encapsulation efficiency of IFN-α microspheres, but also strongly influenced the in vitro release. With smooth and porous surface, the drug loading and encapsulation efficiency of the MPs prepared by 15% 0.89 dL g^{-1} PLGA were 7.736% and 77.38%, respectively. The degradation of MPs was homogeneous and the mass loss was over 80% in 6 weeks. The release profile of microspheres showed a sustained fashion and the IFN-α released from MPs maintained its bioactivity for 7 days [38]. Similar studies were carried out by Zhang et al. [39] and Diwan et al. [40]. Zhang et al. investigated pharmacokinetic-pharmacodynamic properties of IFN-α-2b-loaded PLGA MPs (average diameters were 46, 81, and 110 μm for three different viscosities 0.39, 0.89, and 1.13 dL/g, respectively) in rhesus monkey primates [39]. MPs were able to improve the pharmacodynamic and pharmacokinetic features of IFN-α-2b, maintain longer biological effects and effectively increase the residence time in the rhesus monkey. Study carried out by Diwan et al., showed that pegylated IFN-α is able to retain its native aqueous solubility in comparison to native IFN-α after being exposed to detrimental conditions of microencapsulation which resulted in a continuous release in vitro [40]. The author suggested that a long-acting dosage form for IFN-α can be prepared using a combination of pegylation and microencapsulation techniques.

All the studies explained above dealt with microspheres. Sánchez et al. [41] studied PLGA micro and nanoparticles (size ranging from 280 nm to 40 μm) containing IFN-α co-encapsulated with stabilizer poloxamer and HSA prepared by double emulsion technique, which comply with our study. Use of PVA generally offers lower particle size than poloxamer. In 2011, Giri et al. studied PLGA nanoparticles for IFN-α delivery targeted to hepatocytes [42]. The author claimed that their novel formulation of nanoparticles has potential application in hepatic-targeted drug delivery. The purpose of

that study was to develop hepatitis B surface antigen (HBsAg) surface-adsorbed cationic PLGA nanoparticles.

2.9 Surface modification of PLGA particles

The plasma proteins of our body are being adsorbed on exogenous particles, which is very significant part of defense mechanism of the human body. Due to the quick detection of drug loaded particles by macrophages, they are engulfed and removed quickly from the bloodstream. Hence, they cannot reach the target site(s) or don't get sufficient time to release the drug, which will lead no effect of medication. Tri-block copolymer poloxamers are successfully employed for reducing adsorption of proteinous molecules onto hydrophobic surfaces, which will protect them from quick engulfing and give them prolonged life time [43]. The poly(propylene oxide) (PPO) blocks of poloxamers are capable of attaching the hydrophobic polymeric surfaces and the poly(ethylene oxide) (PEO) blocks are extended outside the surface of hydrophobic polymeric carriers, transforming the surface of drug loaded hydrophobic NPs to hydrophilic to make them stealth. As a result, the MPS fails to recognize the particles due to their hydrophilic nature.

Poloxamer is able to totally inhibit protein adsorption onto the PLGA microsphere and can show continuous release of drugs without any burst effect as found by Paillard-Giteau et al., [44]. Continuous release of lysozyme over 3 weeks without any burst effect was observed for PLGA microspheres due to Poloxamer 188 treatment. After 3 weeks, a plateau was reached due to additional destabilizing mechanisms concomitant with polymer degradation. Poloxamer coating is capable to generate higher residence time in the plasma than uncoated NPs. Fluorescently labelled PLGA particles coated with PEG and Pluronic F127 (one type of poloxamer) had higher plasma concentration than the uncoated ones while used in oral formulations [45]. PLGA carriers without poloxamer (Pluronics F127) coating were detected in the brain, heart, liver, spleen, lungs and kidneys over a period of 7 days. In the plasma, no particles were detected for 0.5% Pluronics F127 coating over the 3 days [45]. Sánchez et al. [41] observed release of IFN-α up to 96 days for PLGA/poloxamer blend microspheres.

Poloxamer coating even can assist PLGA NPs in crossing blood brain barrier (BBB). Loperamide, an opioid drug cannot cross the BBB, although effective as antinociceptive if injected directly to the brain. P188-coated PLGA-PEG-PLGA (PEP)

NPs containing Loperamide showed 14.4 to 21.2% penetration, which was much higher than either with PLGA NPs (4.3%) or with PEP NPs (8.2%) [46]. The in vitro BBB permeation percentage of PEP obtained was 13.7 folds higher than just the loperamide solution.

3 MATERIALS AND METHODS

3.1 Materials

PLGA (50:50, M_w = 8,000, Resomer® RG 502H) containing free carboxyl end-groups was purchased from Boehringer Ingelheim, Germany. Model drug HSA (human serum albumin) solution, natural IFN-α solution and BSA (bovine serum albumin) were kind gifts from Trigon Biotechnological Ltd., Hungary. The concentration of HSA and IFN-α in the bulk solution used was 36.87 mg/ml and 0.213 μg/ml, respectively. Poly(vinyl alcohol) (PVA; M_w = 30,000–70,000), poloxamer (M_w = 8350, BASF, Ludwigshafen, Germany, Pluronic® F68) and phosphate-buffered saline (PBS, pH 7.4) were purchased from Sigma-Aldrich. Solvent dichloromethane (DCM) was obtained from VWR International (Hungary). Magnetite was synthesized by co-precipitation method described in section 4.2.1. Micro BCA (bicinchoninic acid) protein assay kit was purchased from Pierce Biotechnology, Inc. $FeCl_2 \cdot 4H_2O$ and $FeCl_3 \cdot 6H_2O$ were purchased from Fluka (Buchs, Switzerland). Sodium hypochlorite solution (NaClO) and sodium citrate dihydrate were purchased from Bochemie (Bohumín, Czech Republic) and Lachema (Brno, Czech Republic), respectively. Oleic acid was purchased from LachNer (Neratovice, Czech Republic). The ELISA (enzyme-linked immunosorbent assay) kit for specific evaluation of natural IFN-α was purchased from IBL International GmbH (Hamburg, Germany). Sodium azide and protease inhibitor (Pefabolc® SC) were purchased from Sigma-Aldrich and Boehringer Mannheim Ltd., respectively.

3.2 Methods

3.2.1 Synthesis of oleic acid-coated superparamagnetic iron oxide nanoparticles

Neat superparamagnetic nanoparticles were prepared by coprecipitation of $FeCl_2$ and $FeCl_3$ in aqueous ammonia solution by modification of an earlier published method [47]. Briefly, $FeCl_3 \cdot 6\ H_2O$ (24.32 g) and $FeCl_2 \cdot 4\ H_2O$ (11.92 g; molar ratio 2:1) were stirred at 400 rpm in distilled water (50 ml) under nitrogen atmosphere. To this solution, 28% NH_4OH solution (50 ml; 50% excess) was added over a period of 20–30 min. To

coat the nanoparticles, oleic acid (5 ml) was added to the reaction mixture at 90°C and the reaction proceeded for 5 h until the NH_3 odor disappeared. After cooling to room temperature, the Fe_3O_4 nanoparticles were washed with distilled water for 4 days (three times 200 ml a day) using separation by a magnet and decantation; they were then dried at 80°C. Finally, the Fe_3O_4 particles were resuspended under sonication in DCM to a concentration of 5.7 wt%. The size of magnetite obtained was 10 ± 5 nm.

3.2.2 Preparation of IFN-α (or model drug HSA) loaded magnetic PLGA NPs

Both model- (HSA) and active drug (natural IFN-α) loaded magnetic PLGA NPs were prepared by double emulsion solvent evaporation method [48,49]. Fig. 3 schematically shows the preparation of HSA loaded magnetic PLGA NPs. IFN-α loaded magnetic PLGA NPs were prepared in the same way, though IFN-α containing protein solution was used instead of HSA, and hence not described separately.

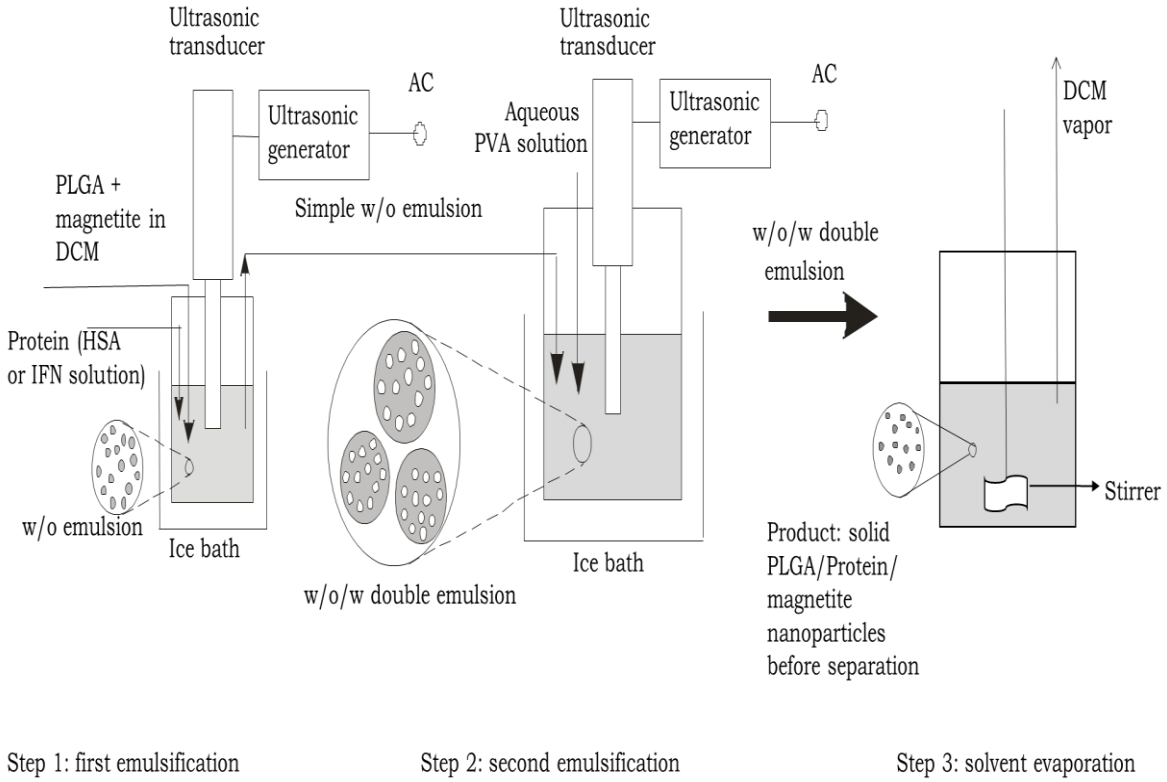

Fig. 3: Schematic diagram of the double emulsion solvent evaporation method applied for preparation of PLGA nanoparticles with encapsulated HSA (model drug) or IFN and Fe_3O_4 particles.

At first PLGA (0.05-0.2 g) was dissolved in DCM using blade stirrer. Fe_3O_4 (1 to 20% by weight related to the weight of PLGA) was added to the solution and sonicated with a Model W-220 probe sonicator (Heat Systems-Ultrasonics) for 30 s. The power of sonicator was 70 W, frequency 20 kHz. The total volume of DCM in the system was fixed at 5 ml. Then 0.5 ml model drug solution of preset concentration, diluted with PBS, was added to the system and the two-phase system was emulsified for 60 s using the same sonicator, which resulted in a W/O emulsion. This emulsion was dispersed in the outer water phase containing 2 wt% PVA (10-30 ml) using the same sonicator for 1-3 min to obtain W/O/W double emulsion. The DCM was evaporated to solidify PLGA NPs under continuous stirring (800 rpm) for 2 h using a blade stirrer. After the evaporation of DCM, dispersed solid PLGA NPs with encapsulated model drug and Fe_3O_4 were obtained and stored in a freezer for further experimental analysis. Utilization of an ultrasonic probe leads to an increase in bulk temperature. If the temperature is not controlled using ice bath, some undesired effects may occur. The most obvious is the degradation of compounds of interest. In addition, as the temperature is increased, the physical characteristics of the liquid media change in such a way that the ultrasonic transmission can be affected and no cavitation is achieved. This phenomenon is known as “decoupling” [50]. Therefore sonication process was always carried out in an ice bath.

3.2.3 Process parameters

Performing some preliminary tests, five process variables (factors F1–F5) have been found to influence mostly the hydrodynamic particle size and/or the encapsulation process. These five process variables were used to make an experimental design carried out by statistical software (section 3.2.4). These variables are the amount of iron oxide in the organic phase (F1) relative to the weight of PLGA used for encapsulation, concentration of PLGA in the organic phase (F2), concentration of HSA in the inner aqueous phase (F3), the outer aqueous/organic phase volume ratio (F4), and time of the ultrasonic treatment in the second emulsification (F5).

3.2.4 Experimental design

Experimental design is probably the best tool to quantify and understand how process variables interact with each other. In case of a complex process having many variables, change in one variable at a time is unable to discover whether there will be

cross effect(s) (or interaction of the independent variables) in that process. Application of various experimental designs is generally useful in developing a formulation, especially if the formulation is complex, and the process is dependent on many factors. Traditional approaches for process development are time consuming since one factor is generally varied at a time to examine its effect, which requires a large number of experimental runs. Without experimental design, more effort, time, and materials are needed when a complex formulation needs to be developed. Moreover, analysis of the results obtained after experimental design provides 3D diagrams from which change of variables in three dimensional space can be more clearly represented.

To elucidate the effect of process conditions on the mean hydrodynamic particle size and to decrease the number of the studied parameter combinations, and thus, the number of experiments, a $3^{(p-1)}$ type fractional factorial experimental design was carried out using STATISTICA® (version 10.0, StatSoft Inc., USA) software, where "p" is the number of factors (variables). The obtained experimental data were evaluated by statistical analysis, similarly to the method described by Feczkó et al. [51] for bovine serum albumin encapsulated in PLGA nanoparticles and Biró et al. [52] for chitosan microparticles.

Table 1 shows the value of studied range of process variables suggested by statistical design.

Table 1: Process variables (factors) in experimental design and their studied ranges.

Factor	Symbol	Variable	Studied intervals
F1	X_{Fe3O4}	Fe_3O_4/PLGA weight ratio	1-20 wt%
F2	X_{PLGA}	PLGA concentration in the organic phase	1-4 wt%
F3	X_{HSA}	HSA concentration in the inner aqueous phase	0.74-3.69 wt%
F4	X_{VOLR}	Outer aqueous (w_2)/organic phase (o) ratio volume ratio.	2-6 vol/vol
F5	X_{time}	Time of the ultrasonic treatment in the second emulsification	1-3 minutes

As a result of the experimental design (DOE), $3^{(5-1)}$ = 81 experiments were needed without repetitions due to variation of five variables. However, to estimate the pure error, 9 repetitions of experiments were also carried out. This resulted in 90 experiments altogether. For each variable 3 different levels (the lowest, mean and highest) were taken into consideration. The main advantage of applying experimental design was the vast reduction of the experimental work without remarkable loss of useful information. Without this, it would have been needed to perform 3^5 = 243 experiments. The experimental program determined by STATISTICA® (including the repetition) is shown in the first six columns of the table in the Appendix. From the table it is seen that repetitions were carried out at the central point of each variable intervals indicated by C with bold numbers. In the second last column of the table, the measured mean particle sizes are listed. In the last column of that table encapsulation efficiency of the model drug is listed.

3.2.5 Redispersion of PLGA NPs

Prepared NPs were redispersed either in distilled water or PBS or poloxamer solution based on intended experiment or analysis using probe sonicator after ultracentrifugation. For small volume (up to 5 ml), ultracentrifugation was carried out for 25 minutes at 10°C using the speed 50,000 rpm (Beckman Coulter Optima™ MAX-E ultracentrifuge, USA). For larger volume (more than 10 ml), different ultracentrifuge was used (Sorvall UltraCentrifuge by Hitachi) and the sample was subjected for 30 minutes at 10°C using the speed 40,000 rpm. Preliminary redispersion was done manually using pipette tips with intense care. After that, sonication with low amplitude was carried out for very short time, until big aggregates of NPs were broken down, which was observed visually by naked eyes. Special attention was given during sonication since longer sonication will generate heat and (model) drug might start to release from the particles. As a result, not only more porous particles might form, but also lower encapsulation efficiency can be obtained.

3.2.6 Surface modification of PLGA NPs

Aqueous solution of poloxamers (Pluronics F68, PF68) were used to treat PLGA surfaces. Poloxamer solutions of different concentrations (PF68 0.1, 0.25, 0.5, 0.75 and 1% wt/vol) were prepared by dissolving them in distilled water. At first NPs were ultracentrifuged (50,000 rpm, 30 min, 10°C), and then redispersed in different PF68

solutions. A fraction of PVA will remain associated with the nanoparticles despite repeated washing, because PVA forms an interconnected network with the polymer at the interface and cannot be removed from the surface of NPs completely [53]. After redispersion of NPs in PF68 solution, the solution was stirred for few hours, and kept overnight in the refrigerator to allow more time for poloxamers to adsorb on NPs.

3.2.7 Hydrodynamic size, electrophoretic mobility and zeta (ζ) potential measurements

Hydrodynamic size of the NPs were analyzed by dynamic light scattering (DLS) method (also called as photon correlation technique) using Zetasizer Nano ZS (Malvern Instruments, Malvern, UK) at 25°C. Electrophoretic mobility and zeta (ζ) potential measurements were also carried out using the same equipment at the same temperature. The Zetasizer system determines the hydrodynamic size of particles in colloids first by monitoring the Brownian motion of the particles in a sample using DLS, and then interpreting a size from this using established theories. Laser light source of Zetasizer Nano ZS illuminates the particles and analyzes the intensity fluctuations in the scattered light. For each sample, five parallel size measurements were carried out.

Electrophoretic mobility and ζ-potential are studied to determine the surface charge of the particles in colloids. The velocity of a particle in an applied electric field is generally referred to as its electrophoretic mobility. The Zetasizer Nano ZS determines the electrophoretic mobility first, and then calculates the zeta potential by applying the Henry-equation. An electrophoresis experiment is performed, and the velocity of the particles is measured using Laser Doppler Velocimetry (LDV) to obtain electrophoretic mobility. Zeta potential is an important tool for understanding the state of the particle surface, and predicting the stability of a colloidal system. For ζ-potential and electrophoretic mobility, number of parallel measurements was three.

3.2.8 Determination of encapsulation efficiency (EE%) for model drug and iron oxide

Encapsulation efficiency of model protein drug was determined by micro BCA protein assay indirectly. The amount of HSA encapsulated into the PLGA NPs was determined by analyzing the protein content in the supernatant (i.e. non-encapsulated fraction of the protein introduced). The resultant encapsulation efficiency (EE_{HSA}) was defined as the percentage of HSA model protein encapsulated into the PLGA

nanoparticles relative to the total amount of protein dissolved in the inner aqueous phase according to eqn. (1):

$$EE_{HSA} = \frac{m_{HSA\,encaps}}{m_{HSA_{\text{int}}}} \times 100\% \qquad (1)$$

In micro BCA protein assay, peptide bonds in protein reduce cupric (Cu^{2+}) to cuprous ions (Cu^{+}). Two molecules of bicinchoninic acid chelate with each Cu^{+} ion, forming a purple-colored product that strongly absorbs light at a wavelength of 562 nm, and is analyzed spectrophotometrically [54]. The amount of Cu^{2+} reduced is proportional to the amount of protein present in the solution.

Encapsulation efficiency of iron oxide in the PLGA NPs was determined after separation of non-encapsulated iron oxide from the particles. At first, suspension of magnetic PLGA particles was centrifuged at 30,000 rpm for 30 min using a Beckman Optima Max-E ultracentrifuge (Brea, USA) to remove PVA solution partly stabilizing the non-encapsulated iron oxide. The magnetic PLGA particles were then resuspended in distilled water, whilst the aggregated iron oxide nanoparticles remained in the precipitate, since they were not stabilized anymore. After removal of the supernatant, the iron oxide content was determined in the precipitate by a colorimetric method using Prussian Blue staining [55]. The iron oxide was dissolved by 6M HCl, the resulting Fe^{3+} solution was diluted with 1% HCl and reacted with equal amount of 1% potassium ferrocyanide solution producing a deep blue color. The absorbance was measured after 15 min by a UV-VIS spectrophotometer at 700 nm. Calibration was done with a stock solution of iron(III) oxide powder, 99.998% of purity.

3.2.9 Morphology of NPs

Nanoparticle morphology was characterized by transmission electron microscopy (TEM) and scanning electron microscopy (SEM), using a Tecnai Spirit G2 transmission electron microscope (FEI, USA) and a Quanta S200 scanning electron microscope (FEI, USA).

3.2.10 Process Optimization

From economic point of view, the efficiency of encapsulation is extremely important, especially when the active agent is very expensive. In certain applications, such as production of injectable drug formulations, the smallest possible particle size

with highest potential encapsulation efficiency must be achieved, which obviously depends on the process variables. Although encapsulation efficiency is generally higher for larger nanoparticles, they are detected and eliminated by macrophages easily and on the other hand, their sterilization after production is difficult. Due to the high number of variables, it was necessary to determine the optimum process conditions mathematically to achieve higher model drug loading with the smallest PLGA capsules. For this purpose the GAMS™/MINOS Large Scale Nonlinear Solver for Windows Ver. 5.51 (System Optimisation Laboratory, Stanford University) software was applied, which suggested the optimum process conditions by precise mathematical tools.

3.2.11 Protein adsorption studies

IFN-α loaded magnetic PLGA NPs may be quickly covered by plasma proteins after intravenous administration and macrophages can detect and engulf them leading to their removal from the bloodstream. The surface modification by PF68 makes the PLGA NP surfaces able to evade macrophages by reducing plasma protein adsorption. To investigate the effectiveness of PF68 coating to reduce plasma protein adsorption on the prepared PLGA NPs, bovine serum albumin (BSA) adsorption was monitored on both surface modified and unmodified PLGA NPs.

BSA was dissolved in distilled water and then added to both unmodified and modified samples. Before the addition of BSA, both types of NPs, respectively were redispersed in distilled water. 5 ml portions of NP suspension (1.19 mg/ml PLGA) was mixed with 4 ml BSA solution (0.1 mg/ml) for 2 h using magnetic stirrer. The obtained solution was then kept overnight in the refrigerator to allow more time for protein to adsorb on NPs. After ultracentrifugation (50,000 rpm, 30 min, 10°C), the degree of adsorption was determined indirectly by analyzing the non-adsorbed portion with UV/VIS spectrometry using micro BCA protein assay kit at the wavelength of 562 nm. The adsorption was also examined by measuring and comparing the size and the zeta potential of the modified and unmodified NPs before and after BSA adsorption by Zetasizer Nano ZS.

Finally, an isothermal titration calorimeter VP-ITC (MicroCal, Northampton, MA, USA) was applied to investigate the protein adsorption. The concentrations of NPs and BSA were 1.19 mg/ml (wt/vol) and 10 mg/ml (wt/vol), respectively. Modified or unmodified samples and BSA were dialyzed against PBS at 4°C, thoroughly degassed

by stirring under vacuum before sampling for the titration. 200 µl suspension of modified and unmodified PLGA NPs, respectively, were loaded into the titration cell, and 280 µl BSA was loaded in the injection syringe from which 20 µl was introduced to the titration cell during every injection. The temperature of the titration cell was fixed at 25°C. Single injection method (SIM) was also applied for both modified and unmodified PLGA NPs to confirm the result obtained by multiple injections. Data were analyzed by MicroCal Origin software.

3.2.12 In vitro IFN-α release

In vitro IFN-α release from magnetic PLGA NPs was determined by enzyme-linked immunosorbent assay (ELISA). ELISA is widely used as diagnostic tool in medicine and in various industries as quality control measure. It is also used as analytical tool in biomedical research for both detection and quantification of specific antigens or antibodies in a given sample.

Samples for analysis were prepared inside sterile box. Distilled water after sterilization was used. All the apparatus were sterilized prior to use. An autoclave (Sanyo Labo Autoclave MCS-3780, Japan) was used for sterilization maintaining a temperature of 121°C. The release study was carried out using an incubator (New Brunswick Scientific, USA) maintaining a constant temperature of 37°C with continuous gentle shaking (rpm 200). Both modified and unmodified particles were redispersed in PBS. Sodium azide (0.03% wt/vol) and protease inhibitor (0.25 mg/ml PBS) were added to the system. Sodium azide can prevent bacterial growth and protease inhibitor prevents proteolytic cleavage of proteins. Samples were collected after specific time intervals (1 h, 2 h, 4 h, 6 h, 1 day, 2 days, 4 days and 7 days), ultracentrifuged for 25 minutes at 10°C using the speed 25,000 rpm (Beckman Coulter Optima^{TM} MAX-E ultracentrifuge, USA) and then the supernatants were stored in a freezer. Prior to ELISA test, the frozen samples were kept at room temperature until complete melting.

Microwells with adsorbed anti-human IFN-α coating antibody were used for ELISA test. Upon addition of the samples to the microwells, IFN-α present in the sample binds to the antibodies. Then, HRP-conjugate (horseradish peroxidase) is added, which binds to IFN-α captured by the first antibody. Substrate solution reactive with HRP is added to the wells, and a colored product is formed, which is proportional to the amount of human IFN-α present in the sample, and is measured at 450 nm using ELISA reader (Multiskan MCC/340 Microplate Reader). A standard curve is prepared from 7

human IFN-α standard dilutions (7.8 pg/ml to 500 pg/ml), and human IFN-α concentration determined.

4 RESULTS AND DISCUSSIONS

Saturation magnetization (Ms) of pure magnetite was 45 emu/g which comply with the result obtained by Sun et al. [56]. The author studied Ms values of Fe_3O_4 nanoparticles and found that Ms values for Fe_3O_4 NPs increase from 41.60 to 49.24 emu/g when the sizes of magnetite increase from 8 to 20 nm. The maximal encapsulation efficiency of iron oxide (X_{Fe3O4}=1.0% wt/wt) was 99.6 %. Optimum process condition selected for the preparation of NPs for surface modification and release studies involved 1% wt/wt Fe_3O_4 (section 4.5, Table 4).

After preparing magnetic PLGA NPs by double emulsion solvent evaporation method, particles were characterized.

4.1 Morphology of HSA loaded magnetic PLGA NPs

SEM image shown in Fig. 4a reveals that prepared NPs are spherical as was expected.

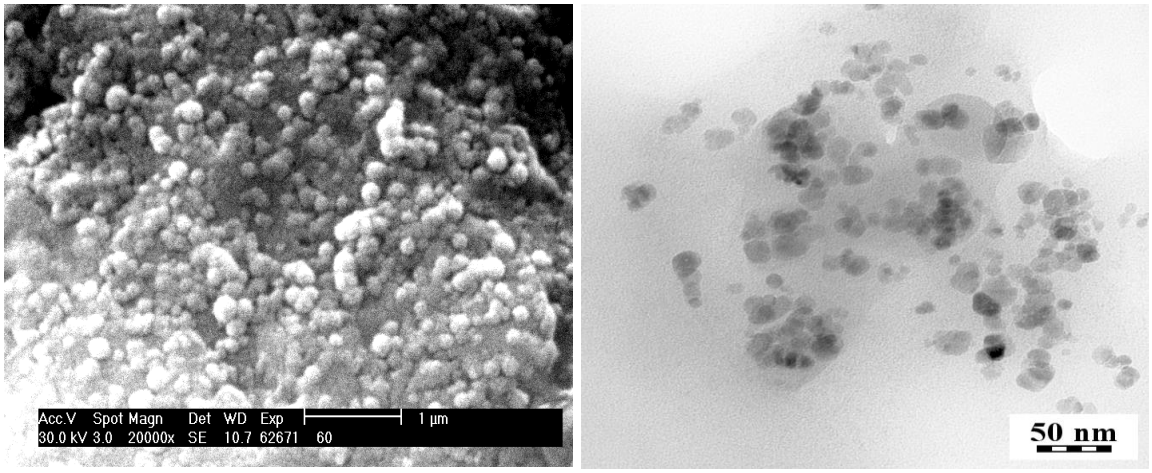

Fig. 4: (a) SEM and (b) TEM micrographs of HSA-loaded magnetic PLGA NPs.

In order to get a better contrast compared to SEM image and to confirm encapsulation of Fe_3O_4 in the polymer, HSA-loaded magnetic PLGA particles were viewed also by TEM (Fig. 4b). Fig. 4b shows that aggregates of oleic acid-coated Fe_3O_4 nanoparticles were dispersed inside the PLGA particles.

4.2 Hydrodynamic size and size distribution

The influencing variables were systematically changed according to the research plan determined by the scheme obtained from the DOE. During this study, the measured size distributions and mean hydrodynamic particle sizes showed characteristic variations depending on the values of independent variables applied in the different experiments. Fig. 5 shows typical particle size distributions selected from the 90 experiments, with various resulted size ranges corresponding to relatively low, medium and high mean particle sizes. It is seen that the studied process variables, such as PLGA concentration in the intermediate organic phase, or the time of the second sonication influenced strongly the obtained size distribution and the mean particle size. For example, low PLGA concentration and long sonication time resulted in smaller mean particle sizes, while high PLGA concentration and short ultrasound treatment during the second emulsification gave larger particle sizes. These diagrams show smooth and quite regular curves similar to the usual lognormal distribution. The dependence of the mean hydrodynamic particle size on the process parameters offers good opportunity for optimization. Therefore, statistical evaluation on the effects of different variables and process optimization has been carried out for this purpose.

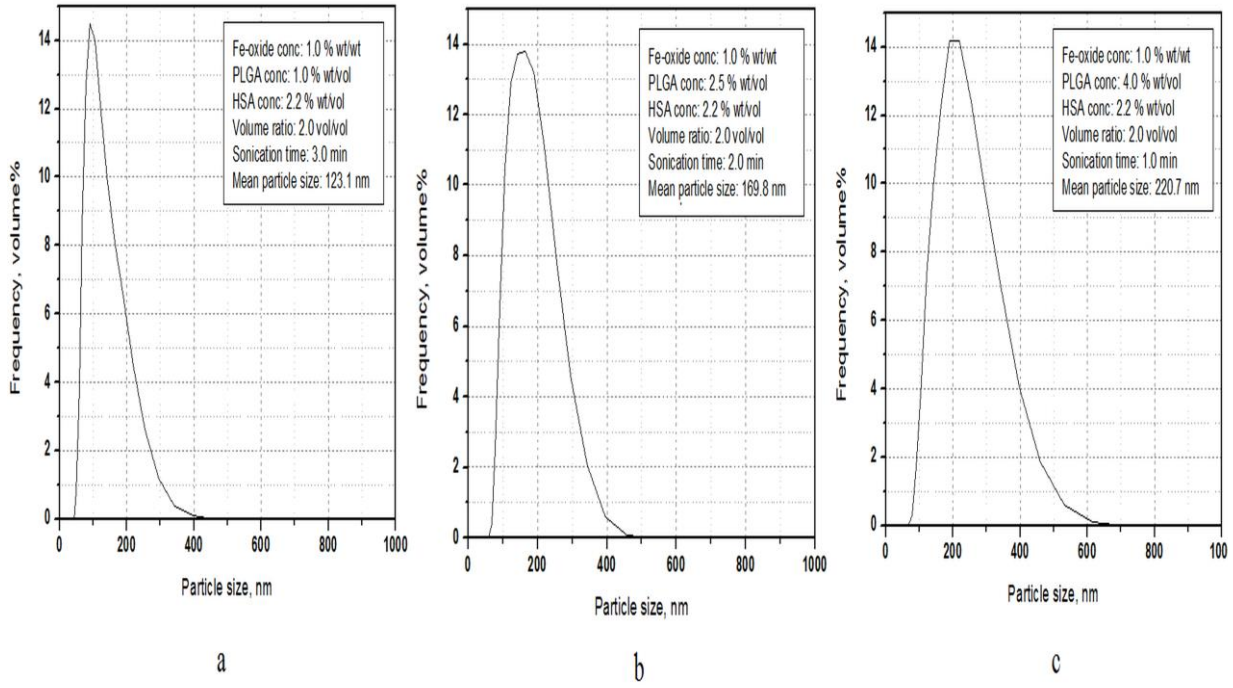

Fig. 5: Typical size distributions of the PLGA nanoparticles obtained with different process variables: a – small, b – medium, and c – relatively high size region.

As a result of the statistical analysis, the significance and importance of the studied variables influencing the mean hydrodynamic particle size were characterized by ANOVA table (Table 2) and Pareto chart of the standardized effects. From Table 2 it is seen that four factors F1, F2, F4 and F5 (i.e. the relative amount of magnetite, the PLGA concentration, the external aqueous/intermediate organic phase volume ratio, and sonication time, respectively), and the interaction of factors F1 and F4 show statistically significant influences, all of them having much lower *p* values than the widely accepted significance level ($p = 0.05$). Table 2 also shows that the mean square of residuals (MS) was 762.37 nm^2, i.e. the mean deviation between the measured and estimated mean particle sizes is $\sqrt{762.37} = 27.6$ nm, which was considered acceptable. The histogram of residual values showed almost normal distribution. Therefore, the estimation made by the multivariable regression was accepted. The pure error of experimental data determined from the 9 repeated runs was $\sqrt{181.3} = 13.5$ nm, which provides reasonable accuracy.

Table 2: Result of statistical analysis on the dependence of the measured mean particle sizes as a function of the influencing factors (ANOVA table).

Factor	ANOVA; Var.:Mean particle size, nm 5 3-level factors, 90 Runs; MS Residual=762.4 Mean error=27.6 nm				
	SS	df	MS	F	p
F1 Fe_3O_4 conc. (L)	12343.9	1	12343.89	16.19139	0.000125
F2 PLGA conc. (L)	31447.1	1	31447.08	41.24891	0.000000
F4 Volume ratio W_2/O (L)	4183.7	1	4183.68	5.48771	0.021516
F5 Time of sonication, min (L)	18699.7	1	18699.73	24.52829	0.000004
interaction F1L by F4L	7898.1	1	7898.09	10.35987	0.001831
Error	64039.4	84	762.37		
Total SS	138611.9	89			

The Pareto chart (Fig. 6) shows that mean hydrodynamic size was affected most strongly by PLGA concentration (F2) followed by the duration of ultrasonic treatment (F5). Iron oxide/PLGA weight ratio (F1), volume ratio (F4), and the linear-linear interaction of the latter factors (F1L×F4L) also played significant roles. Letter "L" on the scale of the diagram refers to the linear correlation between the given variable and the dependent variable (the mean hydrodynamic particle size). Among the studied five variables, the concentration of HSA in the inner aqueous phase (F3) has no significant influence on the particle size, although this variable affected encapsulation efficiency strongly as can be found in section 4.3.

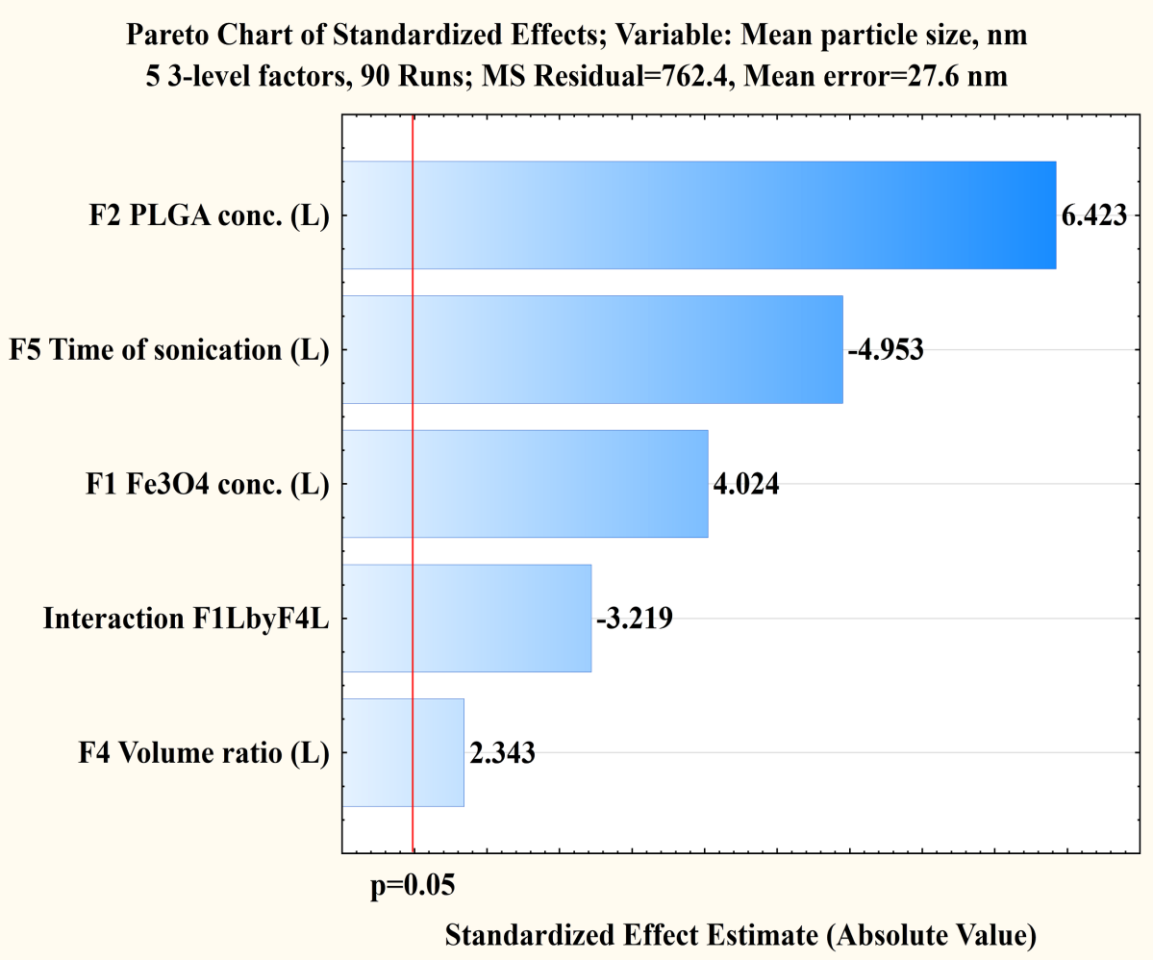

Fig. 6: Pareto chart on the standardized effects of the independent process variables on the mean hydrodynamic particle size.

As a result of the statistical analysis, a regression equation was obtained by which the dependence of the mean hydrodynamic particle size D_{mean} can be estimated for various combinations of the studied independent variables:

$$D_{mean} = 4.7097 \cdot X_{Fe3O4} + 16.088 \cdot X_{PLGA} + 12.5864 \cdot X_{VOLR} - 18.6089 \cdot X_{time} - 0.7796 \cdot X_{Fe3O4} \cdot X_{VOLR} + 143.667 \quad (2)$$

4.2.1 Effect of Fe_3O_4/PLGA weight ratio

As can be seen from the 3D diagram of Fig. 7, the increase in the relative amount of the Fe_3O_4 nanoparticles (relative to the weight of PLGA) dispersed in the intermediate organic phase (DCM), caused considerable increase in the mean particle size of the final NPs.

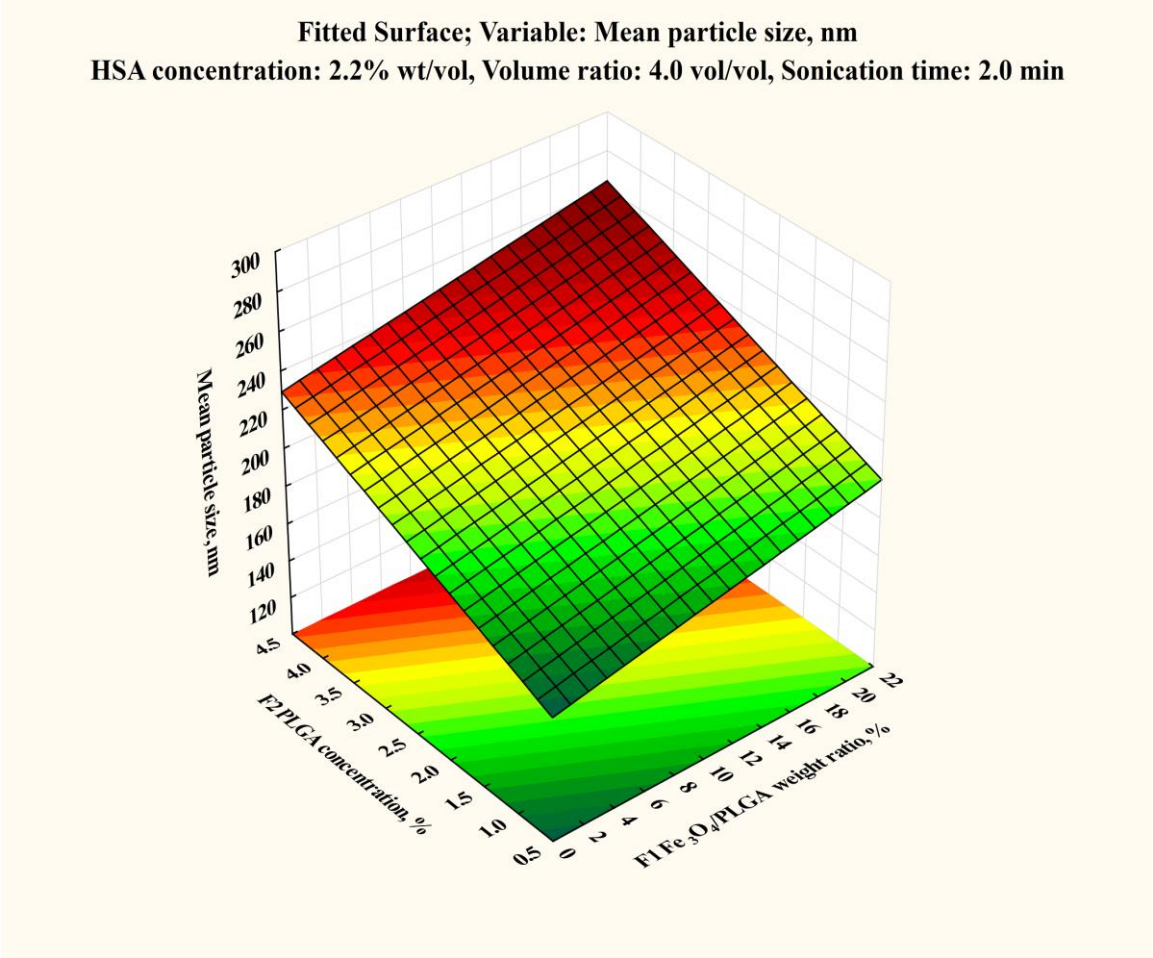

Fig. 7: The effect of Fe_3O_4/PLGA weight ratio and PLGA concentration on the mean particle size.

At medium values of the three other variables (HSA concentration, W/O volume ratio, and sonication time) the predicted (using eqn. 2, for 1% PLGA) mean particle size of the composite PLGA NPs increases from 174 to 205 nm, when Fe_3O_4/PLGA weight ratio is increased between 1 and 20% wt/wt. On the other hand, at higher amounts of

iron oxide NPs, the distribution of the obtained composite PLGA nanoparticles was much broader or highly distorted (often having a second peak). The latter corresponded to another solid product differing from the HSA and iron-oxide-containing PLGA NPs. This precipitate was mainly composed of iron-oxide nanoparticles and also contained other unidentified materials, probably a mixture of PLGA, HSA and PVA.

Both of the precisely non-identified precipitate containing iron oxide and the increase of PLGA nanoparticle size were obtained at high concentrations of iron oxide nanoparticles. This can be explained by the hydrophobic interactions between the oleic acid tails of Fe_3O_4 nanoparticles. These interactions are probably responsible for Fe_3O_4 clustering [55] which explains the shifting of the particle size towards the higher values. The latter explanation may be supported by the study Zhou et al. [37] who studied the size of interferon loaded magnetic PLA and PLGA microspheres. The authors used Fe_3O_4 and found that size of both types of microspheres increased, and the size distribution broadened with the increasing amounts of magnetic NPs. On the other hand, it is also expected that higher number of Fe_3O_4 nanoparticles inside the PLGA nanoparticles may adsorb more PLGA, which increases the amount of polymer in a particle, increasing its mass and size.

The effect of Fe_3O_4 is also shown in Fig. 8 at different HSA concentrations in which the sonication time was 1 min longer than that in Fig. 7 (in Fig. 7 the time is 2 minutes whereas in Fig. 8, it is 3 minutes). As a consequence of the latter, smallest mean particle size of the product expected at low iron oxide/PLGA weight ratio (1% wt/wt) was lower, namely 180 nm.

4.2.2 Effect of PLGA concentration

As is seen in Fig. 7, particle size significantly enhances with the increase in PLGA concentration. At medium HSA concentration (2.2% wt/vol), volume ratio of the intermediate and outer phases (4.0 vol/vol), sonication time (2.0 minutes), low magnetite/PLGA weight ratio (1.0% wt/wt), and the highest PLGA concentration (4.0% wt/vol), large PLGA particles of 223 nm volume mean size forms as calculated by eqn. 2. By decreasing the concentration of PLGA in the organic phase to 1.0% wt/vol, the mean particle size decreases considerably to 174 nm while other four parameters were kept constant.

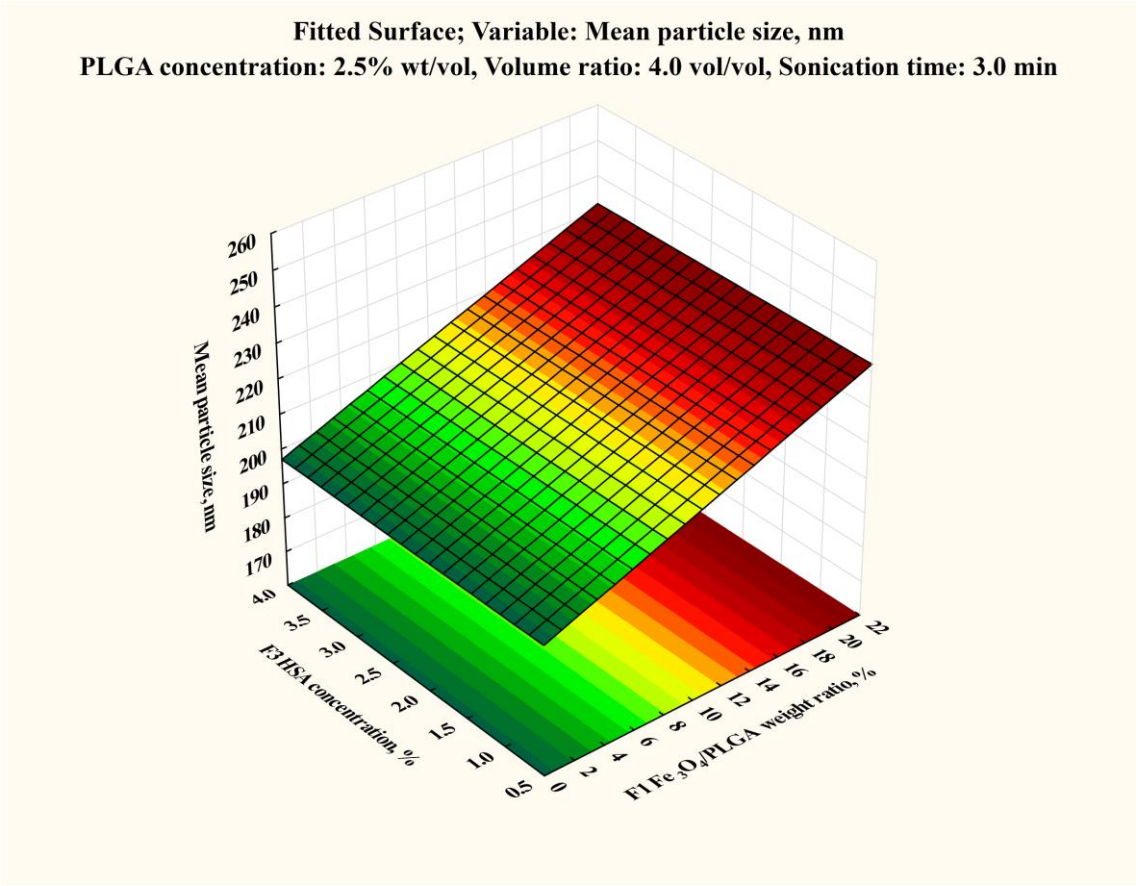

Fig. 8: The effect of HSA concentration and Fe_3O_4/PLGA weight ratio on the mean particle size after longer sonication time.

The effect of PLGA concentration can also be observed in Fig. 10, discussed later in relation to the effect of sonication time. The explanation can be the change of rheological behavior of the mixture during the second emulsification. With the increase in polymer concentration in the organic phase, its viscosity increases. High viscosity provides higher resistance against the shear forces during the second emulsification and restricts the formation of nanodroplets that are the basis of the formation of final composite PLGA nanoparticles. If cohesive forces in correlation with the viscosity and surface tension are higher in a liquid, it is more difficult to attain better dispersion by cavitation during ultrasonic treatment applied for emulsification. Therefore, high viscosity slows down the rapid dispersion of the polymer containing organic phase, which may considerably influence particle size. It means that insufficient dispersion of phases will result in larger particles with wide size distribution [57]. If the viscosity of polymeric solution is high, it will slow down the rapid dispersion of organic phase into aqueous phase resulting in the formation of bigger droplets or aggregates [58]. The viscous forces in the aqueous and organic phases oppose the shear stresses in the

organic phase. Reducing the organic phase viscosity reduces the viscous forces, which results in better dispersion effect of shear stress in the organic phase, hence decreasing PLGA nanoparticle size [59]. With an increase in the applied ultrasonic energy, it may be possible to overcome this viscosity problem. But too high sonication intensities can promote some undesired effects, such as analyte degradation. The increase in the particle size with the polymer concentration was observed by other authors with PLA [60,61] or PLGA [62]. Devi Kusum et al. found that if drug to polymer (Acyclovir:PLGA) ratio increases from 1:1 to 1:2, particle size increases significantly and drug entrapment also increases [63]. It was also found by other researchers that for each solvent, above a critical concentration of polymer, large amorphous polymer aggregates were formed in addition to the desired nanoparticles [64]. Hence, use of polymer above a certain concentration is not beneficial.

4.2.3 Effect of HSA concentration

According to the eqn. 2, also seen in Fig. 8, the HSA concentration in the inner aqueous phase has no significant effect on the particle size. Because this protein was used as a model drug in this study, this information is important. However, apart from the size, the concentration of HSA applied in the inner aqueous phase is essential in respect to achieve desired drug concentration within the carrier NPs. Concentration of HSA also influences the efficiency of encapsulation i.e. the proportion of the utilized amount of the model drug during the encapsulation process. The latter aspects will be discussed in section 4.3.

4.2.4 Effect of volume ratio of the W_2 and O phases

Volume ratio also has significant effect on the particle size as is seen on Fig. 9. Namely, if the ratio between the volumes of external and internal phases of emulsion increases, particle size also increases. This finding is in agreement with the observation of other researchers, [57] who pointed out that this ratio play an important role influencing the stability of the emulsion and the size of dispersed globules.

The basic principle governing the size of NPs is that the external energy source (e.g. ultrasound energy) provides shear stresses to the internal organic phase, which results in the formation of nanodroplets, and finally nanoparticles from it. The size of the droplets is inversely correlated to the magnitude of shear stresses [59]. Any

change(s) in process variables or parameters that reduces these shear stresses will increase the nanoparticle size. The most direct influence on the shear stresses in the system is exercised by the energy density (external energy applied per unit total volume) [59]. Increase in energy density directly increases the shear stresses and results in more efficient droplet breakdown which will reduce the nanoparticle size. In our experiments, the introduced ultrasonic energy was constant for different volume ratios. The higher the volume ratio, the higher the liquid volume is, which in turn reduces the available energy per unit volume, generating weaker emulsification, consequently larger particles are obtained.

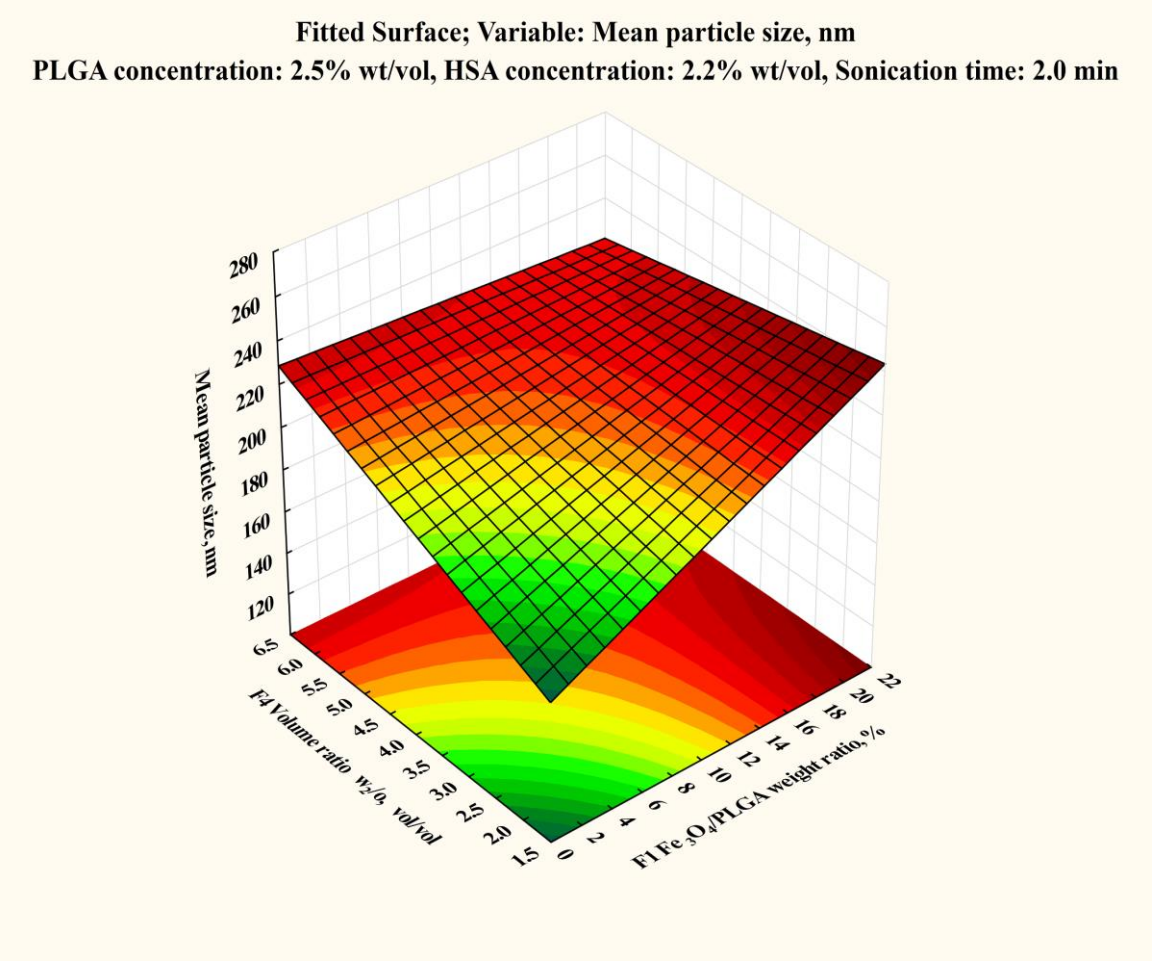

Fig. 9: The effect of volume ratio and Fe_3O_4/PLGA weight ratio on the mean particle size.

From Fig. 9 (also confirmed by eqn. 2), it can be found that volume ratio and magnetite/PLGA weight ratio have combined effect on mean size. It is seen that decrease in both the iron oxide/PLGA ratio and the volume ratio reduces the particle size very rapidly. This phenomenon can be well utilized for the production of very small nanoparticles, e.g. with mean size below 200 nm.

4.2.5 Effect of sonication time during second emulsification

From the Pareto chart, it can be seen that sonication time has the second strongest influence on particle size (after the PLGA concentration). Fig. 10 shows that

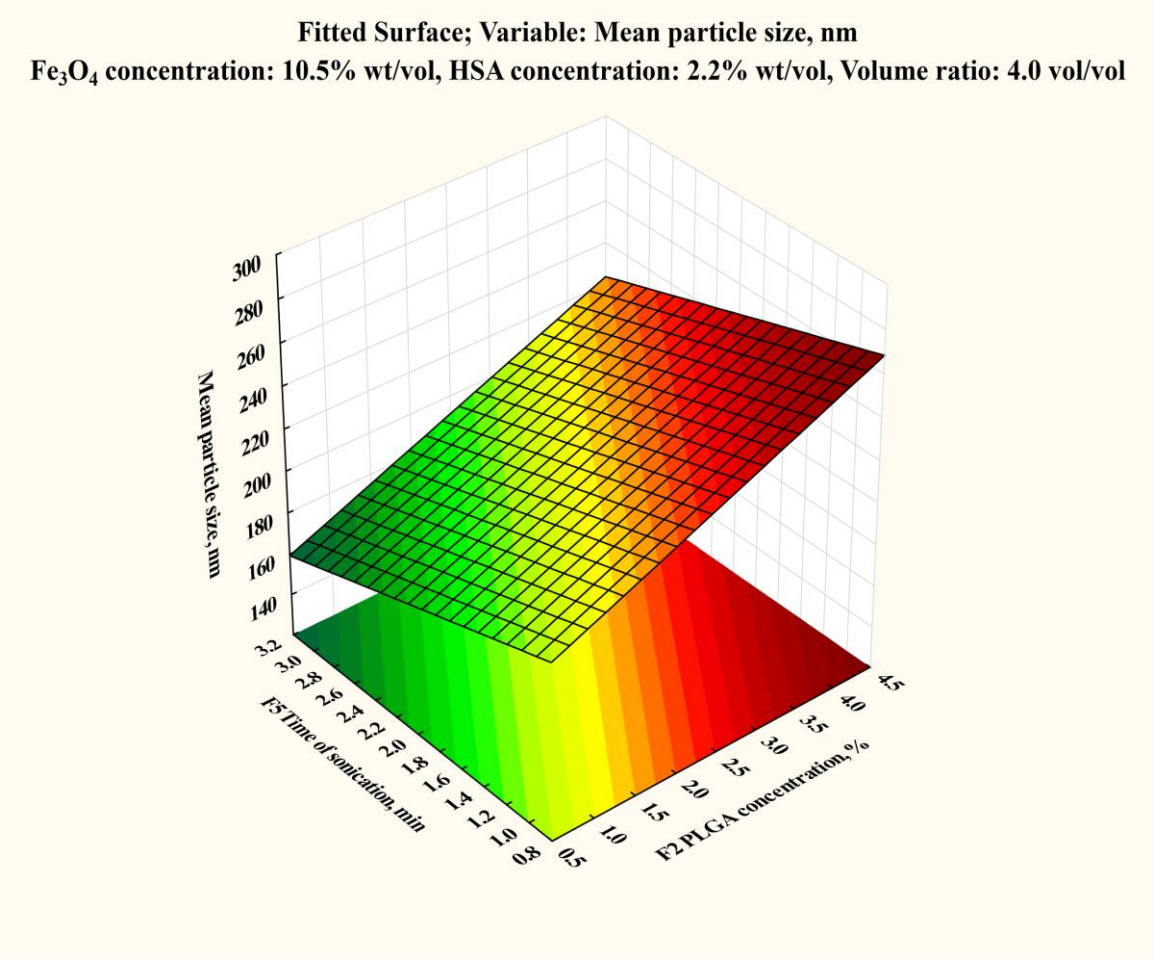

Fig. 10: The effect of PLGA concentration and sonication time on the mean particle size.

particle size drops substantially with the prolongation of sonication time. The reason is that increasing the power and/or the duration of sonication decreases the mean diameter of nanoparticles, which may also change the population distribution. Higher power and/or longer duration of sonication increases the effect of shear stress and the energy causing more droplet breakdown, resulting in a decrease in particle size [59]. The great reduction of particle size is the consequence of stronger disintegration of droplets, due to the longer emulsification process [51]. Applying prolonged sonication (e.g. 3 minutes in our case), shear stress is acting for more time in the process leading to better dispersion of polymeric organic phase as nanodroplets of small size. On the contrary, short time of sonication, i.e. insufficient dispersion of phases results in large particles

with wide size distribution. Mainardes and Evangelista et al. reported a decrease in particle diameter with increasing sonication time for PLGA nanoparticles system [65].

4.2.6 Prediction of the expected mean particle size

As was seen in the discussion above on the effects of various process variables, the magnetite weight ratio to that of the polymer (PLGA) matrix, the concentration of PLGA in the intermediate organic phase, the volume ratio of the external aqueous and intermediate organic phases, and sonication time influenced the produced composite (model drug and magnetite loaded) nanoparticles. Knowing the exact values of these variables, the correlation obtained by linear regression (also considering the possibility of quadratic correlation and linear-linear interactions of variables, eqn. 2), the mean particle size of the product can be predicted in a range of about 100 and 340 nm with a mean error of 27.6 nm. Fig. 11 gives a comparison between the measured and predicted

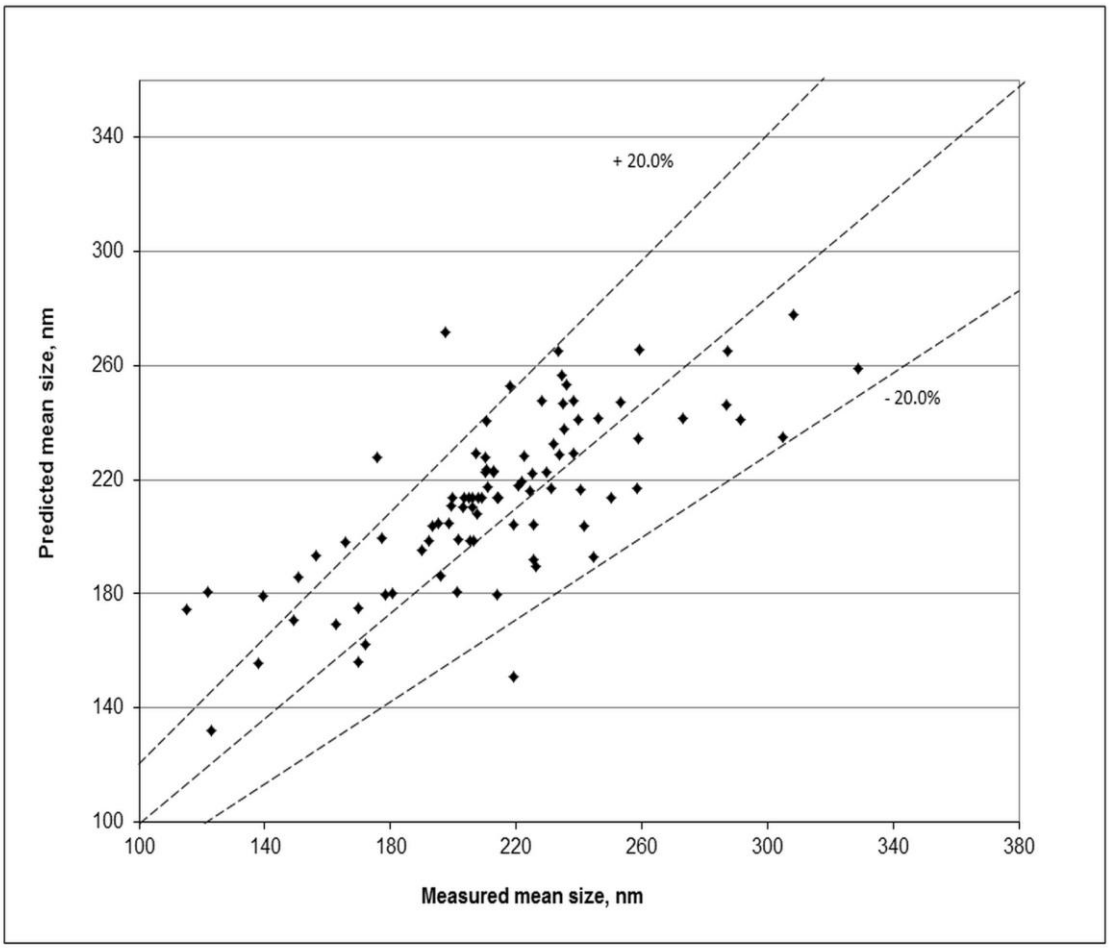

Fig. 11: Comparison of the measured and predicted mean particle sizes.

mean particle sizes. It is seen that the measured and predicted values well correlate along the whole studied size interval. The mean relative deviation between the

measured and predicted values is 9.5%, and the great majority of the data are within the ±20% range (shown by dotted lines). However, along the studied size interval, there is slight tendency that in the lowest size region the predicted values are a bit overestimated, whereas it is somewhat underestimated at the highest region. Considering that, the aim is generally to achieve the smallest possible particle size; this tendency gives more safety than uncertainty.

4.2.7 Optimization of the process variables to achieve smaller sized NPs

The formal model offered by the statistical evaluation in form of a regression equation (eqn. 2), gives sufficient opportunity to find out the optimal conditions for producing NPs of required smallest mean particle size in the studied region. As was mentioned, small particle size is advantageous for different reasons e.g. sterilizing them by ultrafiltration is only eligible, if the size distribution does not exceed much above 220 nanometer (the mean size in this case should be much lower, at least 130-160 nm). Small size of NPs is also required to avoid or reduce harmful interactions with the human organisms. To achieve this goal, the independent i.e. decision variables have to be set to optimal values in this respect.

Optimization was relatively easy by the GAMS program package. The program showed that the optimal values of variables to get the smallest mean particle size were at the borders of their studied intervals. The optimal conditions were as follows: magnetite/PLGA weight ratio, X_{Fe3O4}=1.0% wt/wt (the lowest value), PLGA concentration in the intermediate organic phase, X_{PLGA}=1.0% wt/vol (the lowest value), volume ratio of the external aqueous phase to the intermediate organic phase X_{VOLR}= 2.0 vol/vol (the lowest value), time of second sonication X_{time}=3.0 minutes (the highest value). The concentration of HSA in the inner aqueous phase had no influence in this relation, therefore it does not constrain process optimization. Under these conditions the predictable volume mean particle size is 132 nm, which is more than acceptable in respect of the properties for sterilization and utilization of the product NPs.

Therefore, there is no special reason to use process variables outside the studied parameter intervals, which also may cause technical or economical difficulties (e.g. using too low PLGA concentration decreases the productivity of a given reaction vessel,

or applying excessively long time of sonication may lead to degradation of the valuable drug substances).

However, if the magnetite/PLGA ratio X_{Fe3O4}=1.0% wt/wt during encapsulation of the magnetic nanoparticles proves not to be sufficient to achieve suitable level of magnetism in the product NPs, it can be increased with the consequence of obtaining somewhat larger sizes. To clear up this consequence, optimization was carried out with constrain of different volume mean product particle sizes (this time not regarding the efficiencies of HSA and magnetite encapsulation). The results are shown in Fig. 12. In the diagram it is seen that the increase of magnetite/PLGA ratio causes a linear increase of the achievable mean particle size, providing optimal conditions regarding the best values of the three other decision variables (X_{PLGA}=1.1% wt/vol, X_{VOLR}=2.0 vol/vol, X_{time}=3.0 minutes). As a conclusion, if a mean particle size of 160 nm is allowed for the sterilization by ultrafiltration and in respect of suitable properties as drug carrier, as high as 10% wt/wt magnetite/PLGA ratio can be applied to achieve suitable magnetic behavior of the product nanoparticles.

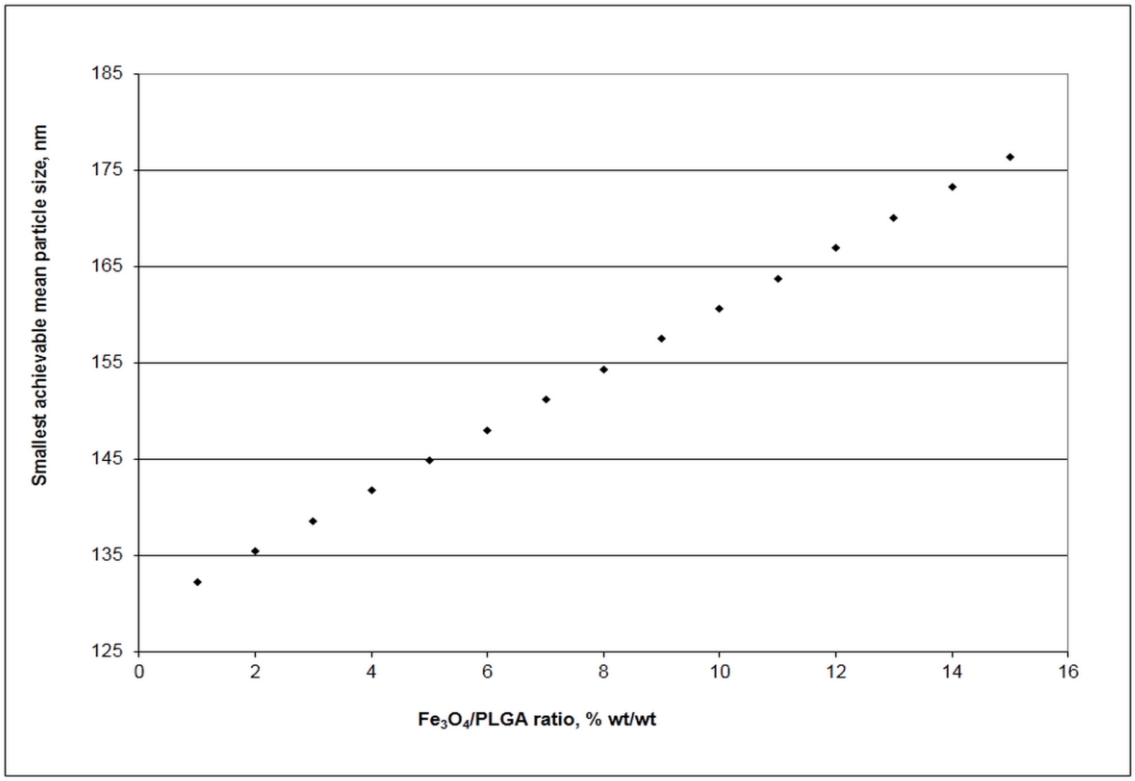

Fig. 12: The smallest achievable mean particle size with constrain of various magnetite/ PLGA ratios at optimized other process variables.

4.3 Encapsulation efficiency of model drug

As a result of the statistical analysis carried out on the measured encapsulation efficiency data, the influences of the studied process variables were characterized by the ANOVA table (Table 3) and Pareto chart of the standardized effects. From Table 3 it is seen that linear (L) and quadratic (Q) effects of PLGA concentration (factor F2), the linear effect of HSA concentration (factor F3), and the cross-effect (linear-linear interaction) of these two factors (F2*F3) had the strongest influences. The quadratic (Q) effect of the weight ratio of magnetite/PLGA (factor F1), and the linear-linear interactions of the PLGA concentration and the volume ratio of external aqueous and intermediate organic phases (F2*F4), and that of the HSA concentration and volume ratio (F3*F4) also possessed significant effects, respectively. From ANOVA table it is seen that all of these effects are statistically significant, since the related *p* values are much below the commonly accepted p=0.05 criterion.

Table 3: ANOVA table obtained by statistical analysis of the measured encapsulation efficiencies obtained with different combinations of the influencing factors.

Factor	ANOVA; Dependent Variable: Encapsulation efficiency (HSA EE%), 5 3-level factors, 90 Runs; MS Residual=84.425				
	SS	df	MS	F	p
F1 Fe_3O_4 conc. (Q)	*734.44*	*1*	*734.436*	*8.69928*	*0.004147*
F2 PLGA conc. (L+Q)	*12025.95*	*2*	*6012.976*	*71.22274*	*0.000000*
F3 HSA conc. (L)	*3918.52*	*1*	*3918.519*	*46.41423*	*0.000000*
Interaction F2*F3	*2909.34*	*1*	*2909.344*	*34.46071*	*0.000000*
Interaction F2*F4	*558.06*	*1*	*558.062*	*6.61015*	*0.011946*
Interaction F3*F4	*456.04*	*1*	*456.036*	*5.40167*	*0.022592*
Error	6922.85	82	84.425		
Total SS	27943.57	89			

Table 3 also shows that the mean square of residuals (MS) was 84.425, i.e. the mean deviation between the measured and estimated encapsulation efficiencies was $\sqrt{84.425} = \pm 9.19\,\%$, which can be considered as an acceptable deviation. The histogram of residuals (not presented here) showed almost normal distribution, therefore the estimation made by the multivariable regression applied in the STATISTICA® software was acceptable. The pure error of experimental data determined from the mean square of the deviations of the encapsulation efficiencies measured in 9 repeated runs at the central values of all variables was $\pm$5.8%, which is regarded as good accuracy.

The Pareto chart (Fig. 13) shows that the encapsulation efficiency was affected mostly by: PLGA concentration in the intermediate organic phase (F2 - linear (L) and quadratic (Q) effects), HSA concentration in the inner aqueous phase (F3 - linear effect (L)) and linear-linear interaction of these two factors. The iron oxide/PLGA weight ratio (F1) had lower and quadratic effect. Although the linear-linear interaction of volume ratio (F4) with PLGA concentration and also with HSA concentration was significant,

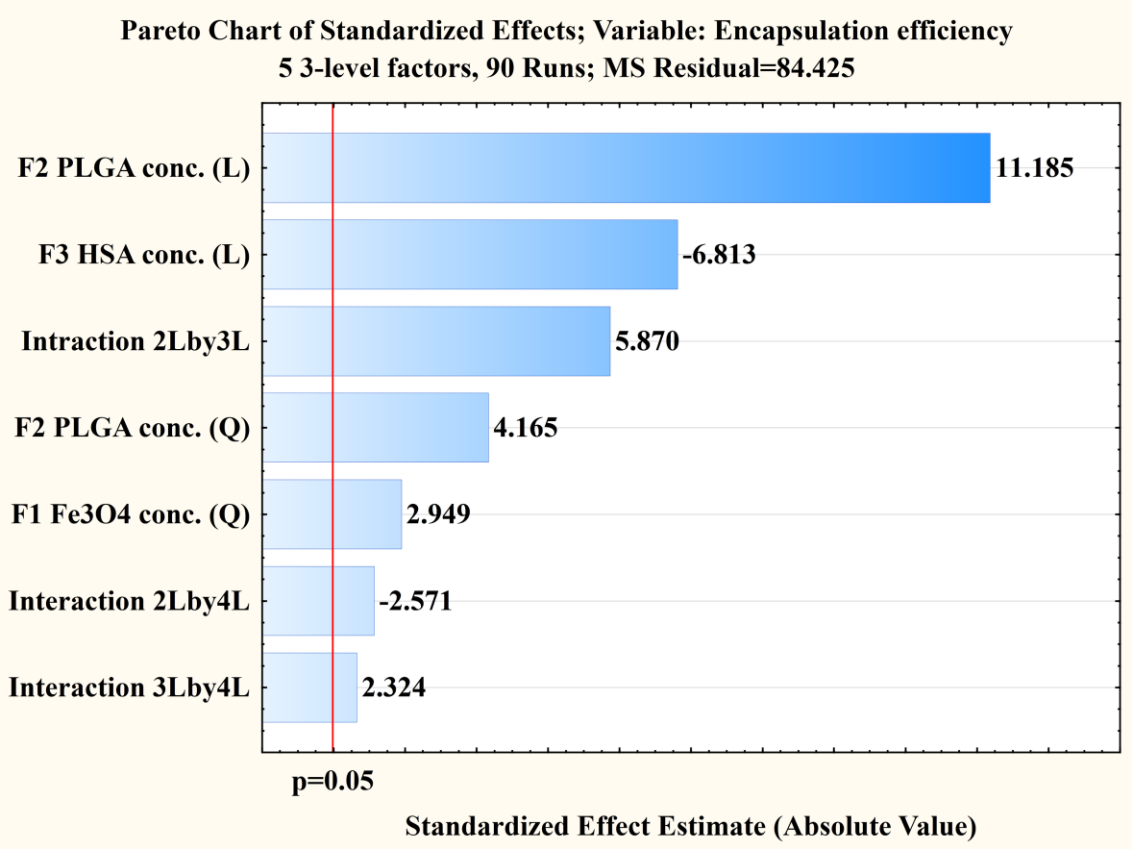

Fig. 13: Pareto chart on the standardized effects of the independent process variables on the encapsulation efficiency.

they had minor effects. Among the studied five variables, the duration of sonication had no direct effect at all on the encapsulation efficiency. The explanation is given in section 4.3.5.

As a result of the statistical analysis, a regression equation was obtained to describe the dependence of the encapsulation efficiency EE_{HSA} on the studied process variables:

$$EE_{HSA} = 25.3189 \cdot X_{PLGA} - 4.0993 \cdot X_{PLGA}^{2} - 21.4573 \cdot X_{HSA} - 0.0075 \cdot X_{Fe3O4}^{2} + 4.0632 \cdot X_{PLGA} \cdot X_{HSA} - 1.1217 \cdot X_{PLGA} \cdot X_{VOLR} + 1.3810 \cdot X_{HSA} \cdot X_{VOLR} + 72.2188 \quad (3)$$

These effects are demonstrated by the diagrams in Fig. 14-17 and discussed in details below.

4.3.1 Effect of PLGA and HSA concentrations

Increased PLGA concentrations can generally be beneficial to achieve higher encapsulation efficiency, but this effect can be diminished under certain conditions due to the influence of other process variables. Among them, the most important one is the concentration of HSA in the inner aqueous phase. Fig. 14 clearly shows this effect at fixed magnetite/PLGA mass ratio (3.0% wt/wt), volume ratio of W_2 and O phases (4.0 vol/vol) and sonication time (3.0 min). It is seen that the encapsulation efficiency varies non-linearly with the change of PLGA concentration: the increase in the encapsulation efficiency is most rapid at the highest model drug concentration (X_{HSA}=3.7% wt/vol), which can grow from 45.1 to 91.1% when X_{PLGA} changes from 1.0 to 4.0% (wt/vol). The increment of encapsulation efficiency is gradually decreasing with the increase in PLGA concentration for medium and low HSA concentration, i.e. rapid growth is seen around X_{PLGA}=1.0% (wt/vol), which slows down at higher PLGA concentrations, e.g. above 2.5% (wt/vol). However, at low HSA concentration (X_{HSA}=0.7% wt/vol) the effect of PLGA is much more moderate, starting from an encapsulation efficiency of about 80.1%, reaching to a maximum of about 90.1%.

Due to the cross-effect (interaction) between the PLGA and HSA, the influence of HSA concentration depends on the actual level of PLGA concentration. As is seen on Fig. 14, if lowest amount of PLGA is used (X_{PLGA}=1% wt/vol) in the intermediate organic phase, the increase of X_{HSA} causes a reduction in the encapsulation efficiency

from the mentioned 80.1% to about 45.1%. However, if PLGA concentration in the organic phase is high, e.g. its maximal value of 4.0% (wt/vol), the increase of HSA concentration to its maximal value (X_{HSA}=3.7% wt/vol) results in a slight increase in the achievable encapsulation efficiency from about 90.1 to 91.1%. The explanation of this interaction lies in the fact that greater amount of PLGA matrix material can absorb more model protein drug. If the presence of PLGA is not sufficient, relatively smaller proportion of the total amount of HSA can be captured in the particles resulting lower encapsulation efficiency.

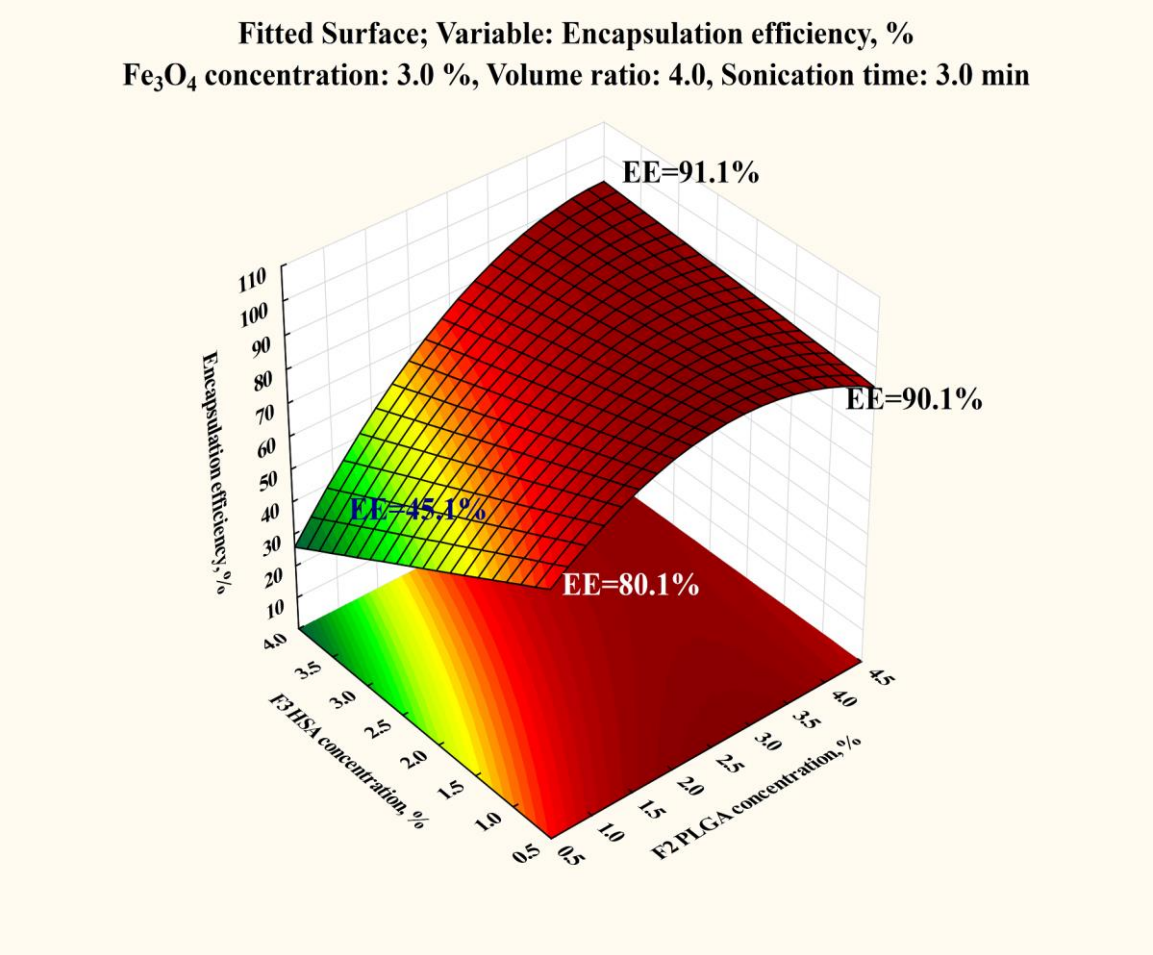

Fig. 14: The effect of PLGA and HSA concentration on the encapsulation efficiency.

The literature data support our findings on the effect of PLGA, because it is known that the efficiency of encapsulation generally grows with the increase in the relative amount of the polymer matrices. Another effect may be that at certain conditions, particle size can also rise with the polymer concentration [66] and the encapsulated drug content is known to increase with the increase in particle size [59,67].

Further explanation can be that with the increase in the concentration of polymer in the organic phase, the viscosity of the organic phase increases. The more viscous organic phase provides higher mass transfer resistance [64] and prevents protein diffusion towards the external phase, which in turns results in higher encapsulation efficiency. Increasing the PLGA concentration at a given HSA concentration will decrease the HSA/PLGA ratio in the droplets of the organic phase. This also may reduce the possibility of its escaping from these droplets. Devi Kusum et al. found that if drug (Acyclovir):polymer (PLGA) ratio increases from 1:1 to 1:2, particle size increases significantly and drug entrapment also increases [63].

As for the effect of HSA concentration, it is seen that the increase in the HSA concentration decreases the encapsulation efficiency. The high model drug loadings typically issue in lower encapsulation efficiencies due to high concentration gradient causing the drug to diffuse out of the droplets [68]. So, the lower encapsulation efficiencies obtained with higher HSA concentrations could be explained by the higher protein loss by diffusion towards the external aqueous phase. During the solidification of droplets, the quantity of solvent in the dispersed phase decreases, and the drug shows the tendency to be expelled from the dispersed phase [22]. Some researchers also pointed out that microspheres with high drug loadings are more porous and have rather irregular shapes; highly porous surface is responsible for the rapid loss of drug [22]. This can be also a reason for the loss of HSA from PLGA nanospheres. Too high drug loading increases the risk of drug leakage due to the limited space inside the nanospheres and the shrinkage of the nanospheres during its solidification. Pamujula et al. studied amifostine drug-loaded PLGA microcapsules [69]. It was found that the efficiency of encapsulation decreased with an increase in drug loading, which complies with our result.

The HSA/PLGA ratio is also an important parameter compared to the protein concentration in the inner aqueous phase. Insufficient concentration of the PLGA can result in more non-encapsulated HSA. In previous studies, it was found in this respect that if the initial protein concentration is not higher than 10% (wt/vol) of the initial PLGA amount, more than 90% of protein can be encapsulated by using a suitable emulsifier [70].

4.3.2 Effect of the magnetite/PLGA mass ratio

As is seen from the very small coefficient of X_{Fe3O4} in eqn. 3, and also from Fig. 15, the presence of magnetite has only slight influence on the encapsulation of HSA into the PLGA nanoparticles. With the increase in magnetite/PLGA ratio from 1.0 to 20.0% (wt/wt), the predicted encapsulation efficiency shows slight reduction only from EE_{HSA}=65.2 to 62.2% at low PLGA concentration (X_{PLGA}=1.0% wt/vol), and from EE_{HSA}=90.6 to 87.6% at the highest studied polymer content (X_{PLGA}=4.0% wt/vol), respectively.

This decrease may be due to the possibility that with the higher Fe_3O_4/PLGA mass ratio, more magnetite particles can escape from the model drug loaded PLGA nanoparticles and can be dispersed into the outer aqueous phase. In this process some model protein drug may be adsorbed on the surface of the escaped magnetite nanoparticles, hence, representing lower encapsulation efficiency.

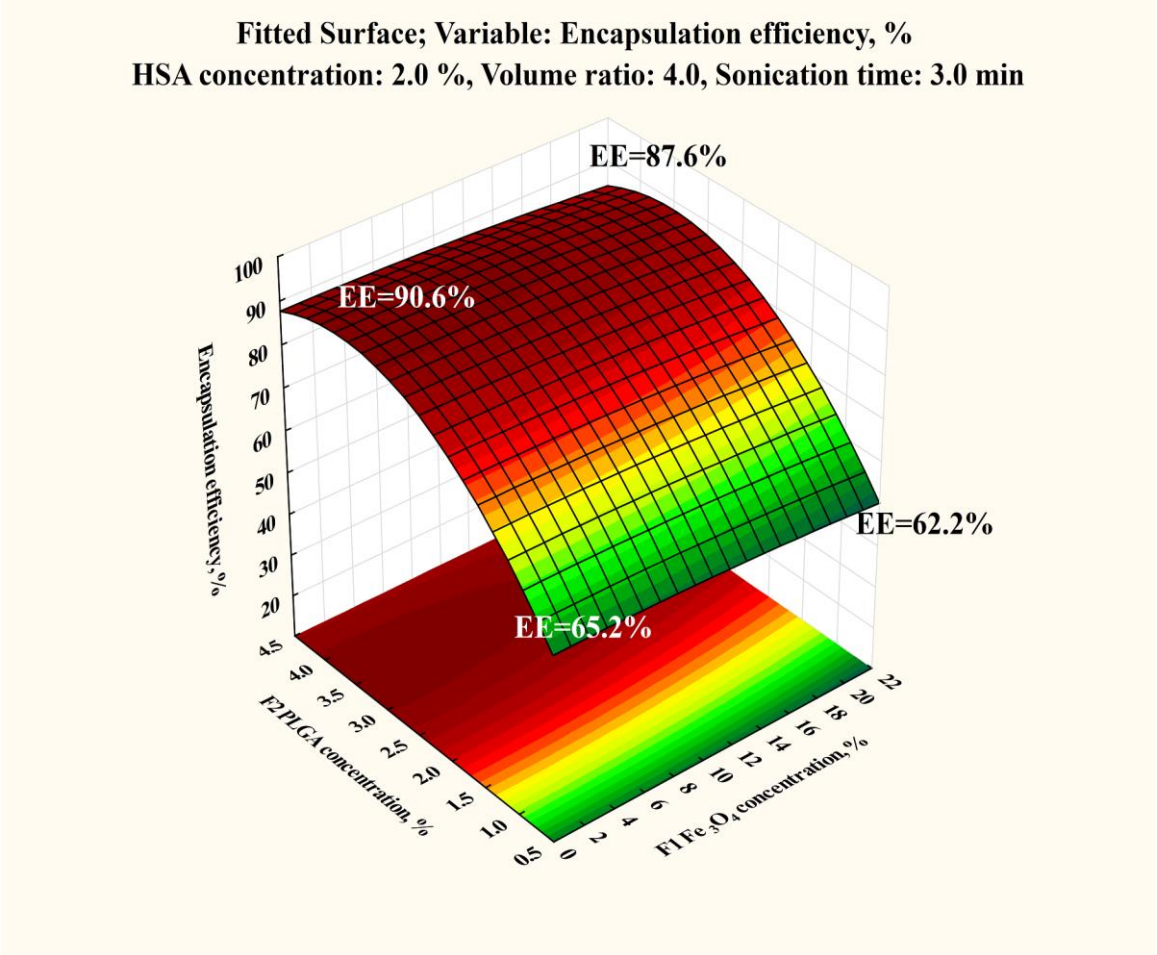

Fig. 15: The effect of the PLGA concentration and the magnetite ratio to the mass of PLGA on the encapsulation efficiency.

4.3.3 The interaction of the PLGA concentration and the volume ratio

It can be seen from the Pareto chart (Fig. 13) and Eqn. 3 that the volume ratio of the external aqueous and the intermediate organic phases (X_{VOLR}) does not have its own independent effect on the encapsulation efficiency, because it interacts with two other process variables. Namely, the effect of the volume ratio can be influenced by both of the PLGA and HSA concentrations, and vice versa. Fig. 16 shows certain cross-effect of the volume ratio and PLGA concentration. Cross-effect can be seen from the fact that the increasing or decreasing tendencies of encapsulation efficiency at low and high PLGA concentration are different ones.

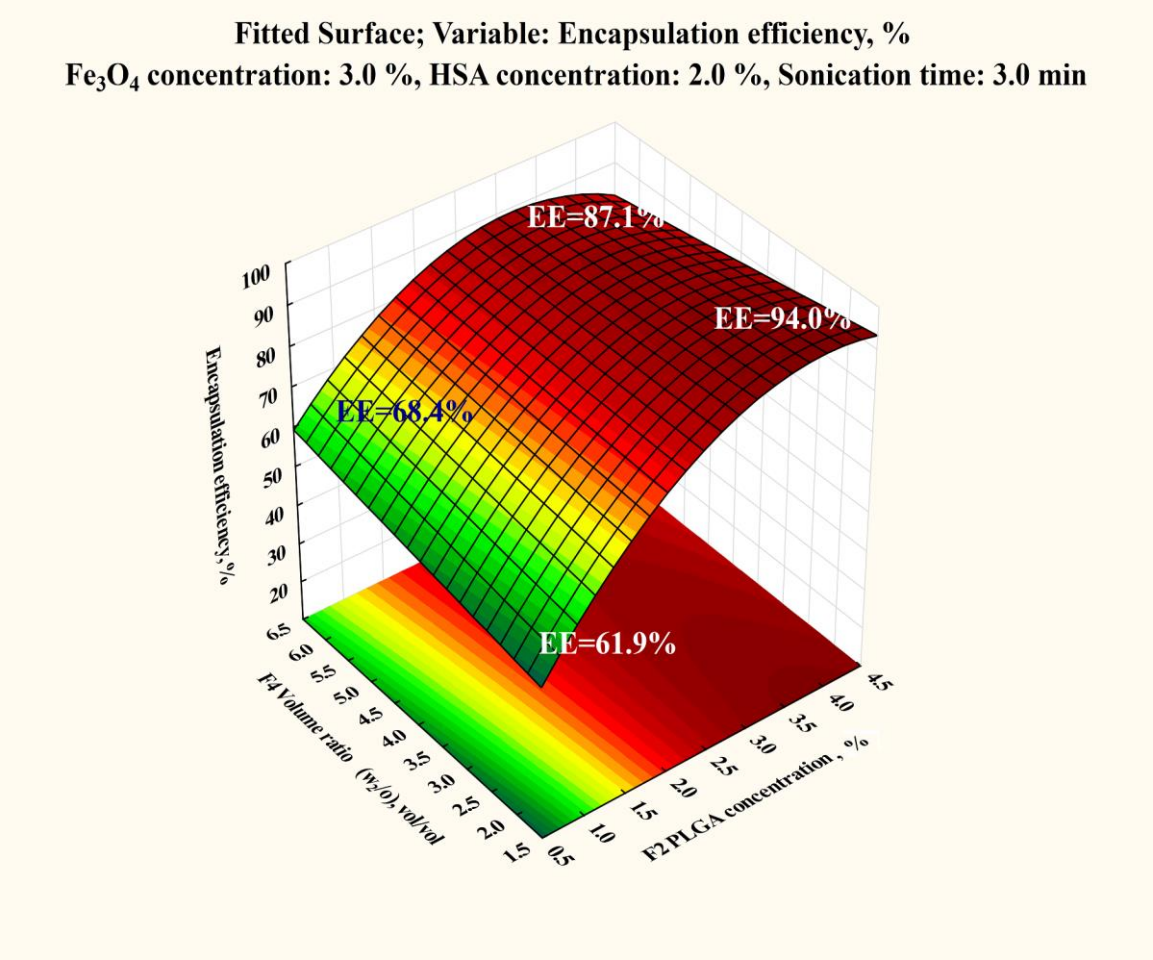

Fig. 16: The interaction of the PLGA concentration and the volume ratio of the external and intermediate phases.

As was seen earlier, an increase in PLGA concentration results in a rapid increase of encapsulation efficiency, especially in the lower region of the studied interval. The change of volume ratio of the W_2/O phases can slightly modify the achievable degree of encapsulation in a considerable range of PLGA concentrations. At

the lower end of the polymer concentration, i.e. at around X_{PLGA}=1.0% (wt/vol), the increase of volume ratio from X_{VOLR}=2.0 to 6.0 (vol/vol) causes a rise in the encapsulation efficiency from EE_{HSA}=61.9 to 68.4% at fixed values of three other variables indicated on Fig. 16. At the higher end of the PLGA concentration range (X_{PLGA}=4.0% wt/vol), the effect of the volume ratio of phases W_2/O is opposite: the increase of volume ratio from 2.0 to 6.0 (vol/vol) results in the decrease of encapsulation efficiency from EE_{HSA}=94.0 to 87.1%.

This phenomenon may be explained by a general principle that governs the size of nanodroplets during shearing the given three-phase system by an external energy source. It is known from the literature that the size of droplets is inversely proportional to the magnitude of shear stresses [59]. Any change in process variables that reduces these shear stresses will increase the nanodroplet size. In our experiments the introduced ultrasonic energy was constant for different volume ratios. Therefore the higher the volume ratio, the higher the liquid volume is, which in turn reduces the available energy per unit volume, i.e. less energy density, resulting in weaker emulsification. It leads to the production of larger particles if all the other variables are fixed. From larger droplets (or particles) less protein can escape to the external aqueous phase.

On the other hand, at higher energy density during shearing the intermediate organic phase droplets (containing the already dispersed inner aqueous phase, HSA solution) increase the probability that the tiny droplets of the HSA solution can get into direct contact with the outer aqueous phase, which allows intermingling and their fusion, thus causing protein loss and lower encapsulation efficiencies. This could be a reasonable explanation of the increase of encapsulation efficiency with increasing volume ratio at the lower end of PLGA concentration. The controversial effect at high PLGA concentration may be the consequence of higher PLGA concentration that increases the viscosity of the intermediate organic phase which may protect the inner aqueous phase from the direct contact with the external aqueous phase during shearing, or at least can diminish the fusion of the droplets of the inner aqueous phase with the outer continuous aqueous phase. The increase of encapsulation efficiency with decreasing volume ratio at higher PLGA content can be caused by reduced HSA extraction from high viscous organic phase by the relatively small amount of the external aqueous phase.

It should be noted that the cross-effect between the PLGA concentration and the volume ratio, and their combined influence on the encapsulation efficiency is

statistically significant, and thus, has to be considered, but this is not the most important effect as a whole.

4.3.4 The interaction of HSA concentration and volume ratio

The interaction between the HSA concentration in the inner aqueous solution and the W_2/O phases volume ratio is clearly seen in Fig. 17, where the magnetite to PLGA ratio, the PLGA concentration in the organic phase, and the time of sonication are fixed (X_{Fe3O4}=3.0% wt/wt, X_{PLGA}=2.5% wt/vol, and X_{time}=3.0 min).

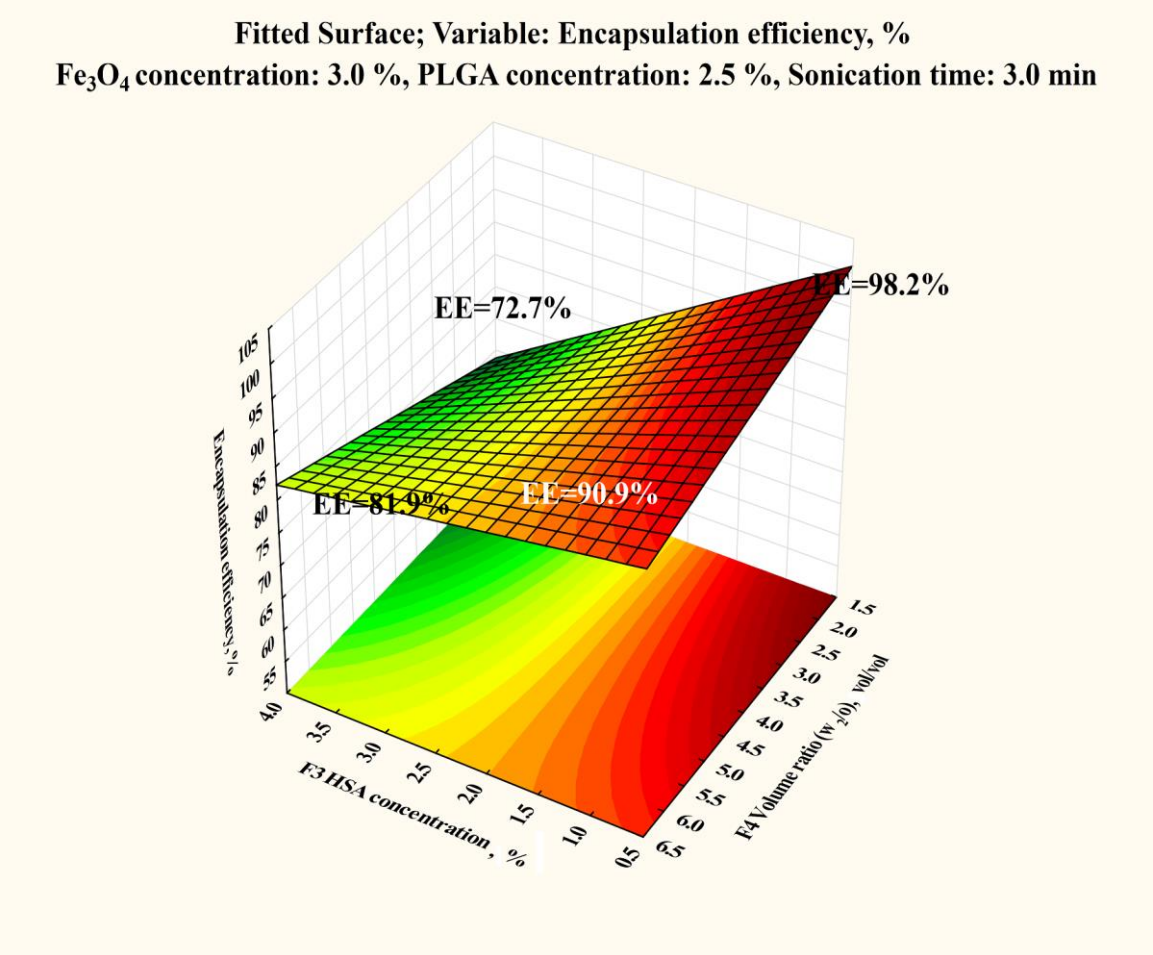

Fig. 17: The interaction of the HSA concentration and the volume ratio of the external and intermediate phases.

Namely, at low volume ratio (X_{VOLR}=2.0 vol/vol), the decrease of HSA concentration from 3.7 to 0.7% (wt/vol) results in significant increase in the encapsulation efficiency (from 72.7 to 98.2%), while for same change in HSA at high volume ratio (X_{VOLR}=6.0 vol/vol) the encapsulation efficiency changes from 81.9 to 90.9%. On the other hand, the effect of volume ratio at high HSA concentration (X_{HSA}=3.7% wt/vol) is also

significant: by increasing the volume ratio from 2.0 to 6.0 vol/vol, the efficiency of encapsulation grows from 72.7 to 81.9%. At low HSA concentration (X_{HSA}=0.737% wt/vol), the tendency is just opposite: the same increase of the volume ratio leads to the decrease of the encapsulation efficiency from 98.2 to 90.9%. The beneficial effect of the increase in the volume ratio at high HSA concentration has already been explained above by the lower energy density and small shear stress, which leads to larger particles and minimizes protein loss. The decrease of encapsulation efficiency with growing volume ratio at lower HSA concentration seems to be contradictory for the first sight, but it becomes understandable by the fact that more external water phase can extract more HSA from the droplets of the first W_1/O emulsion during shearing them in the external continuous W_2 phase.

4.3.5 Effect of sonication duration on the second emulsification

It has been shown in section 4.2.5 that at given values of other influencing variables, the increase in sonication time has decreased the achievable mean particle size of the HSA/magnetite loaded nanoparticles significantly. In spite of this fact, the statistical analysis of the data obtained for entrapping of HSA does not show any significant direct effect of sonication time on the degree of encapsulation. This was especially interesting because it is known from other studies that particle size greatly influences the encapsulation efficiency, which usually increases with increasing particle size and vice versa. Several authors have pointed out for drug-loaded particles that in general the larger the particle size, the higher the encapsulation efficiency for drugs [71,72]. This is the reason why the encapsulation efficiency of nanospheres is usually lower than that of microspheres [73,74]. The lower encapsulation efficiencies obtained with the smaller particles was explained by the larger surface area of smaller droplets. Hence, during the emulsification step, a more direct contact between internal and external phases occurred, which resulted in higher loss of model drug (HSA) by diffusion to the external medium [75]. Inversely, for larger droplets, the surface area per unit mass is comparatively smaller. So, the loss of model drug is lower, and thus higher encapsulation efficiencies are obtained. Such an explanation agrees with the results of Gorner et al. and Feng et al. [67,71]. Moreover, rising particle size increases the length of diffusional pathways into the aqueous phase, thereby reducing the drug loss through diffusion and enhancing the drug content [59]. Dey et al. have also found that encapsulation efficiency of nanoparticles increased from about 68 to 86% with the

increment of their mean diameter from 64 nm to 255 nm [75]. Similar results were found by Gorner et al. [67] where drug encapsulation efficiency grew with the increase in the particle size from about 19% for small particles to about 34% for medium and up to about 57% for large nanospheres which also complies with our earlier result [70], and strongly supports our present finding.

Although the mean particle size was influenced by the duration of second onication (section 4.2.5), no direct relation was obtained between the latter and the encapsulation efficiency. The explanation of this apparent contradiction can be that, besides the duration of ultrasonic treatment, both particle size and the encapsulation efficiency were strongly influenced by other process variables as is seen in Fig. 18a and 18b. It is clearly seen from these plots that along the increasing sonication time both the

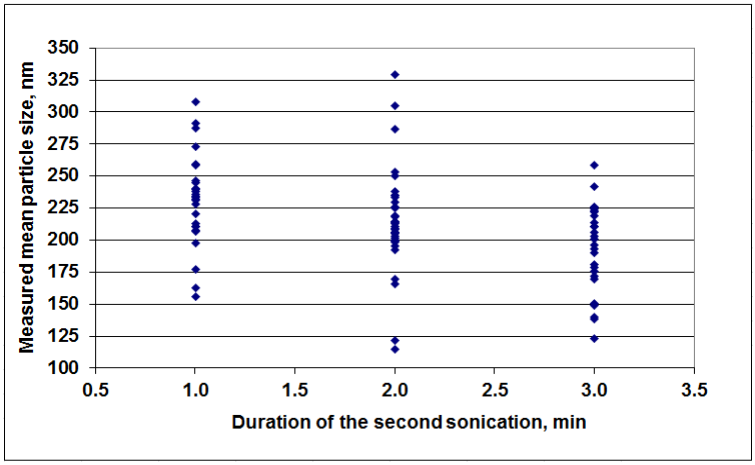

a

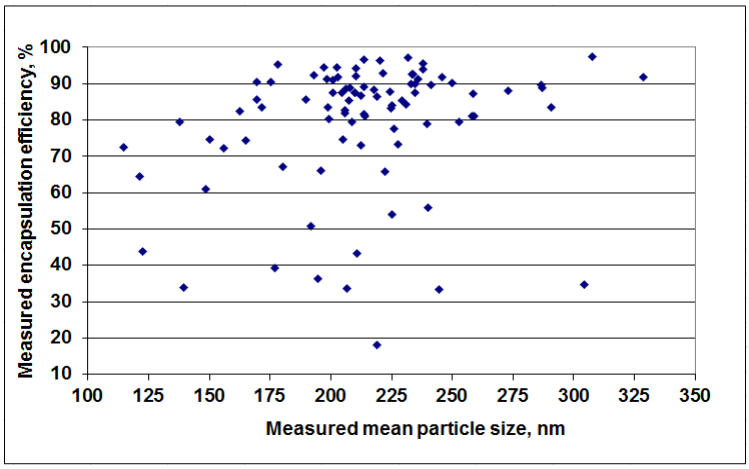

b

Fig. 18: Experimental data on the relation between the mean particle size, duration of second sonication and encapsulation efficiency, a - obtained mean particle size vs. sonication time without separation of the particular effects of different process variables, b – measured encapsulation efficiencies vs. measured mean particle sizes.

mean particle size and the encapsulation efficiency are highly scattered due to the variation of the other influencing parameters at given sonication time. Therefore, the real effect of sonication time and particle size can only be explored by statistical analysis of the data, suitable to study the particular effects of different process variables. The effect of mean particle size on encapsulation efficiency can be explored by the optimization of the results also at various constraints, which will be discussed in details in section 4.4.

From Fig. 18a and 18b it is obvious that, depending on other process variables, at given sonication time, quite different particle sizes can be produced (Fig. 18a), and even for a given mean particle size quite different encapsulation efficiencies were achieved (Fig. 18b). However, process variables are optimized (section 4.4) in respect to get various predefined mean particle sizes with maximal encapsulation efficiency utilizing the descriptive model equations.

4.3.6 HSA loading in the particles

The concentration of the active ingredient in the nanoparticles is also of primary importance in respect of their applications as drug preparations. Therefore the model drug loading (i.e. HSA concentration (% wt/vol) in the total mass of particles) can be calculated as:

$$X_{HSA_{encaps}} = \frac{m_{HSA_{encaps}}}{m_{PLGA} + m_{Fe3O4_{encaps}} + m_{HSA_{encaps}}} \times 100\% \qquad (4a)$$

$$X_{HSA_{encaps}} = \frac{V_{HSA} \cdot X_{HSA} \cdot EE_{HSA}}{V_{PLGA} \cdot X_{PLGA} \cdot (100 + \frac{X_{Fe3O4} \cdot EE_{Fe3O4}}{100}) + V_{HSA} \cdot X_{HSA} \cdot EE_{HSA}} \times 100\% \qquad (4b)$$

In the planned application studies, the concentration of superparamagnetic magnetite NPs in the capsules of final product will be kept at relatively low level (few percent only). Thus for the sake of simplicity, the mass of magnetite in Eqn. 4 can be neglected.

Since the value of any protein type drug ingredient is several order of magnitude higher than the price of iron oxide, the purpose of our study was to determine the influence of process variables on the encapsulation of the model drug. The degree of iron oxide encapsulation was therefore of secondary importance, and served only to ensure a suitable magnetic behavior of particles after their administration in living

organism. On the other hand, to minimize any side effects, as small amount of iron oxide nanoparticles should be present in the final drug formulation as possible, which can be realized at relatively low magnetite/PLGA mass ratios. According to our observations, the encapsulation efficiency of magnetic nanoparticles was close to 100%, when the initial iron oxide was 1% (wt/wt) related to the PLGA mass; viz. no detectable amount of non-encapsulated iron oxide remained in the supernatant after the separation of PLGA nanoparticles. It should be noticed that at higher magnetite/PLGA ratio the degree of encapsulation could not quantitatively be determined because of the difficulty of separation of the encapsulated and non-encapsulated magnetic nanoparticles.

4.4 Optimization of the process variables

In the production of drug-loaded NPs, the general goal is to achieve suitable small particle size and at the same time, high encapsulation efficiency. From the results of our study it was revealed that simultaneous achievement of the two requirements is not an easy task because the effects of some process variables may be opposite (or at least competitive) in respect of these two requirements. From the results it is seen that, low PLGA concentration is beneficial for obtaining smaller NPs (section 4.2.7), whereas it is just disadvantageous in respect of the encapsulation efficiency. Other variables may help to achieve both requirements at the same time, and there are variables which influence only one of them: e.g. magnetite/PLGA ratio and sonication time have significant influence on the mean particle size exclusively, but do not have significant effects on encapsulation efficiency (from eqn. 3, X_{Fe3O4} has coefficient of -0.0075 which is quite low) whereas HSA concentration influences only the encapsulation efficiency, not the mean particle size.

Fig. 18b shows that for given mean particle sizes quite different encapsulation efficiencies can be achieved by varying the process conditions, which offers good opportunity for optimization of the process. To elucidate the best conditions to obtain suitably small NPs and high encapsulation efficiency at the same time, mathematical optimization was carried out by GAMS^{TM}/MINOS software package, using the descriptive model equations: eqn. 2 and eqn. 3, referring to the achievable mean particle size and encapsulation efficiency as a function of process variables, respectively. The reason behind the optimization was to find out suitable conditions (process variables) to get maximum encapsulation efficiency with a constraint of obtaining various

(allowable) mean particle sizes. Because the required magnetic properties of the model drug loaded NPs may be different, and are influenced by the relative amount of Fe_3O_4 nanoparticles applied in the organic phase, the optimization has been carried out at various magnetite/PLGA ratios. The results are shown on the composed diagrams in Fig. 19.

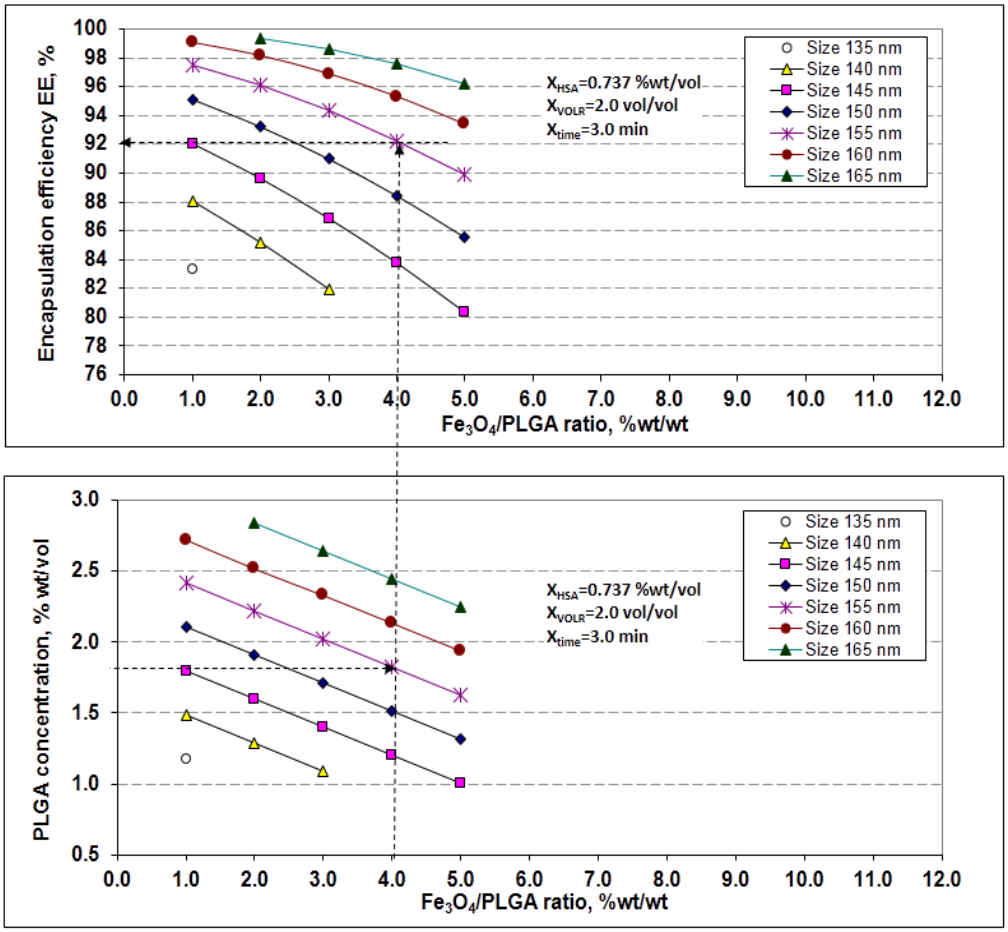

Fig. 19: Results of optimization at different magnetite/PLGA ratio. At optimal values of other process variables, PLGA concentration and magnetite/PLGA ratio determines the achievable smallest mean particle size (lower diagram) and the highest encapsulation efficiency (upper diagram).

In the bottom diagram in Fig. 19, the combined effect of PLGA concentration and magnetite/PLGA mass ratio is shown on the achievable mean particle size with maximal encapsulation efficiency (upper diagram), at fixed (optimal) values of the other three process variables. Among them, maximal sonication time (X_{time}=3.0 min) was chosen, because it was the most beneficial to get the smallest achievable mean particle size, but had no significant direct effect on the encapsulation efficiency. The

concentration of HSA practically had no influence on the mean particle size, but its smallest studied value, X_{HSA}=0.737% (wt/vol) offered the highest encapsulation efficiency, especially at the smallest studied volume ratio of X_{VOLR}=2.0 (vol/vol) (see Fig. 17). The latter volume ratio was the best selection to obtain the smallest mean particle size (section 4.2.7).

According to the lower diagram, two independent variables, i.e. PLGA concentration and Fe_3O_4/PLGA ratio determine the achievable mean particle size at fixed values of the other three variables. An example is shown by dotted lines for X_{PLGA}=1.83% (wt/vol) and X_{Fe3O4}=4.0% (wt/wt), resulting in a mean diameter of about 155 nm (crossing point of the dotted lines). In the lower diagram it is also obvious that increasing the PLGA concentration at constant magnetite/PLGA ratio increases the mean particle diameter, and vice versa. Similarly, at constant PLGA concentration, the increase of magnetite/PLGA ratio enhances particle size and vice versa.

If we follow the vertical line upward to the upper diagram at a given Fe_3O_4:PLGA ratio (in Fig. 19, we have taken the example of X_{Fe3O4}=4.0% wt/wt), it is seen that arriving at the point on the curve referring to the same mean particle size (155 nm in this case) will give EE_{HSA}=92.3% which is the highest encapsulation efficiency achieved under these conditions (Fig. 19, the horizontal dotted line of the upper diagram). We can conclude that if HSA-loaded nanoparticles of 155 nm mean size should be produced (with given magnetite content determined by the Fe_3O_4/PLGA ratio), under optimal conditions as high as 92.3% encapsulation efficiency can be achieved. If smaller particles should be produced by using lower PLGA concentration (the crossing point of the dotted lines in the lower diagram of Fig. 19, that will be shifted downwards e.g. to the curve of 145 nm), the expectable encapsulation efficiency will be decreased to about 84% (the ordinate value in the upper diagram where the vertical dotted line crosses the curve of 145 nm mean size). It means the general opinion widely accepted in the literature is clearly confirmed: the larger is the particle size, the higher is the expected encapsulation efficiency and vice versa, if certain parameters such as the drug/polymer ratio in the emulsion are kept constant (at their optimal value).

In addition to the particle size and encapsulation efficiency, several other requirements may be also important during producing PLGA nanoparticles loaded with protein type drug and magnetic NPs. Such requirements can be e.g. the concentration of the active ingredient in the nanocapsules, and/or the productivity of the applied process or equipment (product yield mass per unit volume of equipment and unit time).

Economical aspects, such as the cost of production per unit mass of product can be very important too. However, we have dealt only with the requirements of particle size and encapsulation efficiency as optimization criteria, also taking the magnetite/polymer ratio into consideration, which may be important to achieve suitable levels of magnetic properties of the produced nanoparticles (examination of the latter will be the subject of a separate study).

Another aspect can be the concentration of the encapsulated HSA in the composite nanoparticles. It was also determined from the available experimental data according to eqn. 4a-b, where concentration of HSA was changing from about 1.5 to 18.3% (wt/wt) depending on the applied process variables (Fig. 20). Considering these

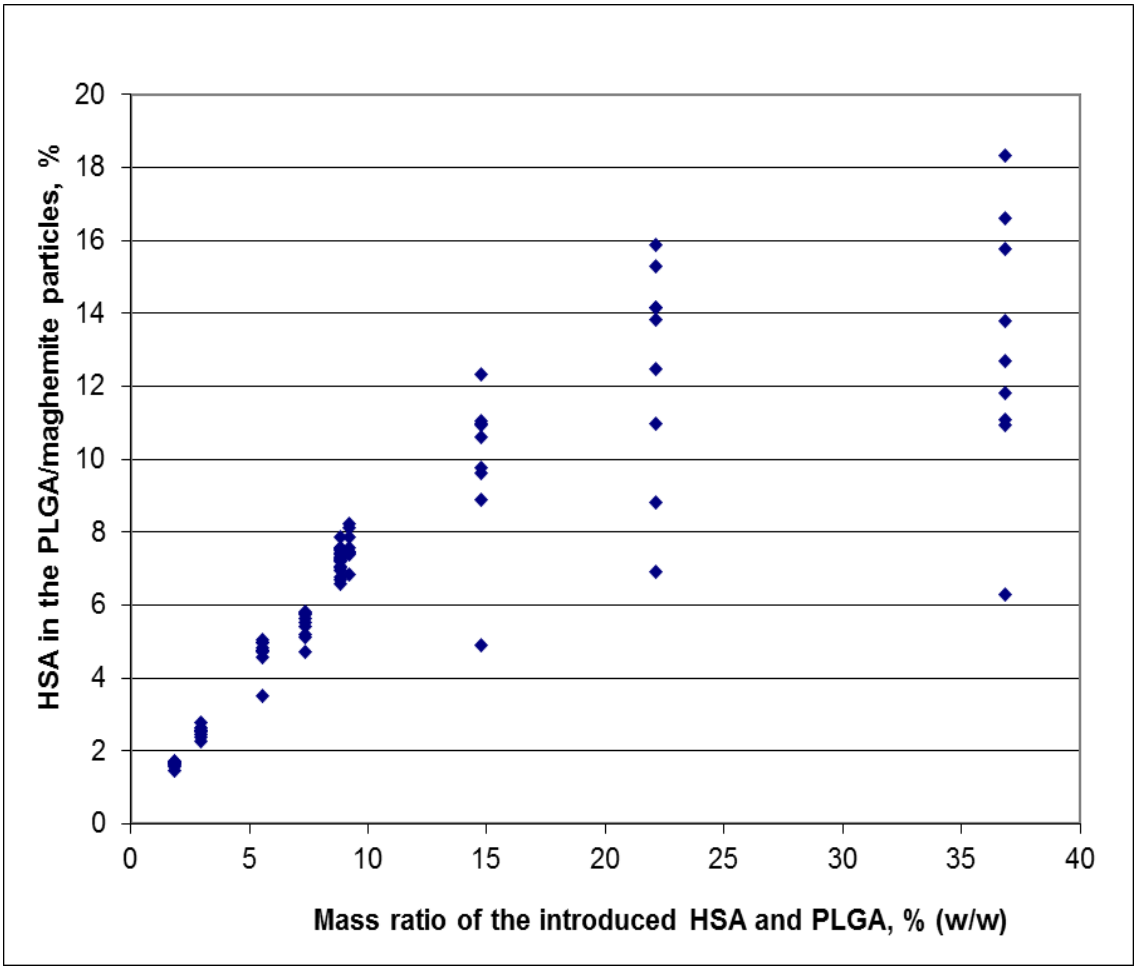

Fig. 20: Experimental data on the concentration of encapsulated HSA within the composite PLGA-magnetite particles at different mass ratios of HSA and PLGA introduced into the W/O/W double emulsion.

scattered values, the actual protein concentration encapsulated into the particles was primarily determined by the mass ratio of the introduced HSA and PLGA (both of them could be varied independently) and the encapsulation efficiency, influenced by the studied process variables. Fig. 20 also shows the increasing tendency of HSA concentration in particles with increasing HSA/PLGA mass ratio. It is also seen that the scattering of data also grows in this direction, mainly due to the increasing effect of other process variables on encapsulation efficiency.

In section 4.2.3, it was seen that the HSA concentration in the inner aqueous phase had no significant influence on the particle size. Therefore, suitably small particles can be produced at relatively high HSA/PLGA mass ratio, if the PLGA concentration is not too high. However, at the same time, increasing the HSA/PLGA ratio may have detrimental effect on the encapsulation efficiency (see Fig. 14) resulting in relatively high amount of non-encapsulated protein in the mother solution, remaining there after solidification and separation of the model drug loaded NPs, which may increase the loss of the valuable ingredient. Fig. 17 shows that applying low volume ratio of the external aqueous and intermediate organic phases (X_{VOLR}=2.0 vol/vol) which is optimal for obtaining small particles, the achievable encapsulation efficiency steeply decreases from 98.2 to 72.7% with the increase of HSA concentration at fixed other variables. This, especially for expensive drug ingredients may extremely deteriorate the economy of the process.

As an example, considering the conditions suitable for a high encapsulation efficiency (EE_{HSA}=92.3%), shown by the dotted line in the upper diagram on Fig. 19, the achievable HSA content can be calculated which is about 3.6% (according to eqn. 4). If higher protein content is needed in the particles, higher HSA/PLGA ratio should be applied which will diminish the efficiency of HSA encapsulation, and thus leads to an increase in protein loss.

4.5 Surface modification

Poloxamers are triblock copolymers consisting of PPO and PEO block and can interact with hydrophobic particles like PLGA to modify their surfaces. The structure of poloxamer and their adsorption onto hydrophobic PLGA NPs are shown in Fig. 21.

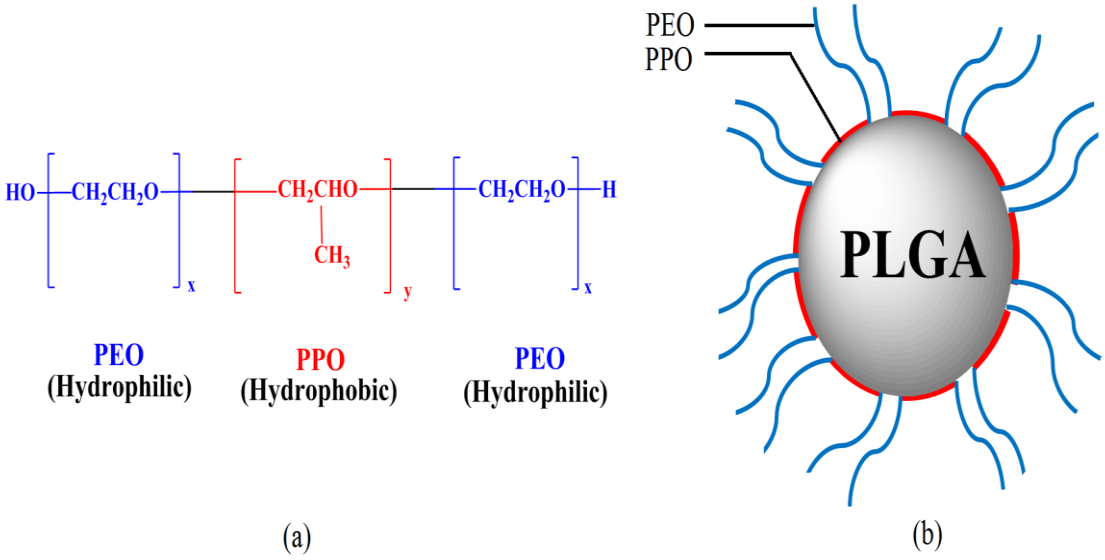

Fig. 21: (a) Structure of poloxamer, (b) adsorption pattern of poloxamer (simple brush type) onto a PLGA NP.

HSA loaded magnetic PLGA NPs subjected for surface modification were prepared using optimum process condition (Table 4) obtained after process optimization (section 4.4).

Table 4: Optimum values of process variables (factors) used for preparing PLGA NPs for surface modification.

Factor	Symbol	Variable	Optimum value
F1	X_{Fe3O4}	Fe_3O_4/PLGA weight ratio	1 wt%
F2	X_{PLGA}	PLGA concentration in the organic phase	1 wt%
F3	X_{HSA}	HSA concentration in the inner aqueous phase	0.74 wt%
F4	X_{VOLR}	Outer aqueous (w_2)/organic phase (o) volume ratio.	2 vol/vol
F5	X_{time}	Time of the ultrasonic treatment in the second emulsification	3 minutes

4.5.1 The surface charge of PLGA NPs

The PLGA used in this study has free carboxyl end groups and forms negatively charged surface in aqueous solution (Fig. 22a). This was also confirmed by electrophoretic mobility (μ) study which was measured as a function of the pH of the medium (Fig. 22b). The pH changes were made by the addition of dilute HCl and

NaOH. In all cases the μ values sharply increased when the pH changed to more acidic pH values (from 6 to 3), whereas more constant values were observed at basic pHs (from 8 to 10), which is in agreement with the study of Ortega et al [76]. Since used PLGA is negatively charged, addition of acid starts to minimize surface negativity, and between pH 4 and 5, the surface has no net charge, which represents the isoelectric point. Further addition of acid enables accumulation of positive charges on the surface providing positive zeta potential.

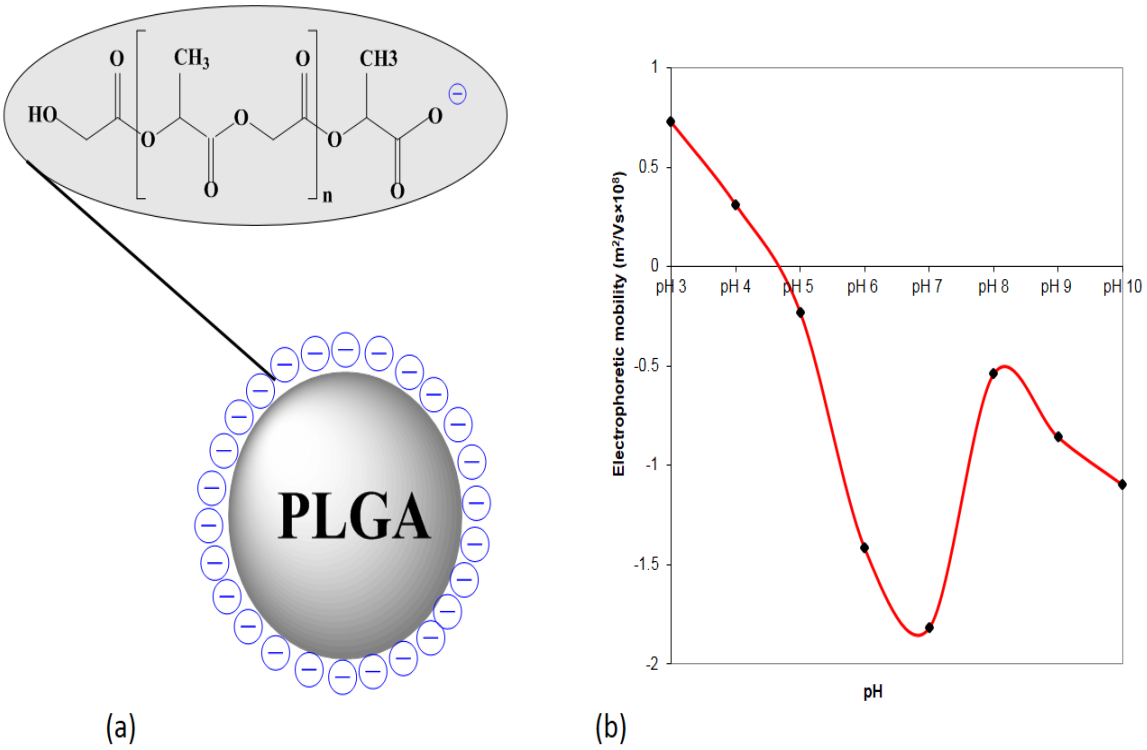

Fig. 22: (a) Negatively charged PLGA NP, (b) electrophoretic mobility (μ) as a function of pH.

4.5.2 Surface attachment of poloxamer

Surface attachment of PF68 was confirmed by size and zeta potential (ZP) study. The increase in size and change in ZP values obtained indicated the surface attachment of PF68 on PLGA NPs. The size and ZP of control PLGA NPs and PF68 modified PLGA NPs are shown in Table 5.

Table 5: Average size and zeta potential of uncoated and PF68 coated PLGA NPs.

Percentage of PF68	Size (nm)	Zeta potential (mV)
0% (control)	142±3.9	-35±0.5
0.1% PF68	165±9.1	-43.8±1.5
0.25% PF68	167±8.4	-45.2±0.9
0.5% PF68	177±2.5	-49±0.6
0.75% PF68	181±2.9	-49.5±0.7
1% PF68	191±4.3	-53.9±0.2

Size distribution curves (Fig. 23) makes it clear that there is no aggregation. Thus, it can be considered that it was a real size increase which was due to the poloxamer attachment onto PLGA.

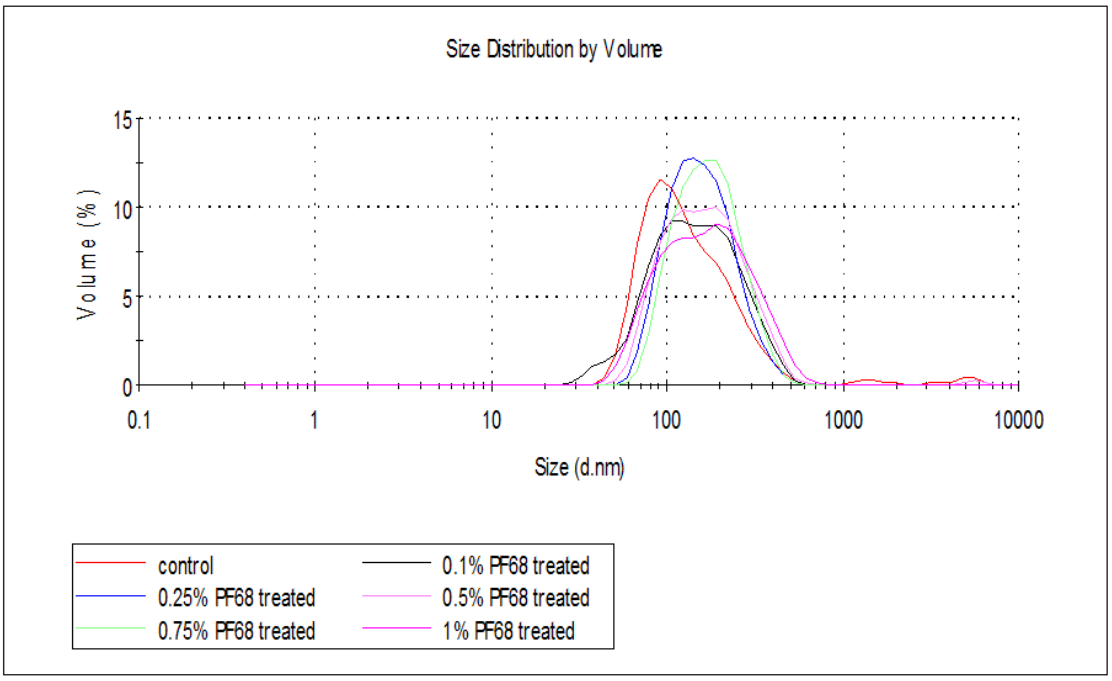

Fig. 23: Size distribution curves of unmodified and PF68 modified PLGA NPs (each drawn from five parallel measurements).

Volume mean size of the control sample was 142 nm and for coating with 1% PF68, almost 50 nm enhancement in size was observed which is comparable to the result obtained by Greenwood [77]. It was found that with the increase in poloxamer concentration, the size distributions of PF68 coated PLGA NPs shifted toward higher particle size region with significant simultaneous increase in volume mean particle size.

The increase is sharp and high for up to 0.5% poloxamer concentration, however, above that concentration, it is quite steady (Table 5). Ortega et al. [78] found a sharp increase in adsorption isotherm of PF68 coating on PLGA particles for low PF68 concentration (up to 100 mg/L), whilst above that value, the increase was quite steady, and reached a plateau, which supports our findings. If number of poloxamer attached is higher, the surface will be highly crowded. Consequently, adlayer thickness increases [79]. With the increase in concentration of PF68, micelle formation appears followed by micellar aggregation [80].

Considering the problem of micelle formation and aggregation, 0.5% PF68 was selected for PLGA NP treatment, and used for further analysis in this study. Moreover, the size of 0.5% PF68 modified NPs is about 40 nm below the membrane cut-off value, which is used for ultrafiltration.

ZP values of modified and unmodified samples are shown in Table 5. Absolute differences in ZP values should be at least 10 mV to allow prediction of distinct stability [81]. Modified PLGA NPs were fairly more stable even after few days of treatment showing comparatively little sedimentation, which could be clearly observed by naked eyes, and also supported by the ZP values shown in Table 5. On the other hand, control sample formed observable coagulates or flocculates after few hours of preparation which increased with time. This is also supported by our ZP values shown in Table 5. In all cases, visual observation strongly supported the ZP values obtained in this study. The addition of poloxamer leads to an increase in surface negativity.

4.5.3 Protein adsorption studies

Eqn. (5) was used to calculate protein adsorption from amount of protein left in the supernatant and the total amount of protein added in the beginning.

$$\%\ BSA\ adsorbed\ = \frac{(m_{BSA_{\text{int}}} - m_{BSA_{\text{supernatant}}})}{m_{BSA_{\text{int}}}} \times 100\% \qquad (5)$$

where m_{BSAint} = total amount of the introduced BSA (mg) and $m_{BSAsupernatant}$ = total amount of BSA in the supernatant.

For both unmodified and PF68 modified PLGA NPs, absorbance of reference samples (without BSA) were measured and subtracted from the total absorbance of samples since disturbance is expected due to the presence of residual PVA and non-

encapsulated model drug. Fig. 24 shows percentage of protein adsorbed for both modified and unmodified PLGA NPs. Almost 50% protein adsorption can be reduced by treating PLGA NPs with PF68 which is sufficiently enough for drug delivery purpose.

Comparison of this result with other published results is not so easy, since protein adsorption depends on the type of protein and the surface charge of NPs. From Table 5, it can be understood that the PLGA NPs studied have high negative ZP indicating high number of negative charges on the NP surface. To substantiate the result of protein adsorption shown in Fig. 24, size and ZP analysis were carried out (Table 6).

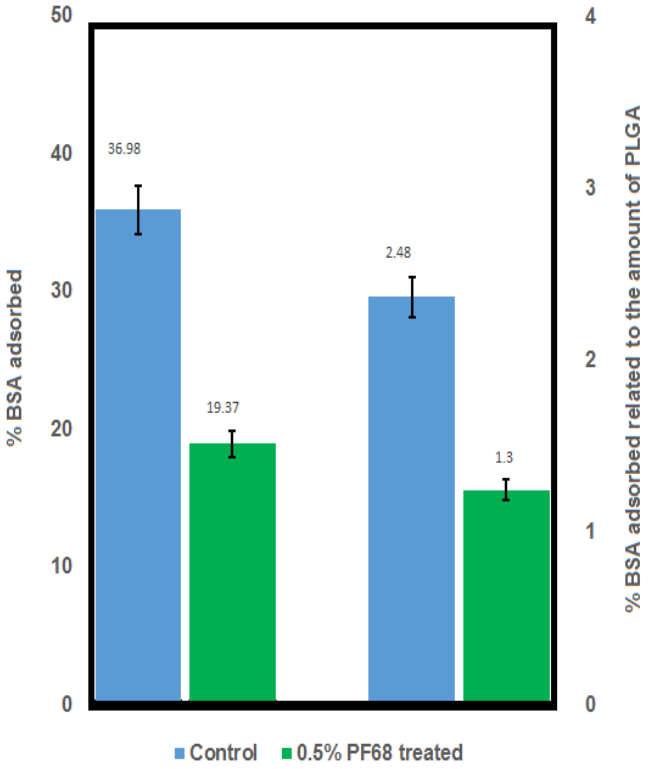

Fig. 24: Percentage of BSA adsorbed for unmodified and modified PLGA NPs.

Table 6: Size and ZP values of modified and unmodified sample before and after protein adsorption.

Sample	Size (nm)		ZP (mV)	
	Before BSA adsorption	After BSA adsorption	Before BSA adsorption	After BSA adsorption
Control	145.6±1.5	174.4±2.7	-36.1±7.2	-24.2±0.9
0.5% PF68 modified	173.2±0.9	181.2±2.8	-45.5±2.8	-34.4±1.2

From Table 6, it is clear that BSA adsorption increases the size and decreases the ZP of control sample significantly in comparison to the modified sample, which indicates that less protein was adsorbed on modified NPs supporting results of Fig. 24.

The adsorption of BSA to negatively charged PLGA surface is somewhat puzzling, because the isoelectric point of BSA is 4.6, and therefore BSA is negatively

charged at pH 7 [82]. The adsorption mechanism is quite interesting and is explained schematically by the Fig. 25.

Aspartic acid and glutamic acid in BSA are negatively charged due to the presence of side chains with carboxylate groups. BSA also contains slightly positively charged amino acids, namely lysine and arginine [83,84]. Lysine has a side chain amino group, which can become positive by accepting proton from water and arginine has protonated guanidinium group.

The net charge shown by BSA at pH 7 is negative as mentioned above. Although, BSA undergoes conformational changes on the PLGA surfaces (described in the next subsection), positively charged amino acids will be closer to the negatively charged PLGA surface than negatively charged amino acids like aspartic and glutamic acid. Negative PLGA surface repels negative amino acids to take them away from the surface as far as possible whereas they will pull and attract positively charged amino acids as close to the surface as possible (Fig. 25b).

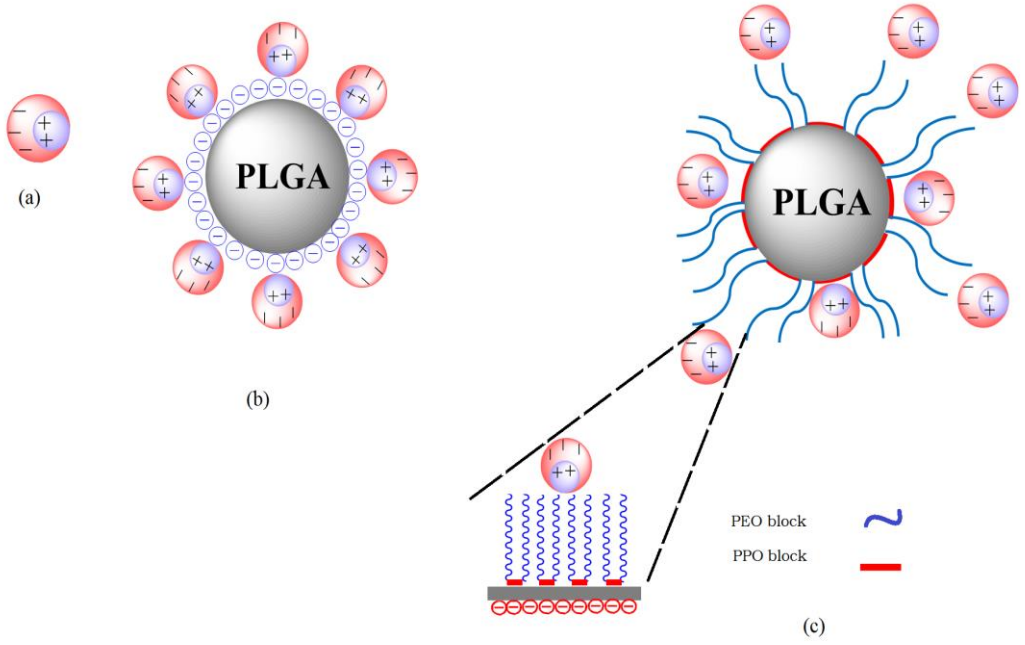

Fig. 25: (a) BSA protein having net negative charge (light blue and light red color regions carry local net positive and negative charges, respectively), (b) adsorption of BSA onto a unmodified PLGA NP and (c) prevention of protein adsorption onto PLGA NP by PF68 coating.

It is also confusing that BSA which has net negative charge reduces the surface negativity (Table 6). From Fig. 25, it can be understood that when BSA is adsorbed on

PLGA, positively charged amino acids will be close to PLGA surface e.g. positive arginine. Hence, it can be considered that positively charged amino acids will cover the surface reducing surface negativity of PLGA showing lower ZP values.

4.5.4 Isothermal calorimetric analysis

The protein binding energetics for BSA adsorption onto unmodified and 0.5% PF68 modified PLGA NPs were studied using the isothermal titration calorimetry (Fig. 26). The observed heat effects indicate definite interaction between BSA and NPs. One-site model was used to fit the data (lower panels in Fig. 26).

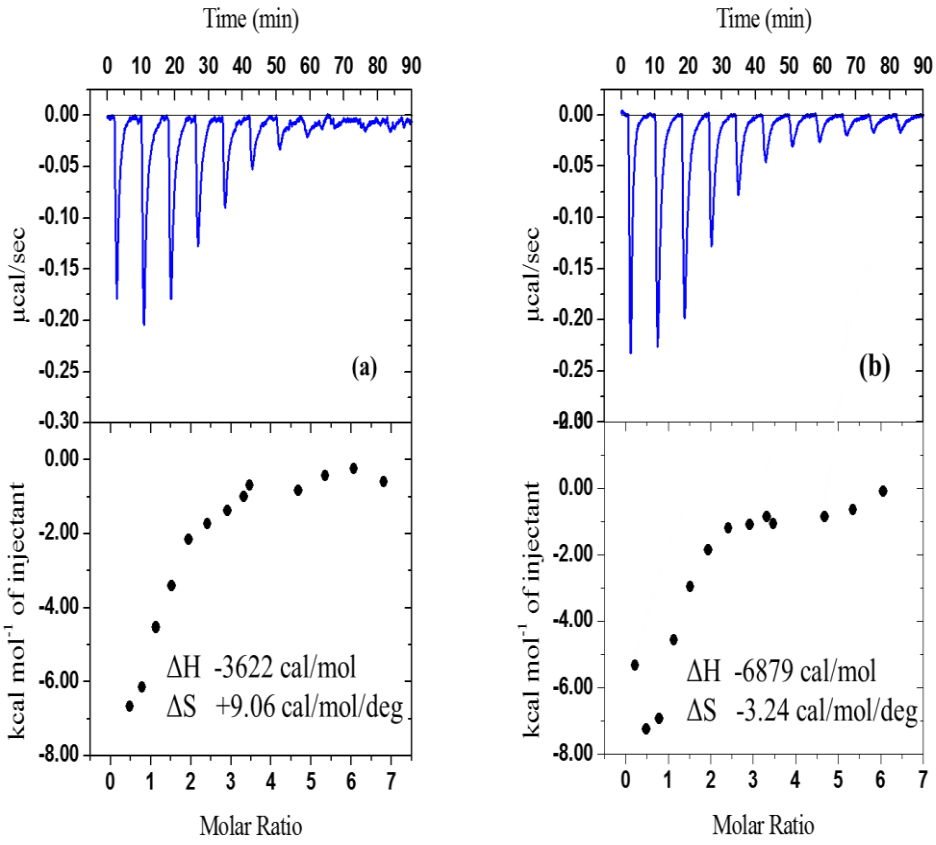

Fig. 26: Calorimetric data (top panel: raw data; bottom panel: binding isotherms) for BSA adsorption onto (a) unmodified PLGA NPs and (b) modified PLGA NPs.

Adsorption of BSA on NP surfaces is spontaneous and Gibbs free energy (ΔG) is negative. For unmodified NPs, heat release (ΔH) is lower than for modified ones and entropy change is also favorable, indicating that the process is entropy driven involving primarily hydrophobic interactions. Larger heat release (ΔH) and unfavorable entropy

change (-TΔS is positive) for modified samples indicate that the process is enthalpy driven involving hydrogen bonding in addition to hydrophobic interactions [85].

Protein adsorption is a very complicated process. Hydrophobic interaction is the main mechanism for protein adsorption on hydrophobic surface. Electrostatic interaction is observed for protein adsorption on hydrophilic surface, which is unfavorable but not impossible for hydrophobic surface. BSA is charged protein and charged amino acids are hydrophilic. They exist on the surface of a protein interacting with the surrounding water keeping hydrophobic amino acids away from water. Thus, for BSA, charged amino acids are in the water side (opposite to the PLGA NP surface), whereas hydrophobic amino acids are located close to the NP surfaces leading to BSA adsorption on NP surfaces. Since, hydrophilic charged group can be in the water side, hydrogen bond between BSA and PLGA is not expected. Due to hydrophobic interaction between protein and hydrophobic PLGA, entropy gain is observed (from Fig. 26, it is 9.06 cal/mol/deg), which is because of releasing water molecules from the hydrophobic surface. "Soft" proteins like BSA show conformational change (Fig. 27) when adsorbed onto hydrophobic particle [86].

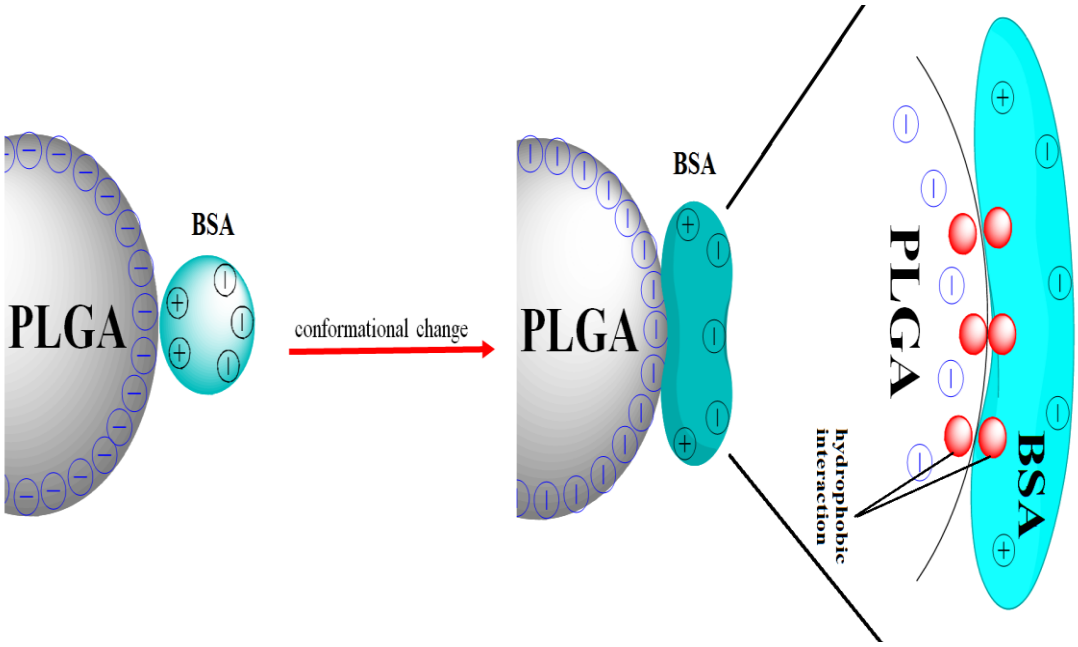

Fig. 27: Soft protein adsorption on a hydrophobic PLGA NP.

Poloxamers are surfactants and readily dissolve in water which forms strong hydrogen bonds with surfactants. It is expected and from Fig. 26 can be assumed that hydrogen bond will be formed between BSA and poloxamer, since both of them are hydrophilic. H-bond formation will release heat to a greater extent than simple

hydrophobic interaction between BSA and PLGA NPs, as can be seen from Fig. 26 (ΔH is significantly higher for modified nanoparticles than that for unmodified one). Scheme in Fig. 28 shows how lysine and arginine of BSA can form H-bonds with poloxamer.

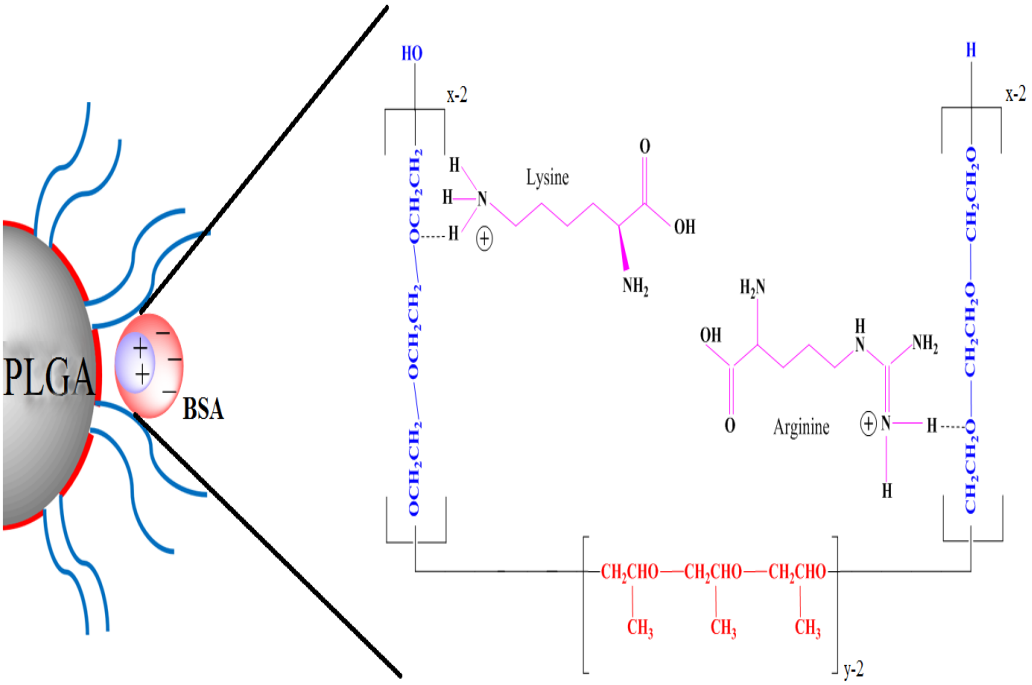

Fig. 28: Hydrogen bonding between poloxamer and amino acids of BSA.

Although before the experiments it was expected that more protein adsorption (for modified NPs) would show larger peaks and occupy more area in raw ITC Fig., whereas obtained result was opposite. To confirm the finding, single injection method (SIM) was also applied. The result shown in Fig. 29 clearly shows larger exothermic peak for modified NPs indicating high heat release due to H-bonding which is in agreement with the result shown in Fig. 26.

This result is novel and not easy to compare with other published work due to incorporation of model drug (HSA) and oleic acid coated magnetite. Interaction of poloxamer and PLGA have already been examined by ITC, but NPs containing PLGA, poloxamer, HSA and oleic acid coated magnetite have not been studied before using ITC. Iseult et al. investigated binding of protein HSA (human serum albumin) to hydrophobic polymeric NPs with and without oleic acid (OA) [87]. Very different interaction patterns were observed in the presence and absence of OA. Hydrophobic NP-HSA interaction was exothermic in absence of OA, whereas presence of OA gave endothermic signal. This study gives an idea that presence of other molecules/ions can

affect heat release pattern during ITC analysis, and can even change the release pattern from exothermic to endothermic.

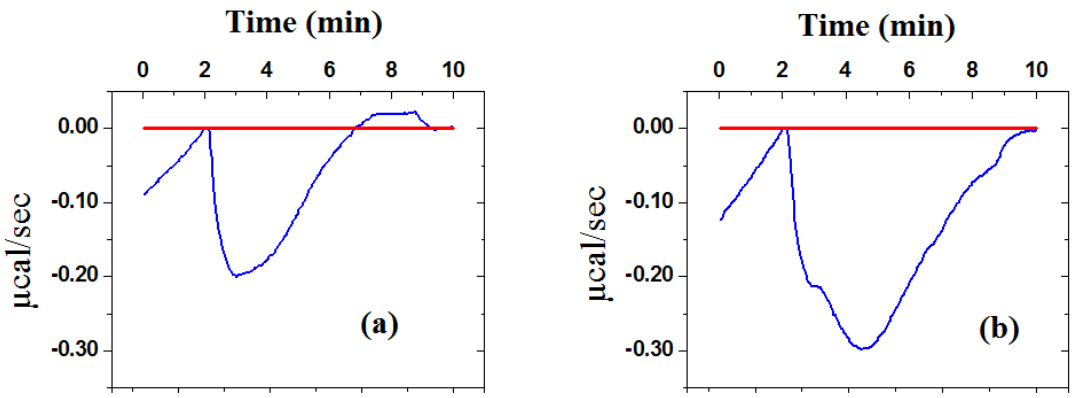

Fig. 29: Raw ITC data using single injection method for BSA adsorption onto (a) unmodified PLGA NPs and (b) modified PLGA NPs.

4.6 In vitro IFN-α release

In vitro IFN-α release study was carried out using ELISA test under conditions which are similar to the physiological circumstances in human body, i.e. the rate of dissolution of interferon was investigated at 37°C in PBS buffer, under gentle shaking the buffer solution after introducing the drug loaded particles. Two kinds of particles, i.e. surface modified with poloxamer and non-modified particles were investigated in the drug release tests and compared to non-encapsulated IFN.

Fig. 30 shows the release of surface modified and unmodified NPs, as well as free IFN degradation. It can be recognized that the IFN concentration of NPs in the first hour was suddenly increased in an initial burst, due to the rapid release of IFN from the nanoparticles, then, it was continuously decreasing, because of the simultaneous decomposition of the dissolved interferon. However, comparing these data to the results of native IFN decomposition, a substantial difference can be recognized: while the free IFN concentration decreased almost to zero level, where continuous supply of interferon took place from the nanoparticles to the buffer solution, the IFN concentration level remained quite high till the same time (i.e. till 48 hours), almost 30 pg/ml, and it was also high after 168 hours (almost 15 pg/ml). It means that encapsulation of interferon into the PLGA nanoparticles gives a good potential for realization of controlled release of the very sensitive biologically active substances, such as natural IFN alpha. The

nature of concentration variation in the modified NPs is similar to the non-modified particles, but the level of IFN activity is generally lower. The main reason of lower level during the whole investigation can be that while surface modification occurs, additional ultrasonic treatment is necessary, which undoubtedly can drop active IFN content. The surface covering with poloxamer might also retard the IFN release.

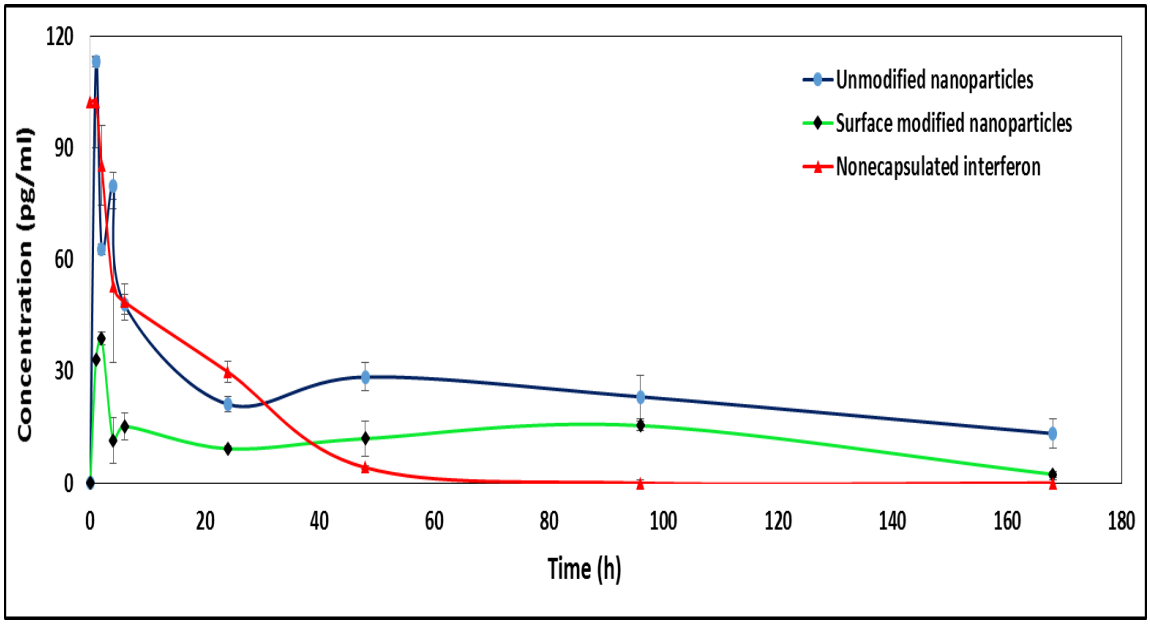

Fig. 30: Activity loss of IFN-α for the particles encapsulating IFN-α (both unmodified and modified) and control IFN-α (non-encapsulated).

It is supposed that the IFN released from the particles and being present in the buffer solution continuously decomposes, mainly due to the elevated temperature. It means that three processes take place simultaneously: 1. the release of the interferon from the particles increasing its concentration in the buffer, 2. chemical decomposition of the IFN in the nanoparticles and 3. Degradation of IFN dissolved in the liquid phase, decreasing its concentration in the buffer. The actual concentration of interferon in liquid phase is therefore determined by the rates of these three processes and the initial condition. This is analogues to the variation of the middle product concentration in case of three consecutive reactions, and also similar to the variation of the drug level in the body in case of simultaneous drug release from drug loaded particles together with the elimination of the active ingredient from the organism e.g. by renal clearance. Therefore the actual concentration alone does not give full information on the release rate, i.e. the elimination or decomposition rates should also be taken into consideration.

4.6.1 IFN-α decomposition kinetics

To get information on the rate of decomposition, non-encapsulated interferon was added to the buffer in order to measure the decay of interferon concentration as a function of time caused merely by the decomposition, applying the same conditions as during measuring the release from the drug loaded particles.

Using non-encapsulated interferon in 102 pg/ml initial concentration in 200 ml buffer solution at 37°C, the measured variation of IFN activity as a function of time is shown in Fig. 31. The duration of measurement was 7 days (168 hours), but due to the rapid decay, only the data points obtained in the first 48 hours (see also the data points in Fig. 30) were plotted in the diagram. It seems that the initial concentration decays rapidly due to its chemical decomposition under the applied conditions. It is highly probable that decomposition was primarily caused by the elevated temperature in the applied buffer composition.

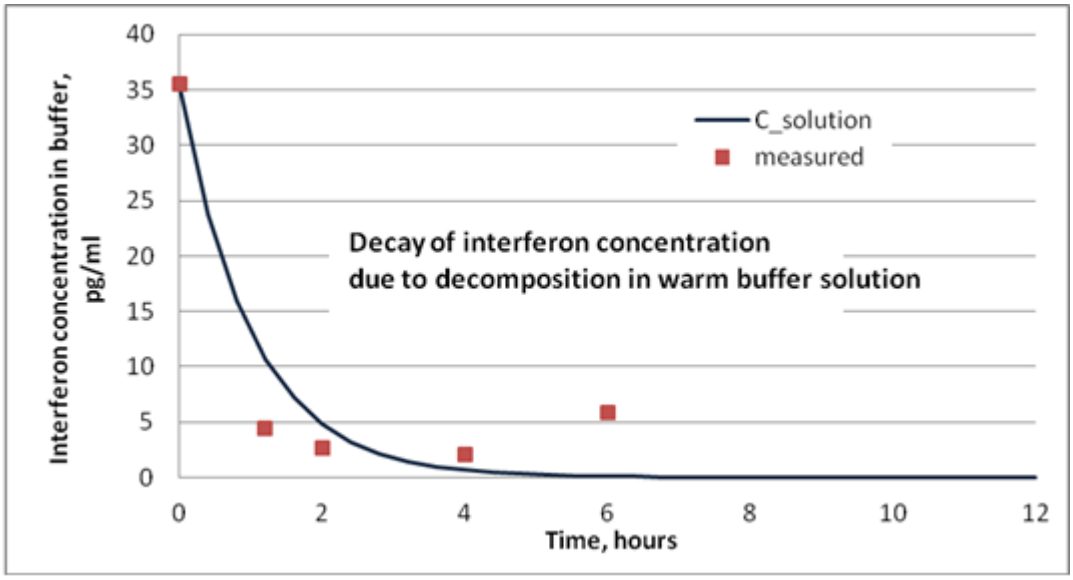

Fig. 31: Comparison of the measured and calculated data obtained with K_{decomp}=1.0 $hour^{-1}$ decomposition rate coefficient.

It was supposed that decomposition of interferon takes place in form of a first order reaction rate, i.e. the rate of inactivation of interferon molecules by chemical transformation to other compounds is proportional to the actual concentration of IFN in the buffer. That means:

$$\frac{dC_{IFN,buffer}}{dt} = -K_{decomp} \cdot C_{IFN,buffer} \qquad (6)$$

where $C_{IFN,buffer}$ is the actual concentration of interferon in the buffer (pg/ml), and K_{decomp} is the rate coefficient of decomposition ($hour^{-1}$).

The simulation of decomposition was carried out supposing different rate coefficients K_{decomp}, and the obtained concentration decay curves in the buffer were fitted to the measured concentration data to estimate the probable value of K_{decomp}. With a value of K_{decomp}=1.0 $hour^{-1}$ reasonable fit was obtained. The data plotted in Fig. 31 gives a comparison of the measured and calculated concentration data.

4.6.2 Modelling IFN-α release from NPs

Knowing the decomposition rate coefficient of IFN in the solution, it can be supposed that the decomposition of the released IFN from the studied particles takes place with the same kinetics. Although, it is emphasized that during the preparation process of NPs the activity loss of IFN cannot be estimated, and unfortunately, we have no reliable method to measure the real IFN concentration in the particles.

With the available data, change of the interferon concentration in the particles can be described as follows:

$$\frac{dC_{IFN,part}}{dt} = -\frac{dM_{IFN,part}}{V_{particle} \cdot dt} = -K_{release} \cdot \left(C_{IFN,part} - C_{IFN,buffer}\right) - K_{decomp,part} \cdot C_{IFN,part} \quad (7)$$

$$\frac{dC_{IFN,buffer}}{dt} = -\frac{dM_{IFN,buffer}}{V_{buffer} \cdot dt} = K_{release} \cdot \left(C_{IFN,part} - C_{IFN,buffer}\right) - K_{decomp,buffer} \cdot C_{IFN,buffer} \quad (8)$$

where $C_{IFN,part}$ is the volumetric concentration of interferon in the particles (pg/ml), $C_{IFN,buffer}$ is the concentration of interferon in the buffer (pg/ml), $M_{IFN,part}$ is the total mass of interferon in the drug loaded particles introduced to the buffer for release test (pg), $V_{particle}$ is the total volume of particles (ml), $K_{release}$ ($hour^{-1}$) is the rate coefficient of the IFN release, $K_{decomp,part}$ ($hour^{-1}$) and $K_{decomp,buffer}$ ($hour^{-1}$) are the decomposition rate coefficients of IFN in the particles and in the buffer, respectively. The IFN concentration entrapped in the NPs was 1.98 μg/ml.

The rate constants were determined by fitting the calculated curves to the measured points. The calculated curves were obtained by solving the differential eqns (7)-(8) by ModelMaker software (Fig. 32).

A)

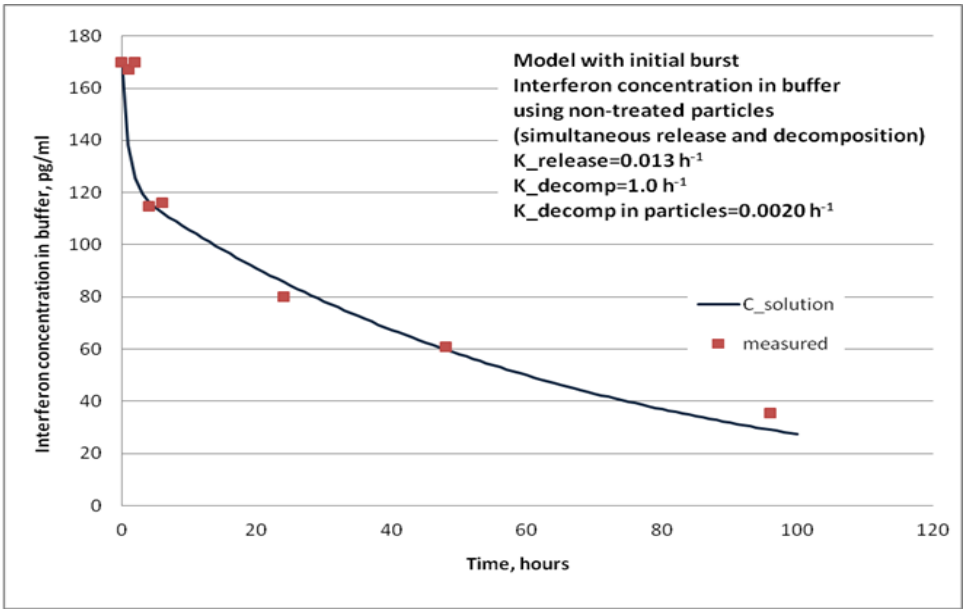

B)

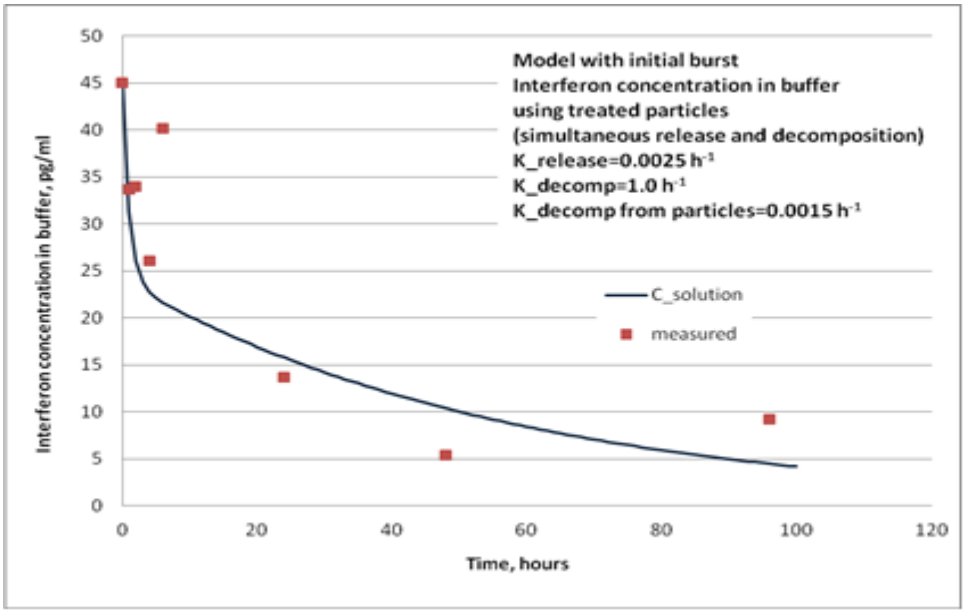

Fig. 32: Measured and calculated concentration of interferon in the buffer as a function of time obtained for non-treated particles, taking the decomposition inside the particles and first burst into consideration (A: unmodified NPs, B: surface modified NPs).

Table 7 compares the rate coefficients for the unmodified and modified particles.

Table 7: Rate coefficients of release ($K_{release}$), decomposition in the solution (K_{decomp}) and decomposition in the particles ($K_{decomp\ in\ part}$) for the unmodified and modified NPs.

	Unmodified particles	Surface modified particles
$K_{release}$, h^{-1}	0.013	0.0025
K_{decomp}, h^{-1}	1.0	1.0
$K_{decomp\ in\ part}$, h^{-1}	0.0020	0.0015

It was found that during the release at 37°C, the IFN entrapped in the NPs decomposes, though with much lower rate than free protein. Regarding both surface modified and unmodified particles the model resulted in reasonable fit, but the release rate constants were very different. It is emphasized that more exact release rate constants could be calculated if the real active IFN content could be measured in the NPs. Significantly lower initial burst and release rate of surface modified NPs might denote the more delayed effect of poloxamer coating, however, it must be also taken into consideration that the additional processing of NPs definitely caused some further loss of IFN activity in surface modified particles.

5 CONCLUSIONS

Co-encapsulation of magnetite nanoparticles (MNPs) and model drug (HSA)/active drug (IFN-α) was carried out into the matrix of biocompatible polymer (PLGA) nanoparticles by double emulsion solvent evaporation method. The influence of main parameter on size and encapsulation efficiency was investigated, which was studied by means of a $3^{(p-1)}$ type fractional factorial experimental design. .

The concentration of PLGA in the intermediate organic phase and the duration of the second sonication affected most strongly the mean hydrodynamic particle size. To achieve the smallest possible mean particle size, relatively low PLGA concentration, high dispersion energy (enough sonication time) and relatively small volume ratio of the intermediate organic/external aqueous liquid need to be applied. On the other hand, to achieve highest possible EE%, high concentration of PLGA and low concentration of HSA need to be applied in the process. It can be concluded that less than 160 nm PLGA NPs with more than 90% EE can be obtained by using optimized condition. Concentration of magnetite was kept minimum (1%) which is believed to provide sufficient magnetic property, higher magnetite concentration might enhance its health risk.

Nanoparticles surface was functionalized by poloxamer in order to increase their blood half-life. Serum protein adsorption was decreased by 50 % due to surface modification.

IFN-α loaded magnetic PLGA NPs prolonged the lifetime of IFN-α in in vitro release test. Finally, surface modified PLGA NPs represented more sustained release of IFN-α than unmodified NPs.

6 NEW SCIENTIFIC RESULTS

Thesis 1: For sustained and targeted delivery of natural interferon alpha (IFN-α), the latter one (IFN-α) and superparamagnetic iron oxide (Fe_3O_4) NPs were co-encapsulated inside poly(lactic-co-glycolic acid) (PLGA) matrix. The effect of five most important process variables (the amount of iron oxide in the organic phase relative to the weight of PLGA; concentration of PLGA in the organic phase; concentration of HSA in the inner aqueous phase; the outer aqueous/organic phase volume ratio; and the time of the ultrasonic treatment in the second emulsification) was investigated on the mean hydrodynamic particle size and the encapsulation efficacy. The mean hydrodynamic size of nanoparticles ranged from 115 to 329 nm depending on the process conditions, and it was affected most strongly by PLGA concentration followed by the duration of ultrasonic emulsification. Iron oxide/PLGA weight ratio, the outer aqueous and organic phase volume ratio and the linear-linear interaction of the latter factors also played significant size affecting roles.

(Reference of own published work: [3])

Thesis 2: Encapsulation efficiency of studied nanoparticles ranged from 18 to 97% depending on the process conditions. Among five important process variables, concentration of PLGA and concentration of HSA in the inner aqueous phase along with their cross-effect had the strongest influence on the encapsulation efficiency. The presence of magnetite had only slight influence on the encapsulation of HSA into the PLGA nanoparticles, while the outer aqueous/organic phase volume ratio and the time of ultrasonic treatment showed no significant effect on the encapsulation efficiency.

(Reference of own published work: [4,5])

Thesis 3: The optimization process, carried out by exact mathematical tools using GAMS^{TM}/MINOS, enabled to find out optimum process conditions to achieve high encapsulation efficiency for relatively small sized NPs. The results showed that smallest possible mean particle size could be achieved by using low polymer concentration and high dispersion energy (sufficient sonication time) along with small aqueous/organic volume ratio. HSA-loaded nanoparticles of 155 nm mean size could be produced under optimal conditions with as high as 92.3% encapsulation efficiency.

(Reference of own published work: [4])

Thesis 4: Proper surface modification of PLGA NPs was carried out using triblock copolymer poloxamer (Pluronic F68, PF68) to increase their lifetime in the bloodstream. Size and zeta potential measurements, protein adsorption study and isothermal titration calorimetry proved the effective surface modification of the NPs.
(Reference of own published work: [1,2])

Thesis 5: In vitro IFN-α release study was carried out by means of enzyme-linked immunosorbent assay. It was supposed that the IFN-α was released from the particles and continuously decomposed both in the nanoparticles and in the liquid phase, decreasing its concentration in the buffer. The actual concentration of interferon in the liquid phase was therefore determined by the rates of these three processes and the initial condition. It was assumed that the decomposition of interferon alpha took place with a first order reaction kinetics. The decomposition rate constants, occurred in the nanoparticles, were found to be similar within the surface modified and unmodified nanoparticles. These solid phase decomposition rates were considerably lower, than that in the liquid phase. The IFN release rate of surface modified particles was substantially lower than that of unmodified particles, which with the significantly lower initial burst are attributed mainly to the more delayed release effect arising from the poloxamer coating.

7 ÚJ TUDOMÁNYOS EREDMÉNYEK

1. tézis

Természetes interferon alfa (IFN-α) késleltetett és célzott hatóanyagleadása érdekében, IFN-α-t és szuperparamágneses vas-oxidot (Fe_3O_4) poli(tejsav-glikolsav) (PLGA) mátrixban mikrokapszuláztam. Az öt legfontosabb eljárási változó (vas-oxid mennyisége a szerves fázisban a PLGA tömegére vonatkoztatva; PLGA koncentráció a szerves fázisban; HSA koncentráció a belső vizes fázisban; a külső vizes fázis/szerves fázis térfogatarány; és az ultrahangos kezelés időtartama a második emulzifikálás során) az átlagos hidrodinamikai részecskeméretre és a kapszulázási hatékonyságra gyakorolt hatását vizsgáltam. A nanorészecskék átlagos hidrodinamikai mérete az eljárási körülményektől függően a 115-329 nm tartományban változott, és leginkább a PLGA koncentráció, azt követően a szonikálás időtartama befolyásolta. A vas-oxid/PLGA tömegarány, a külső vizes- és a szerves fázis térfogataránya és az utóbbi két faktor lineáris-lineáris kölcsönhatása is fontos méret befolyásoló szereppel bírt.
(Kapcsolódó saját publikációk: [3])

2. tézis

A vizsgált nanorészecskék kapszulázási hatékonysága az eljárási körülmények függvényében a 18-97 % tartományban változott. Az öt fontos változó közül a PLGA koncentrációja és a HSA koncentráció a belső vizes fázisban, továbbá ezek kereszthatása bírt a legerősebb hatással a kapszulázási hatékonyságra. A magnetit jelenléte csak kissé befolyásolta a HSA kapszulázást a PLGA nanorészecskékbe, míg a külső vizes/szerves fázis térfogat arány és az ultrahangos emulzifikálás nem mutatott szignifikáns hatást a kapszulázási hatékonyságra
(Kapcsolódó saját publikációk: [4,5])

3. tézis

Az egzakt matematikai eszközökkel (GAMS^{TM}/MINOS) kivitelezett optimalizálás lehetővé tette, hogy az optimális folyamat körülményeket megtaláljam ahhoz, hogy magas kapszulázási hatékonyság mellett relatíve kisméretű nanorészecskéket állítsak elő. Az eredmények azt mutatták, hogy a legkisebb lehetséges átlagos részecskeméret alacsony polimer koncentrációnál, nagy diszpergálási energiánál (elegendő szonikálási idő), illetve alacsony vizes fázis/szerves fázis térfogat aránynál érhető el. A legjobb

körülmények között 155 nm átlagméretű HSA-t tartalmazó nanorészecskéket sikerült előállítanom 92,3 %-os kapszulázási hatékonysággal.
(Kapcsolódó saját publikációk: [4])

4. tézis

A PLGA nanorészecskék megfelelő felületi módosítását poloxamer triblokk kopolimerrel (Pluronic F68, PF68) végeztem annak érdekében, hogy az élettartamuk a véráramban megnövekedjen. Méret és zeta potenciál mérések, fehérje adszorpciós vizsgálat és izotermális titrációs kalorimetria igazolták a nanorészecskék hatékony felületi módosítását.
(Kapcsolódó saját publikációk: [1,2])

5. tézis

In vitro IFN-α leadási vizsgálatot enzimhez kapcsolt *immunszorbens* meghatározással végeztem. Feltételeztem, hogy az IFN-α a részecskékből felszabadult, és folyamatosan lebomlott mind a nanorészecskékben és a folyadék fázisban, ezáltal csökkent a koncentrációja a pufferben. Így az interferon aktuális koncentrációját a folyadék fázisban ennek a három folyamatnak a sebessége és a kiindulási viszonyok határozzák meg. Feltételeztem, hogy az interferon lebomlása első rendű reakció kinetikával írható le. A nanorészecskékben lejátszódó lebomlás sebességi állandójára hasonló értéket kaptam a felületmódosított és a nem módosított nanorészecskék esetén. A szilárd fázisú lebomlási sebességek számottevően alacsonyabbak, mint a folyadék fázisban tapasztaltak. A felületmódosított részecskék IFN kibocsátási sebessége lényegesen alacsonyabb, mint a nem módosított részecskéké, amit a sokkal alacsonyabb kezdeti felszabadulással együtt főképpen a poloxamer borítás miatt fellépő még inkább elnyújtott kibocsátási hatásnak tulajdonítok.

8 REFERENCES

1. Attama A. A., Philip F. Builders P. F., in “Biopolymers in drug delivery: recent advances and challenges”, Adikwu M. U. (ed.). Bentham ebooks, page 85. DOI: 10.2174/97816080507891090101.

2. Kumari A., Yadav S. K., Yadav, S. C. Colloids and Surfaces B: Biointerfaces 2010, 75, 1–18.

3. Yang F., Shu Y. J., Yang Y. Q., Song F. L., Pan Y. F., Long X. Y., Chen G., Zhang, Y. M. Journal of Microencapsulation 2011, 28, 483-489.

4. Roth M. S., Foon K. A. The American Journal of Medicine 1986, 81, 871–882.

5. Belardelli F., Ferrantini M., Proietti E., Kirkwood J. M. Cytokine & Growth Factor Reviews 2002, 13, 119–134.

6. Brassard D. L., Grace M. J., Bordens R. W. Journal of Leukocyte Biology 2012, 71, 565-581.

7. Andrade L. J., Atta A. M., D'Almeida Junior A., Paraná R. The Brazilian Journal of Infectious Diseases 2008, 12, 144-148.

8. Yang F., Bian C., Zhu L., Zhao G., Huang Z., Huang M. Journal of Structural Biology 2007, 157, 348–355.

9. Vyas A., Das S. K., Singh D., Sonker A., Gidwani B., Jain V., Singh M. Trends in Applied Sciences Research 2012, 7, 620-635.

10. Singh M., Manikandan S., Kumaraguru A. K. Research Journal of Nanoscience and Nanotechnology 2011, 1, 1-11.

11. Singh R., Lillard Jr. J. W. Experimental and Molecular Pathology 2009, 86, 215–223.

12. Redhead H. M., Davis S. S., Illum L. Journal of Controlled Release 2001, 70, 353–363.

13. Mahapatro A., Singh D. K. Journal of Nanobiotechnology 2011, 9, 55.

14. Win K. Y., Feng S. S. Biomaterials 2005, 26, 2713–2722.

15. Bamrungsap S., Zhao Z., Chen T., Wang L., Li C., Fu T., Tan W. Nanomedicine 2012, 7, 1253-1271.

16. Champion J., Katare Y., Mitragotri S. Journal of Controlled Release 2007, 121, 3–9.

17. Ramishetti S., Huang L. Therapeutic Delivery 2012, 3, 1429–1445.

18. Wani M. Y., Hashim M. A., Nabi F., Malik M. A. Advances in Physical Chemistry 2011, dx.doi.org/10.1155/2011/450912.

19. Israelachvili J. N., in "Intermolecular and Surface Forces", Israelachvili J. N. (ed.). Elsevier, Amsterdam, 2011, page 255.

20. Jyothi N. V. N., Prasanna P. M., Sakarkar S. N., Prabha K. S., Ramaiah P. S., Srawan G. Y. Journal of Microencapsulation 2010, 27, 187–197.

21. Benichou A., Aserin A., Garti N. Advances in Colloid and Interface Science 2004, 108–109, 29–41.

22. Li M., Rouaud O., Poncelet D. International Journal of Pharmaceutics 2008, 363, 26–39.

23. Acharya S., Sahoo S. K. Advanced Drug Delivery Reviews 2011, 63, 170–183.

24. Lü J-M., Wang X., Marin-Muller C., Wang H., Lin P. H., Yao Q., Chen C. Expert Review of Molecular Diagnostics 2009, 9, 325–341.

25. Athanasiou K. A., Niederauer G. G., Agrawal C. M. Biomoterids 1996, 17, 93-102.

26. Akbarzadeh A., Samiei M., Davaran S. Nanoscale Research Letters 2012, 7, 144.

27. Gubin S. P., Koksharov Y. A., Khomutov G. B., Yurkov G. Y. Russian Chemical Reviews 2005, 74, 489-520.

28. Kolhatkar A. G., Jamison A. C., Litvinov D., Willson R. C., Lee T. R. International Journal of Molecular Sciences 2013, 14, 15977-16009.

29. Chomoucka J., Drbohlavova J., Huska D., Adam V., Kizek R., Hubalek J. Pharmacological Research 2010, 62, 144–149.

30. Jia Y., Yuan M., Yuan H., Huang X., Sui X., Cui X., Tang F., Peng J., Chen J., Lu S., Xu W., Zhang L., Guo Q. International Journal of Nanomedicine 2012, 7, 1697-708.

31. Akbarzadeh A., Mikaeili H., Zarghami N., Mohammad, R. Barkhordari A., Davaran S. International Journal of Nanomedicine 2012, 7, 511–526.

32. Wu W., He Q., Jiang C. Nanoscale Research Letters 2008, 3, 397–415.

33. Kim J-E., Shin J-Y., Cho M-H. Archives of Toxicology 2012, 86, 685–700.

34. Gupta A. K., Gupta M. Biomaterials 2005, 26, 3995–4021.

35. Freese A., Sabel B. A., Saltzman W. M., During M. J., Langer R. Experimental Neurology 1989, 103 234–238.

36. Makadia H. K., Siegel S. J. Polymers (Basel) 2011, 3, 1377–1397.

37. Zhou S., Sun J., Sun L., Dai Y., Liu L., Li X., Wang J., Weng J., Jia W., Zhang Z. Journal of Biomedical Materials Research Part B: Applied Biomaterials 2008, 87B, 189–196.

38. Yang F., Song F. L., Pan Y. F., Wang Z. Y., Yang Y. Q., Zhao Y. M., Liang S. Z., Zhang Y. M. Journal of Microencapsulation 2010, 27, 133-141.

39. Zhang Y. M., Yang F., Yang Y. Q., Song F. L., Xu A. L. Acta Pharmacologica Sinica 2008, 29, 1370–1375.

40. Diwan M., Park T. G. International Journal of Pharmaceutics 2003, 252, 111–122.

41. Sánchez A., Tobío M., González L., Fabra A., Alonso M. J. European Journal of Pharmaceutical Sciences 2003, 18, 221–229.

42. Giri N., Tomar P., Karwasara V. S., Pandey R. S., Dixit V. K. Acta Biochimica Biophysica Sinica 2011, 43, 877-883.

43. Kiss É., Kutnyánszky E., Bertóti I. Langmuir 2010, 26 1440–1444.

44. Paillard-Giteau A., Tran V. T., Thomas O.V Garric X., Coudane J., Marchal S., Chourpa I., Benoît J. P., Montero-Menei C. N., Venier-Julienne M. C. European Journal of Pharmaceutics and Biopharmaceutics 2010, 75, 128-136.

45. Semete B., Booysen L., Kalombo L., Ramalapa B., Hayeshi R., Swai H. S. International Journal of Pharmaceutics 2012, 424, 115-120.

46. Chen Y. C., Hsieh W. Y. Lee W. F., Zeng D. T. Journal of Biomaterials Applications 2013, 27, 909-922.

47. Horák D., Semenyuk N., Lednický F. Journal of Polymer Science Part A: Polymer Chemistry 2003, 41, 1848-1863.

48. Feczkó T., Tóth J., Gyenis J. Colloids and Surfaces A: Physicochemical and Engineering Aspects 2008, 319, 188–195.

49. Panyam J., Dali M. M., Sahoo S. K., Ma W., Chakravarthi S. S., Amidon G. L., Levy R. J., Labhasetwar V. Journal of Controlled Release 2003, 92, 173–187.

50. Santos H. M., Lodeiro C., Capelo-MartRnez J., in "Ultrasound in Chemistry: Analytical Applications", Capelo-Martinez J-L. (ed.). Wiley-VCH, Weinheim, 2009, page 13.

51. Feczkó T., Tóth J., Dósa G., Gyenis J. Chemical Engineering and Processing: Process Intensification 2011, 50, 846–853.

52. Biró E., Németh A. S., Feczkó T., Tóth J., Sisak C., Gyenis J. Chemical Engineering and Processing: Process Intensification 2009, 48, 771–779.

53. Sahoo S. K., Panyam J., Prabha S., Labhasetwar V. Journal of Controlled Release 2002, 82, 105–114

54. Chang S. K. C., in "Food Analysis Part II", Nielsen S. S. (ed.). Springer, New York, 2010, page 142.

55. Astete C. E., Kumar C. S. S. R., Sabliov C. M. Colloids and Surfaces A: Physicochemical and Engineering Aspects 2007, 299, 209-216 .

56. Sun J., Zhou S., Hou P., Yang Y., Weng J., Li X., Li M. Journal of Biomedical Materials Research Part A 2007, 80, 333-41.

57. Duan Y., Sun X., Gong T., Wang Q., Zhang Z. Journal of Materials Science: Materials in Medicine 2006, 17, 509–516.

58. Kollipara S., Bende G., Movva S., Saha R. Drug Development and Industrial Pharmacy 2010, 36, 1377-1387.

59. Budhian A., Siegel S. J., Winey K. I. International Journal of Pharmaceutics 2007, 336, 367–375.

60. Chorny M., Fishbein I., Danenberg H. D., Golomb G. Journal of Controlled Release 2002, 83, 389–400.

61. Quintanar-Guerrero D., Fessi H., Allémann E., Doelker E. International Journal of Pharmaceutics 1996, 143, 133–141.

62. Kwon H. Y., Lee J. Y., Choi S. W., Jang Y., Kim J. H. Colloids and Surfaces A: Physicochemical and Engineering Aspects 2001, 182, 123–130.

63. Kusum V. D., Bhosale U. V. International Journal of PharmTech Research 2009, 1, 644-653.

64. Galindo-Rodriguez S., Allémann E., Fessi H., Doelker E. Pharmaceutical Research 2004, 21, 1428-1439.

65. Mainardes R. M., Evangelista R. C. International Journal of Pharmaceutics 2005, 290, 137–144.

66. Coimbra P. A., De Sousa H. C., Gil M. H. Journal of Microencapsulation 2008, 25, 170-178.

67. Gorner T., Gref R., Michenot D., Sommer F., Tran M. N., Dellacherie E. Journal of Controlled Release 1999, 57, 259–268.

68. Maravajhala V., Dasari N., Sepuri A., Joginapalli S. Indian Journal of Pharmaceutical Sciences 2009, 71, 663-669.

69. Pamujula S., Graves R. A., Kishore V., Mandal T. K. European Journal of Pharmaceutics and Biopharmaceutics 2004, 57, 213–218.

70. Feczkó T., Tóth J., Dósa G., Gyenis J. Chemical Engineering and Processing: Process Intensification 2011, 50, 757– 65.

71. Feng S., Huang G. Journal of Controlled Release 2001, 71, 53–69.

72. Zhao H., Gagnon J., Häfeli U. O. Biomagnetic Research and Technology 2007, 5.

73. Wang Y. M., Sato H., Adachi I., Horikoshi I. Chemical & Pharmaceutical Bulletin (Tokyo) 1996, 44, 1935–1940.

74. Sato H., Wang Y. M., Adachi I., Horikoshi I. Biological & Pharmaceutical Bulletin 1996, 19, 1596–1601.

75. Dey S. K., Mandal B., Bhowmik M., Ghosh L. K. Brazilian Journal of Pharmaceutical Sciences 2009, 45, 585-591.

76. Santander-Ortega M. J., Csaba N., Alonso M. J., Ortega-Vinuesa J. L., Bastos-González D. Colloids and Surfaces A: Physicochemical and Engineering Aspects 2007, 296, 132-140.

77. Greenwood R., Luckham P. F., Gregory T. Colloids and Surfaces A: Physicochemical and Engineering Aspects 1995, 98, 117-125.

78. Santander-Ortega M. J., Jodar-Reyes A. B., Csaba N., Bastos-Gonzalez D., Ortega-Vinuesa J. L. Journal of Colloid and Interface Science 2006, 302, 522-529.

79. Stolnik S., Felumb N. C., Heald C. R., Garnett M. C., Illum L., Davis S. S. Colloids and Surfaces A: Physicochemical and Engineering Aspects 1997, 122, 151-159.

80. Garala K., Joshi P., Shah M., Ramkishan A., Patel J. International Journal of Pharmaceutical Investigation 2013, 3, 29–41.

81. Lu G. W., Gao P., in " Handbook of Non-Invasive Drug Delivery Systems: Science and Technology", Kulkarni V. S. (ed.). Elsevier, California, 2010, page 67.

82. Brewer S. H., Glomm W. R., Johnson M. C., Knag M. K., Franzen S. Langmuir 2005, 21, 9303-9307.

83. Rezwan K., Meier L. P., Gauckler L. J. Biomaterials 2005, 26, 4351–4357.

84. Persaud D. R., Barranco-Mendoza A. Food and Chemical Toxicology 2004, 42, 707–714.

85. Edink E., Jansen C., Leurs R., de Esch I. J. P. The heat is on: thermodynamic analysis in fragment-based drug discovery 2010, 7, 189–201.

86. Nakanishi K., Sakiyama T., Imamura K. Journal of Bioscience and Bioengineering 2001, 91, 233–244.

87. Lynch I., Dawson K. A. Nanotoday 2008, 3, 40–47.

List of publications

Publications related to the Ph.D. thesis

[1] **Quazi T. H. Shubhra**, Judit Tóth, János Gyenis, Tivadar Feczkó (2014). Surface Modification of HSA Containing Magnetic PLGA Nanoparticles by Poloxamer to Decrease Plasma Protein Adsorption. Colloids and Surfaces B: Biointerfaces, Published online on 22 July, doi: 10.1016/j.colsurfb.2014.07.025.

[2] **Quazi T. H. Shubhra**, Judit Tóth, János Gyenis, Tivadar Feczkó (2014). Poloxamers for surface modification of hydrophobic drug carriers and their effects on drug delivery, Polymer Reviews, 54(1): 112-138.

[3] **Quazi T. H. Shubhra**, Andrea F. Kardos, Tivadar Feczkó, Hana Mackova, Daniel Horák, Judit Tóth, György Dósa, János Gyenis (2014). Co-encapsulation of human serum albumin and superparamagnetic iron oxide in PLGA nanoparticles: Part I. Effect of process variables on the mean size. Journal of Microencapsulation, 31(2): 147-155.

[4] **Quazi T. H. Shubhra**, Tivadar Feczkó, Andrea F. Kardos, Judit Tóth, Hana Mackova, Daniel Horak, György Dósa, János Gyenis (2014). Co-encapsulation of human serum albumin and superparamagnetic iron oxide in PLGA nanoparticles: Part II. Effect of process variables on protein model drug encapsulation efficiency. Journal of Microencapsulation, 31(2): 156-165.

[5] **Quazi T. H. Shubhra**, Hana Macková, Andrea F. Kardos, Daniel Horák, Judit Tóth, János Gyenis, Tivadar Feczkó (2013). Encapsulation of human serum albumin in submicrometer magnetic poly(lactide-co-glycolide) particles as a model system for targeted drug delivery. e-Polymers, 13 (1): 310–318.

Proceedings and abstracts related to the Ph.D. thesis

[6] **Q. T. H. Shubhra**, T. Feczkó and J. Gyenis. Surface Modification of PLGA Nanoparticles Co-encapsulating Model Drug and Magnetic Nanoparticles to Prolong Life Time in the Bloodstream. The 7th World Congress on Particle Technology, May 19-22, 2014, Beijing, China, published electronically.

[7] **Shubhra Q.T.H.**, Feczkó T. and Gyenis J. Preparation, Optimization And Surface Modification Of Magnetic PLGA Nanoparticles Loaded With Model Drug. XXI International Conference on Bioencapsulation, August 28-30, 2013, Berlin, Germany, page 96-97.

[8] **Q.T.H. Shubhra**, T. Feczkó, J. Gyenis. Optimization Of Process Variables And Surface Modification Of Model Drug Loaded Magnetic PLGA Nanoparticles. 44th IUPAC World Chemistry Congress, August 11-16, 2013, Istanbul, Turkey, published electronically.

[9] **Quazi T. H. Shubhra**, Tivadar Feczkó, János Gyenis. Surface Modification Of Model Drug Loaded Magnetic PLGA Nanoparticles To Prolong Life Time In The Blood Stream. Particles 2013 conference, August 3-6, 2013, Ohio, USA, pages 48-49.

[10] **Quazi T. H. Shubhra**, Andrea F. Kardos, Tivadar Feczkó, János Gyenis. Co-encapsulation of superparamagneticiron oxide and human serum albumin in PLGA nanoparticles: Effect of process variables on the mean size and encapsulation efficiency. Materials Today Virtual Conference: Nanotechnology; 11-13 December, 2012. Poster published online. (http://view6.workcast.net/?cpak=9984479751519192&pak=6530323889924159).

[11] **Q.T.H. Shubhra**, A.F. Kardos, T. Feczkó, J. Gyenis. Effect Of Process Variables On Size And Encapsulation Efficiency Of Model Drug Loaded Magnetic PLGA Nanoparticles. NanoDDS'12 conference; 2012 December 6-7, Atlantic City, NJ, USA, page 151-152.

[12] **Q.T.H. Shubhra**, A.F. Kardos, T. Feczkó, J. Gyenis. Effect Of Process Variables On Size And Encapsulation Efficiency Of Model Drug Loaded Magnetic PLGA Nanoparticles. Drug Delivery Australia (DDA) conference; 2012 November 26-27; Melbourne, Australia, page 157.

[13] **Quazi T. H. Shubhra**, Tivadar Feczkó, János Gyenis, Andrea F. Kardos. Co-encapsulation of a model drug and magnetic nanoparticles. Conference of Chemical Engineering (MKN'12); 2012 April 24-26; Veszprem, Hungary, page 112 (ISBN 978-615-5044-54-0).

Acknowledgement

Firstly, I would express my most gratitude to my supervisors, Dr. János Gyenis and Dr. Tivadar Feczkó without whom I would not have been able to finish my Ph.D. work in time, although words can't explain everything. A good and complicated research work needs mental support and feedback from persons with facilities and funding, what I always got from my supervisors. I am extremely grateful for the countless opportunities that they provided for my academic and personal growth. By working with them, I learned a great deal not only about science, but also about how to approach difficulties positively, how to run a laboratory, and how to balance work and personal life.

For funding, I would like to gratefully acknowledge the financial support of European Commission granted through the "PowTech" Marie Curie Initial Training Network (Grant Agreement No: 264722), the support of Hungarian National Programme of Social Development TÁMOP-4.2.2/B-10/1-2010-0025 and the bilateral academic exchange program of Hungarian Academy of Sciences and Academy of Sciences of the Czech Republic (project KAN401220801).

The list of those to whom I would like to acknowledge seems to be endless; however, I highlight them, who provided support, without which this PhD thesis would have been difficult. Dr. Judit Tóth is the first person, need to be acknowledged, who supported me with her knowledge and encouragement and was very friendly at work and outside work as well. Special thanks to my other colleagues, Andrea F. Kardos, Laura Amina Dahili, Bence Németh, Eszter Herczeg and Anikó Bakonyvári working in our groups including my retired colleague Erika Szentmarjay, who have been by my side during the course of my studies with helpful discussions and encouraging words.

I would like to sincerely thank to Dr. Ferenc Vonderviszt for his support with knowledge and to let me use his laboratory. László Bali and Zsolt Pallai (Trigon Biotechnological Zrt.) supported this work with interferon and lab facilities. I want to thank Dr. Daniel Horak from Czech Republic for providing magnetic nanoparticles.

Knowledge is priceless, and I am really grateful to get the chance to learn from Dr. Endre Nagy, Dr. János Szépvölgyi and Dr. István Bársony. I am grateful to Hungary and Hungarian people to give me love and so many nice memories.

Finally, I would like to thank my beloved mother Tahmina Hamid and father Quazi Hamidul Haque for everything they did for me especially for making me

educated from childhood until university level to make me qualified for this Ph.D. position. All over the whole Ph.D. period, they supported me mentally from far away by providing me more love to make me mentally strong so that I don’t feel homesick and don’t break down with all difficulties and work pressures.

Appendix

Table: Experimental program obtained by 5-factorial 3-level experimental design with the applied process variables (factors), and the measured mean particle sizes and encapsulation efficiencies

Run # after randomization of their order	F1 (Fe_3O_4/PLGA weight ratio), wt/wt%	F2 (PLGA conc.), wt/vol%	F3 (HSA conc.), wt/vol%	F4 (Volume ratio W_2/O), vol/vol	F5 (Time of sonication), min	Mean particle size, nm	Encaps. efficacy, %
10	1.0	4.0	0.74	6.0	3.0	175.6	90.40
83 (C)	10.5	2.5	2.21	4.0	2.0	203.3	91.77
18	10.5	4.0	0.74	4.0	3.0	221.7	92.80
1	20.0	4.0	2.21	4.0	1.0	197.6	94.40
26	1.0	1.0	0.74	2.0	1.0	162.8	82.40
16	10.5	4.0	3.69	2.0	2.0	238.2	95.66
19	20.0	2.5	3.69	4.0	1.0	228.0	73.24
9	1.0	4.0	2.21	2.0	1.0	220.7	96.32
11	10.5	2.5	0.74	2.0	2.0	198.5	91.24
25	1.0	2.5	2.21	6.0	3.0	193.3	92.40
17	20.0	1.0	3.69	2.0	3.0	225.5	53.98
13	20.0	4.0	0.74	2.0	3.0	210.6	94.30
2	20.0	2.5	0.74	6.0	2.0	210.3	87.60
3	10.5	2.5	3.69	6.0	1.0	291.2	83.48
24	1.0	2.5	3.69	2.0	1.0	156.2	72.20
15	10.5	1.0	2.21	2.0	2.0	121.8	64.50
5	1.0	1.0	2.21	4.0	2.0	114.9	72.60
12	1.0	1.0	3.69	6.0	3.0	139.6	33.82
84 (C)	10.5	2.5	2.21	4.0	2.0	250.3	90.23
6	10.5	1.0	0.74	6.0	1.0	258.6	81.01
21	1.0	2.5	0.74	4.0	2.0	206.4	88.66
14	20.0	1.0	2.21	6.0	2.0	205.2	74.59
4	10.5	2.5	2.21	4.0	3.0	189.9	85.71
22	10.5	1.0	3.69	4.0	3.0	149.0	60.86
8	20.0	4.0	3.69	6.0	2.0	253.3	79.50
7	10.5	4.0	2.21	6.0	1.0	233.2	90.05
23	20.0	1.0	0.74	4.0	1.0	212.6	72.96
20	20.0	2.5	2.21	2.0	3.0	224.5	87.88
82 (C)	10.5	2.5	2.21	4.0	2.0	206.0	82.00
27	1.0	4.0	3.69	4.0	2.0	212.7	86.68
34	10.5	4.0	3.69	4.0	1.0	234.3	92.70
51	10.5	1.0	2.21	4.0	1.0	207.6	85.30

43	10.5	2.5	0.74	4.0	1.0	232.0	97.20
30	10.5	1.0	0.74	2.0	3.0	171.9	83.50
46	20.0	2.5	3.69	6.0	3.0	225.7	84.10
38	1.0	2.5	0.74	6.0	1.0	239.8	78.90
36	10.5	4.0	2.21	2.0	3.0	203.0	94.40
44	1.0	4.0	0.74	2.0	2.0	201.4	91.00
39	1.0	4.0	2.21	4.0	3.0	219.1	86.40
28	20.0	1.0	3.69	4.0	2.0	195.1	36.32
49	20.0	4.0	3.69	2.0	1.0	308.1	90.20
85 (C)	10.5	2.5	2.21	4.0	2.0	214.2	86.40
29	20.0	1.0	2.21	2.0	1.0	207.1	33.54
41	10.5	2.5	3.69	2.0	3.0	196.1	49.50
40	1.0	2.5	3.69	4.0	3.0	178.4	81.30
54	1.0	2.5	2.21	2.0	2.0	169.8	90.50
50	1.0	1.0	0.74	4.0	3.0	138.1	79.39
48	20.0	2.5	2.21	4.0	2.0	233.8	92.50
52	20.0	2.5	0.74	2.0	1.0	236.0	91.22
86 (C)	10.5	2.5	2.21	4.0	2.0	213.8	89.17
45	20.0	4.0	0.74	4.0	2.0	217.9	88.42
32	20.0	1.0	0.74	6.0	3.0	180.6	67.20
47	10.5	1.0	3.69	6.0	2.0	192.0	50.69
42	10.5	2.5	2.21	6.0	2.0	229.5	85.30
35	1.0	1.0	2.21	6.0	1.0	240.3	55.80
33	1.0	4.0	3.69	6.0	1.0	287.4	88.80
31	1.0	1.0	3.69	2.0	2.0	219.1	18.21
53	20.0	4.0	2.21	6.0	3.0	222.4	65.91
37	10.5	4.0	0.74	6.0	2.0	235.0	87.50
87 (C)	10.5	2.5	2.21	4.0	2.0	209.1	79.40
63	1.0	4.0	2.21	6.0	2.0	286.9	89.78
88 (C)	10.5	2.5	2.21	4.0	2.0	214.2	81.10
55	20.0	1.0	3.69	6.0	1.0	211.0	43.42
81	1.0	1.0	2.21	2.0	3.0	123.1	43.79
70	1.0	2.5	0.74	2.0	3.0	169.9	85.50
66	10.5	2.5	3.69	4.0	2.0	199.7	80.30
71	10.5	2.5	0.74	6.0	3.0	241.7	89.58
72	20.0	4.0	2.21	2.0	2.0	328.9	91.80
79	20.0	2.5	0.74	4.0	3.0	206.1	82.60
67	20.0	4.0	3.69	4.0	3.0	258.7	87.20
64	1.0	1.0	0.74	6.0	2.0	165.5	74.50
61	10.5	4.0	2.21	4.0	2.0	235.1	89.90
78	10.5	1.0	2.21	6.0	3.0	213.8	81.70
90 (C)	10.5	2.5	2.21	4.0	2.0	205.1	87.60
58	1.0	2.5	2.21	4.0	1.0	231.1	84.17
75	20.0	2.5	3.69	2.0	2.0	304.8	34.84

57	10.5	1.0	0.74	4.0	2.0	226.2	77.50
80	1.0	1.0	3.69	4.0	1.0	244.8	33.28
62	1.0	4.0	3.69	2.0	3.0	201.1	87.47
74	1.0	2.5	3.69	6.0	2.0	225.0	83.24
69	1.0	4.0	0.74	4.0	1.0	246.3	91.80
76	20.0	2.5	2.21	6.0	1.0	273.2	88.10
73	20.0	4.0	0.74	6.0	1.0	259.2	81.17
56	20.0	1.0	2.21	4.0	3.0	150.7	74.59
59	20.0	1.0	0.74	2.0	2.0	199.2	83.45
77	10.5	1.0	3.69	2.0	1.0	177.3	39.39
65	10.5	4.0	0.74	2.0	1.0	238.1	94.03
68	10.5	2.5	2.21	2.0	1.0	210.6	92.04
60	10.5	4.0	3.69	6.0	3.0	210.3	87.60
89 (C)	10.5	2.5	2.21	4.0	2.0	208.0	88.90